View metadata, citation and similar papers at core.ac.uk
brought to you by CORE
provided by IUScholarWorks

PHYSICAL REVIEW D **80,** 015020 (2009)

Electrodynamics with Lorentz-violating operators of arbitrary dimension

V. Alan Kostelecký[1] and Matthew Mewes[2]
[1]*Physics Department, Indiana University, Bloomington, Indiana 47405, USA*
[2]*Physics Department, Marquette University, Milwaukee, Wisconsin 53201, USA*
(Received 7 May 2009; published 29 July 2009)

The behavior of photons in the presence of Lorentz and *CPT* violation is studied. Allowing for operators of arbitrary mass dimension, we classify all gauge-invariant Lorentz- and *CPT*-violating terms in the quadratic Lagrange density associated with the effective photon propagator. The covariant dispersion relation is obtained, and conditions for birefringence are discussed. We provide a complete characterization of the coefficients for Lorentz violation for all mass dimensions via a decomposition using spin-weighted spherical harmonics. The resulting nine independent sets of spherical coefficients control birefringence, dispersion, and anisotropy in the photon propagator. We discuss the restriction of the general theory to various special models, including among others the minimal standard-model extension, the isotropic limit, the case of vacuum propagation, the nonbirefringent limit, and the vacuum-orthogonal model. The transformation of the spherical coefficients for Lorentz violation between the laboratory frame and the standard Sun-centered frame is provided. We apply the results to various astrophysical observations and laboratory experiments. Astrophysical searches of relevance include studies of birefringence and of dispersion. We use polarimetric and dispersive data from gamma-ray bursts to set constraints on coefficients for Lorentz violation involving operators of dimensions four through nine, and we describe the mixing of polarizations induced by Lorentz and *CPT* violation in the cosmic-microwave background. Laboratory searches of interest include cavity experiments. We present the general theory for searches with cavities, derive the experiment-dependent factors for coefficients in the vacuum-orthogonal model, and predict the corresponding frequency shift for a circular-cylindrical cavity.

DOI: 10.1103/PhysRevD.80.015020 PACS numbers: 11.30.Cp, 11.30.Er, 13.40.−f

I. INTRODUCTION

The properties of electromagnetic radiation have proved a fertile testing ground for relativity since its inception over a century ago. Tests such as the classic Michelson-Morley, Kennedy-Thorndike, and Ives-Stilwell experiments [1–4] were key in establishing Lorentz invariance, the foundational symmetry of relativity. The proposal that minuscule deviations from Lorentz symmetry could emerge from an underlying unified theory [5] has rekindled interest in sensitive relativity tests, and the past decade has seen a broad variety of searches for Lorentz violation at impressive sensitivities [6].

Violations of Lorentz symmetry at attainable energies are described by the standard-model extension (SME) [7,8]. The SME is a comprehensive effective field theory that characterizes general Lorentz and *CPT* violations. It contains both general relativity and the standard model, and so it is a realistic theory that can be applied to analyze observational and experimental data. A Lorentz-violating term in the Lagrange density of the SME is an observer scalar density formed by contracting a Lorentz-violating operator with a coefficient that acts to govern the term. The operator can be characterized in part by its mass dimension d, which determines the dimensionality of the coefficient and can be used as a naive guide to the size of the associated effects [9].

The focus of the present work is Lorentz and *CPT* violation involving photons. Numerous searches for Lorentz violation in electrodynamics have been performed, yielding some of the best existing constraints on SME coefficients. One major class of tests consists of laboratory searches involving electromagnetic resonators or interferometers [10–18], which can be viewed as contemporary versions of the classic tests of relativity. Another major class of tests consists of astrophysical observations searching for tiny defects in the propagation of light that has traveled over cosmological distances [7,11,19–23]. A variety of other analyses involving photons lead to constraints on SME coefficients [24]. There is also substantial literature on various topics in the photon sector of the SME, including renormalization [25], photon interactions [26], vacuum Čerenkov radiation [27], the Chern-Simons term [28], electromagnetostatics [29], and related phenomena involving photons in other contexts [30]. Outside the photon sector, the SME serves as the theoretical underpinning for studies of Lorentz symmetry involving electrons [31,32], protons and neutrons [33–35], mesons [36], muons [37], neutrinos [38], the Higgs boson [39], and gravity [8,40].

In this paper, we extend the existing treatment of Lorentz violation in electrodynamics to include operators of arbitrary mass dimension d. This further develops and consolidates previous systematic studies for operators of

 © 2009 The American Physical Society

renormalizable dimension [7,11], and it incorporates many phenomenological models for Lorentz violation. For definiteness, we focus on an action having the usual U(1) gauge symmetry and invariance under spacetime translations, so that charge, energy, and momentum are conserved. If the Lorentz violation is spontaneous, then the SME coefficients originate as expectation values of operators in an underlying theory, and the requirement of invariance under spacetime translations corresponds to disregarding soliton solutions and any massive or Nambu-Goldstone (NG) modes [41]. In a more complete treatment including gravity, the NG modes may play the role of the graviton [42]. Alternatively, the NG modes may be interpreted as the photon for Einstein-Maxwell theory embedded in a Lorentz-violating vector model called bumblebee electrodynamics [8,43]. The approach discussed here can readily be adapted to these and other scenarios, including applications to the photon sector of the SME in the context of the various topics mentioned above. Our methods are also relevant for other sectors of the SME [44].

The motivation for this work comes in part from current doctrine, which regards the combination of general relativity and the standard model as the low-energy limit of a unified quantum gravity theory that holds sway at the Planck scale, $M_{\text{Planck}} \sim 10^{19}$ GeV. Experience teaches us to expect a smooth transition from the known low-energy physics to the underlying theory, so it is plausible to interpret the low-energy action as the zeroth-order term in a series approximating the underlying theory. Dimensional analysis suggests that operators with larger d correspond to higher-order corrections. For physics involving violations of Lorentz and CPT symmetry, the complete series is given by the SME action, while the leading corrections form the action of the minimal SME. Lorentz-violating operators of larger d are therefore likely to be especially relevant in searches involving very high energies and in theoretical studies of foundational properties such as causality and stability [45]. Under suitable circumstances, nonrenormalizable operators may even dominate the physics. For example, the action of noncommutative quantum electrodynamics [46] incorporates Lorentz-violating effects associated with a nontrivial commutator for the spacetime coordinates. When the action is expressed in terms of conventional photon fields, a subset of the SME emerges in which the lowest-order Lorentz-violating operators have mass dimension six [47]. Similarly, operators of larger d dominate in Lorentz-violating theories with supersymmetry [48].

A comprehensive investigation of all Lorentz-violating operators with arbitrary mass dimensions is a challenging task. Here, we concentrate on terms in the action that are quadratic in the photon field A_μ and therefore contribute to the propagator, which in practice is the quantity of immediate interest in many searches for Lorentz violation. Our basic approach consists of constructing the quadratic action and developing a scheme to classify the operators. Rotations are a prominent subgroup of the Lorentz group, and a spherical decomposition can be performed on any Lorentz-violating operator. We use this fact to classify all Lorentz-violating terms in the action using nine sets of coefficients for Lorentz violation. The classification scheme is well matched to the description of physical Lorentz-violating effects in the photon propagator, including birefringence, dispersion, and anisotropy.

With this classification scheme taming the infinite number of operators, specific analyses of observational and experimental data become feasible. We study a variety of methods for seeking Lorentz violation using predictions from the quadratic action. The sharpest tests involve astrophysical birefringence, which involves propagation in the vacuum. Some Lorentz-violating operators produce no vacuum birefringence at leading order but nonetheless cause dispersion in the vacuum, and these can also be studied using astrophysical observations. In addition, there are many other Lorentz-violating operators that are undetectable at leading order via astrophysical observations and hence are best sought instead in laboratory experiments. The analyses in this work yield several first measurements of coefficients for Lorentz violation, and numerous interesting arenas emerge for future exploration.

The structure of this paper is as follows. The basic theory is discussed in Sec. II, which contains five subsections. The construction and counting of Lorentz-violating operators of all mass dimensions is presented in Sec. II A, while the Lagrange density and constitutive relations are obtained in Sec. II B. We derive the covariant dispersion relation in Sec. II C, discuss the physics of birefringence in Sec. II D, and offer general comments on Lorentz-violating effects in Sec. II E.

The spherical decomposition of the coefficients for Lorentz violation in terms of spin-weighted spherical harmonics is performed in Sec. III. We consider various special limits in Sec. IV, including the minimal SME, isotropic models, the vacuum limit, nondispersive nonbirefringent ''camouflage'' models, the vacuum-orthogonal case, and some limits providing connections to other formalisms. The rotation properties of the spherical coefficients for Lorentz violation are discussed in Sec. V. Other key properties of the spin-weighted spherical harmonics are summarized in the Appendix.

The remainder of the paper applies the results to observations and experiments. Astrophysical observations are studied in Sec. VI. Vacuum-dispersive effects are discussed in Sec. VI A, where new measurements and a summary of existing constraints are obtained. Vacuum birefringence is considered in Sec. VI B, which contains three subsections. Some basic theory for vacuum birefringence is presented in Sec. VI B 1. We apply it to point sources in Sec. VI B 2, using polarimetry from gamma-ray bursts to obtain new measurements, and also to the cosmic microwave back-

ground (CMB) in Sec. VI B 3. In both cases, we tabulate some existing sensitivities.

Laboratory experiments are discussed in Sec. VII. We construct a general theory for resonant-cavity tests in Sec. VII A and apply it in Sec. VII B to derive cavity factors for nonbirefringent operators and the form of the fractional frequency shift predicted by Lorentz violation. Explicit values of some cavity factors for a circular-cylindrical cavity are calculated in Sec. VII C. Section VIII provides a summary and discussion of the results in the paper, including tables compiling essential properties of the spherical coefficients and various limiting cases. Unless otherwise stated, this paper follows the notation and conventions of Ref. [11].

II. BASIC THEORY

This section discusses the theory and basic features of the quadratic action for electrodynamics allowing for arbitrary Lorentz and *CPT* violation. We begin with a discussion of the SME procedure for constructing the Lagrange density associated with the effective photon propagator. Attention is focused primarily on the case with conventional U(1) gauge invariance and translational invariance. The resulting effective field theory conserves charge, energy, and momentum. It represents an explicit presentation of all Lorentz-violating operators for photon propagation that are consistent with observer covariance. Following the construction of the theory, we extract a complete set of coefficients for Lorentz and *CPT* violation and discuss some of their basic properties. A technique for deriving covariant dispersion relations is presented and used to obtain a general covariant dispersion relation for the photon in the presence of arbitrary Lorentz and *CPT* violation. The issue of conditions for birefringence is considered, and we offer some remarks about the connections between birefringence, metricity, and electromagnetic duality.

A. Construction

A low-energy Lorentz-violating theory that is both coordinate independent and consistent with current observational data can be written as a Lagrange density containing sums of standard polynomial tensor operators contracted with coefficients for Lorentz violation [7]. The coefficients may be viewed as background fields inducing Lorentz violation, and they can correspond to vacuum expectation values of fundamental tensor fields. Applying this general idea to source-free linear electrodynamics, we arrive at an action S that is a quadratic functional of the photon field A_μ and its derivatives. The action S can then be expanded in a sum of terms $S_{(d)}$ of the form

$$S_{(d)} = \int d^4x \mathcal{K}_{(d)}^{\alpha_1\alpha_2\alpha_3\ldots\alpha_d} A_{\alpha_1} \partial_{\alpha_3} \ldots \partial_{\alpha_d} A_{\alpha_2}, \qquad (1)$$

where d is the dimension of the tensor operator. Each term $S_{(d)}$ violates *CPT* if d is odd or preserves *CPT* if d is even. The coefficients $\mathcal{K}_{(d)}^{\alpha_1\alpha_2\alpha_3\ldots\alpha_d}$ have mass dimension $4 - d$. In general, they can be dynamical and can depend on spacetime position. We can ensure invariance of S under spacetime translations, and hence obtain the usual conservation of energy and momentum, by restricting attention to the case of constant coefficients. Constant coefficients may arise naturally, but they may also represent the dominant components of dynamical background fields or an averaged effect.

Size estimates for the coefficients for Lorentz violation depend on the details of their origins. Since the effects are expected to be small, it is natural to suppose the Lorentz-violating operators are suppressed by some large mass. The intimate connection between Lorentz symmetry and gravity suggests the relevant scale is set by Planck-scale physics and therefore by the Planck mass M_{Planck}. Various scenarios can be imagined, although the absence of a satisfactory underlying theory combining gravity and quantum physics, and hence the lack of specifics concerning possible Lorentz violations, makes such scenarios a matter of surmise and likely naive. For example, one simple estimate has coefficients varying as $\mathcal{K}_{(d)} \sim \zeta M_{\text{Planck}}^{4-d}$, where ζ is of order 1. This means operators of renormalizable dimension $d \leq 4$ are unsuppressed relative to conventional physics. Observations then imply only the operators $d \geq 5$ are experimentally viable, so the dominant new physics is controlled by nonrenormalizable terms. Another class of scenarios has Lorentz-violating effects suppressed by a factor involving some power of the ratio m/M_{Planck}, where m is an appropriate low-energy scale. In these cases, the Lorentz violation may be related to one or more of the known hierarchies in nature [9]. For example, taking $m \sim 10^2$ GeV as the electroweak scale gives a dimensionless suppression factor of some power of $\sim 10^{-17}$ for Lorentz-violating physics compared to conventional effects.

While a general study of all possible operators of the form (1) would be of interest, it would be rather cumbersome and introduce various features in addition to Lorentz violations, thereby complicating both theoretical and experimental considerations. The possibilities are simplified somewhat by restricting attention to operators that maintain the conservation of energy, momentum, and electric charge. This implies focusing on the case of constant coefficients and requiring U(1) gauge invariance. The latter imposes certain symmetries on the Lorentz-violating operators, thereby reducing the total number of independent coefficients.

The first step in imposing these symmetries is to identify properties of the coefficients $\mathcal{K}_{(d)}^{\alpha_1\alpha_2\alpha_3\ldots\alpha_d}$ that follow from the intrinsic structure of S. One property of the coefficients is total symmetry in the $d - 2$ indices $\{\alpha_3 \ldots \alpha_d\}$. Another can be displayed by integrating Eq. (1) by parts $d - 2$ times. This reveals that the only coefficients contributing

to *CPT*-odd terms are antisymmetric in the first two indices of $\mathcal{K}_{(d)}^{\alpha_1\alpha_2\alpha_3\ldots\alpha_d}$, while the only ones contributing to *CPT*-even terms are symmetric. The same conclusion follows by considering the contributions to the variation of the action:

$$\delta S_{(d)} = \int d^4x \mathcal{K}_{(d)}^{\alpha_1\alpha_2\alpha_3\ldots\alpha_d}(\partial_{\alpha_3}\ldots\partial_{\alpha_d}A_{[\alpha_2})\delta A_{\alpha_1]_\pm} + \text{surface terms}, \tag{2}$$

where the minus and plus signs apply for *CPT*-odd and *CPT*-even terms, respectively, and where the brackets $[\,]_\pm$ indicate symmetrization and antisymmetrization.

With these intrinsic symmetries understood, term-by-term gauge invariance can be imposed and the resulting additional symmetries of $S_{(d)}$ identified. The usual U(1) gauge invariance, representing symmetry of the action under the variations $\delta_g A_\alpha = \partial_\alpha \Lambda$, is achieved by requiring that the variation

$$\delta_g S_{(d)} = -\int d^4x \mathcal{K}_{(d)}^{\alpha_1\alpha_2\alpha_3\ldots\alpha_d}\Lambda\partial_{\alpha_3}\ldots \times \partial_{\alpha_d}\left(\partial_{[\alpha_1}A_{\alpha_2]_\pm} + \frac{1}{2}\partial_{[\alpha_1}\partial_{\alpha_2]_\pm}\Lambda\right) \tag{3}$$

vanish for an arbitrary scalar function Λ. Direct investigation of this equation is possible but awkward. To identify the additional symmetries and hence the coefficients of interest, it is more practical first to perform representation decompositions of the associated Lorentz-violating operators. The intrinsic symmetries drastically limit the number of representations that can appear. The total symmetry in the last $d-2$ indices of $\mathcal{K}_{(d)}^{\alpha_1\alpha_2\alpha_3\ldots\alpha_d}$ implies that all representations that are antisymmetric in any pair of these indices are absent. We can therefore construct the relevant irreducible tensors from a product of symmetric representations. It turns out that this limits the possibilities to only five representations. In terms of Young tableaux, these five representations are displayed in Fig. 1.

For *CPT*-odd coefficients, the antisymmetry condition on the first two indices and the gauge variation (3) imply that tableau (a) is irrelevant, since it is symmetric in the indices $\{\alpha_1\alpha_2\}$. Also, representation (d) is symmetric under the simultaneous permutation of $1 \leftrightarrow 2$ and $3 \leftrightarrow 4$ and so fails to contribute. The antisymmetry in $\{1, 2, 3\}$ of representation (e) directly implies gauge invariance, so it satisfies our restrictions. The remaining two representations (b) and (c) lead to nonvanishing $\delta_g S(d)$ and are therefore gauge violating. We conclude that all gauge-invariant *CPT*-odd operators are associated with coefficients $\mathcal{K}_{(d)}^{\alpha_1\alpha_2\alpha_3\ldots\alpha_d}$ belonging to representation (e). These are antisymmetric in the first three indices and symmetric in the last $d-3$. Since dimension $d \leq 1$ operators are absent in a linear theory, we take $d \geq 3$ for *CPT*-odd operators in what follows.

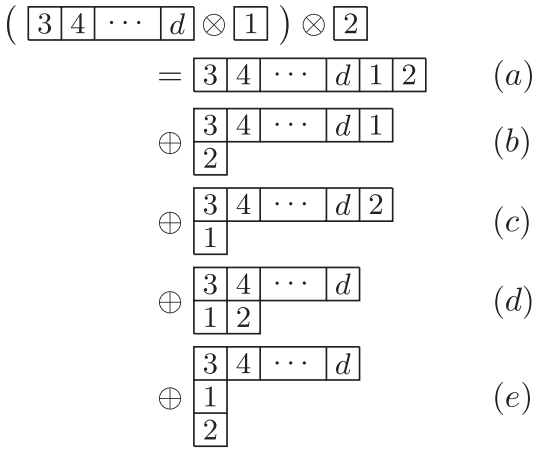

FIG. 1. Representation decomposition for the term $S_{(d)}$ using Young tableaux.

For *CPT*-even coefficients, the antisymmetry of tableau (e) in $\{1, 2\}$ implies it cannot contribute to Eq. (2) and therefore is absent in the theory. The antisymmetry of tableau (d) in $\{1, 3\}$ and $\{2, 4\}$ leads to $\delta_g S(d) = 0$, so this representation is gauge invariant and satisfies our restrictions. The tableau (a) is totally symmetric and leads to $\delta_g S(d) \neq 0$, implying gauge violation. Similarly, tableaux (b) and (c) are also gauge violating. We thus find that all gauge-invariant *CPT*-even operators have coefficients $\mathcal{K}_{(d)}^{\alpha_1\alpha_2\alpha_3\ldots\alpha_d}$ belonging to representation (d). Note that operators with $d = 2$ are gauge violating, so in what follows we take $d \geq 4$ for the *CPT*-even sector.

To simplify handling and to provide a convenient match to the usual coefficients for Lorentz violation in the minimal SME, it is convenient to introduce further definitions. For the *CPT*-odd case, the dual coefficients

$$(k_{AF}^{(d)})_\kappa{}^{\alpha_1\ldots\alpha_{(d-3)}} \equiv \frac{1}{3!}\epsilon_{\kappa\mu\nu\rho}\mathcal{K}_{(d)}^{\mu\nu\rho\alpha_1\alpha_2\ldots\alpha_{d-3}} \tag{4}$$

provide a generalization of the usual coefficients $(k_{AF})_\kappa$ in the minimal SME. The symmetries of tableau (e) translate into total symmetry of the coefficients $(k_{AF}^{(d)})_\kappa{}^{\alpha_1\ldots\alpha_{(d-3)}}$ in the last $d-3$ indices, along with the trace condition $(k_{AF}^{(d)})_{\alpha_1}{}^{\alpha_1\ldots\alpha_{(d-3)}} = 0$. Counting the number of independent components in representation (e) using standard group-theory techniques [49] yields for dimension d the result

$$N_{AF}^{(d)} = \tfrac{1}{2}(d+1)(d-1)(d-2). \tag{5}$$

This number can also be obtained by noting that symmetry in the last $d-3$ indices yields $4(d-2)(d-1)d/3!$ components while the trace condition given above provides $(d-3)(d-2)(d-1)/3!$ constraints, and taking the difference yields $N_{AF}^{(d)}$. Note that the number of these coefficients for *CPT*-odd Lorentz violation grows rapidly as the cube of d: the usual 4 for $d = 3$, then 36 coefficients for $d = 5$, 120 for $d = 7$, etc.

For the *CPT*-even case, it suffices to define

$$(k_F^{(d)})^{\kappa\lambda\mu\nu\alpha_1\ldots\alpha_{(d-4)}} \equiv \mathcal{K}_{(d)}^{\kappa\mu\lambda\nu\alpha_1\alpha_2\ldots\alpha_{d-4}} \tag{6}$$

to obtain coefficients that mimic the definition of $(k_F)^{\kappa\lambda\mu\nu}$ in the minimal SME. The first four indices of $(k_F^{(d)})^{\kappa\lambda\mu\nu\alpha_1\ldots\alpha_{(d-4)}}$ have the symmetries of the Riemann tensor, and there is total symmetry in the remaining $d-4$ indices. Also, one can show that antisymmetrization of $(k_F^{(d)})^{\kappa\lambda\mu\nu\alpha_1\ldots\alpha_{(d-4)}}$ on any three indices produces zero. In this case, counting the number of independent components for dimension d gives

$$N_F^{(d)} = (d+1)d(d-3). \tag{7}$$

This counting includes the total trace term, which is Lorentz invariant and represents a scaling factor. Again, note that the number of these coefficients for *CPT*-even Lorentz violation grows as the cube of d: the usual 20 (19 plus a Lorentz-invariant trace) for $d=4$, then 126 coefficients for $d=6$, 360 for $d=8$, etc.

B. Lagrange density and constitutive relations

The construction outlined in the previous subsection leads to a general gauge-invariant Lagrange density that can be written in a form similar to the photon sector of the minimal SME:

$$\begin{aligned}\mathcal{L} &= -\tfrac{1}{4}F_{\mu\nu}F^{\mu\nu} + \tfrac{1}{2}\epsilon^{\kappa\lambda\mu\nu}A_\lambda(\hat{k}_{AF})_\kappa F_{\mu\nu} \\ &\quad - \tfrac{1}{4}F_{\kappa\lambda}(\hat{k}_F)^{\kappa\lambda\mu\nu}F_{\mu\nu},\end{aligned} \tag{8}$$

where the differential operators $\hat{k}_{AF}$ and $\hat{k}_F$ involve *CPT*-odd and *CPT*-even violations, respectively. These operators are given by the expansions

$$(\hat{k}_{AF})_\kappa = \sum_{d=\text{odd}} (k_{AF}^{(d)})_\kappa{}^{\alpha_1\ldots\alpha_{(d-3)}}\partial_{\alpha_1}\ldots\partial_{\alpha_{(d-3)}}, \tag{9}$$

$$(\hat{k}_F)^{\kappa\lambda\mu\nu} = \sum_{d=\text{even}} (k_F^{(d)})^{\kappa\lambda\mu\nu\alpha_1\ldots\alpha_{(d-4)}}\partial_{\alpha_1}\ldots\partial_{\alpha_{(d-4)}}, \tag{10}$$

where the sums range over values $d \geq 3$. The coefficients $(k_{AF}^{(d)})_\kappa{}^{\alpha_1\ldots\alpha_{(d-3)}}$ are defined in Eq. (4), and they have symmetry properties yielding $N_{AF}^{(d)}$ independent components as given in Eq. (5). The coefficients $(k_F^{(d)})^{\kappa\lambda\mu\nu\alpha_1\ldots\alpha_{(d-4)}}$ are defined in Eq. (6) and have $N_F^{(d)}$ independent components according to Eq. (7). The usual minimal SME terms are $k_{AF} \equiv k_{AF}^{(3)}$ and $k_F \equiv k_F^{(4)}$, where in the latter the overall trace is removed to leave 19 independent coefficients.

In principle, obtaining and interpreting equations of motion for a Lagrange density of the form (8) is problematic due to the infinite sum, whose action cannot be varied in the usual way, and also due to Ostrogradski instabilities [50]. However, these issues can be circumvented by noting that Eq. (8) represents the low-energy limit of a more fundamental theory, with each successive term representing a perturbation on preceding terms. Truncating the sums at any definite value of d and restricting attention to perturbative effects therefore can be expected to provide a good approximation to the low-energy behavior. Only at extreme energies can qualitatively new effects and late terms in the sum play an important role. At these energies, the theory must converge to the underlying fundamental physics, which presumably is free of these issues. Adopting this truncation, we obtain equations of motion given by

$$(\eta^{\mu\alpha}\eta^{\nu\beta}\partial_\nu + (\hat{k}_{AF})_\nu\epsilon^{\mu\nu\alpha\beta} + (\hat{k}_F)^{\mu\nu\alpha\beta}\partial_\nu)F_{\alpha\beta} = 0. \tag{11}$$

Note the explicit gauge invariance of these equations.

In the minimal SME, the coefficients $k_{AF}^{(3)}$ and $k_F^{(4)}$ are known to produce photon behavior analogous to that of conventional electrodynamics in anisotropic and gyrotropic materials [7,11]. This analogy can be extended to the present situation involving Lorentz-violating operators of arbitrary dimension. The first step is to define a field tensor

$$G^{\mu\nu} = F^{\mu\nu} - 2\epsilon^{\mu\nu\alpha\beta}(\hat{k}_{AF})_\alpha A_\beta + (\hat{k}_F)^{\mu\nu\alpha\beta}F_{\alpha\beta}, \tag{12}$$

in terms of which the equations of motion become

$$\partial_\nu G^{\mu\nu} = 0. \tag{13}$$

Note that the latter equation is gauge invariant, even though the definition of $G^{\mu\nu}$ depends on the choice of gauge and is unique only up to a term of the form $\epsilon^{\mu\nu\alpha\beta}(\hat{k}_{AF})_\alpha\partial_\beta\Lambda$ for an arbitrary scalar function Λ.

For conventional electrodynamics in macroscopic media, a constitutive four-tensor χ is typically introduced that maps the two-form field strength F to the macroscopic two-tensor field strength G, via $G^{\mu\nu} = \chi^{\mu\nu\rho\sigma}F_{\rho\sigma}$. In the present context, we can reformulate the situation in terms of a set of unconventional constitutive relations, which may explicitly depend on the choice of gauge. However, we must generalize the usual notion of a constitutive four-tensor to encompass more general operator constitutive tensors. We now require an operator four-tensor $\hat{\chi}^{\mu\nu\rho\sigma}$ and an operator three-tensor $\hat{X}^{\mu\nu\rho}$, defined by

$$\begin{aligned}\hat{\chi}^{\mu\nu\rho\sigma} &= \tfrac{1}{2}(\eta^{\mu\rho}\eta^{\nu\sigma} - \eta^{\nu\rho}\eta^{\mu\sigma}) + (\hat{k}_F)^{\mu\nu\rho\sigma}, \\ \hat{X}^{\mu\nu\rho} &= \epsilon^{\mu\nu\rho\sigma}(\hat{k}_{AF})_\sigma.\end{aligned} \tag{14}$$

Note that the three-tensor controls *CPT* violation. The effective macroscopic field strength G defined in Eq. (12) is then given by

$$G^{\mu\nu} = \hat{\chi}^{\mu\nu\rho\sigma}F_{\rho\sigma} + 2\hat{X}^{\mu\nu\rho}A_\rho. \tag{15}$$

As in conventional electrodynamics, the new constitutive relations remain linear. However, unlike electrodynamics in linear media, the relations (15) inherit a nonlocal aspect due to their differential nature.

Decomposing $G^{\mu\nu}$ into an effective vector displacement field $\boldsymbol{D}$ and an effective pseudovector magnetic field $\boldsymbol{H}$ in the usual way, the equations of motion (13) take the same form as the familiar source-free inhomogeneous Maxwell equations,

$$\boldsymbol{\nabla}\cdot\boldsymbol{D}=0, \qquad \boldsymbol{\nabla}\times\boldsymbol{H}-\partial_0\boldsymbol{D}=0, \tag{16}$$

where

$$\begin{aligned}\boldsymbol{D} &= \boldsymbol{E}+2\hat{\boldsymbol{k}}_{\boldsymbol{AF}}\times\boldsymbol{A}+\hat{\kappa}_{DE}\cdot\boldsymbol{E}+\hat{\kappa}_{DB}\cdot\boldsymbol{B},\\ \boldsymbol{H} &= \boldsymbol{B}-2(\hat{k}_{AF})_0\boldsymbol{A}+2\hat{\boldsymbol{k}}_{\boldsymbol{AF}}A_0+\hat{\kappa}_{HB}\cdot\boldsymbol{B}+\hat{\kappa}_{HE}\cdot\boldsymbol{E}\end{aligned} \tag{17}$$

with

$$\begin{aligned}(\hat{\kappa}_{DE})^{jk}=-2(\hat{k}_F)^{0j0k}, \qquad (\hat{\kappa}_{HB})^{jk}=\tfrac{1}{2}(\hat{k}_F)^{lmrs}\epsilon^{jlm}\epsilon^{krs},\\ (\hat{\kappa}_{DB})^{jk}=-(\hat{\kappa}_{HE})^{kj}=(\hat{k}_F)^{0jlm}\epsilon^{klm}.\end{aligned} \tag{18}$$

The latter equations are operator generalizations of the SO(3) decomposition of the coefficients $k_F^{(4)}$ into 3×3 matrices introduced in Ref. [11].

Using the fields $\boldsymbol{D}$ and $\boldsymbol{H}$, the Lagrange density may be written as

$$\mathcal{L}=-\tfrac{1}{4}F_{\mu\nu}G^{\mu\nu}=\tfrac{1}{2}(\boldsymbol{E}\cdot\boldsymbol{D}-\boldsymbol{B}\cdot\boldsymbol{H}), \tag{19}$$

which also parallels conventional electrodynamics in macroscopic media. We remark that the analogy with electrodynamics breaks down when attempting to construct a conserved energy-momentum tensor. Standard techniques can be used to build a conserved tensor that reduces to the conventional symmetrized energy-momentum tensor in the limit of vanishing Lorentz violations. However, the resulting tensor takes an unconventional form in terms of $F_{\mu\nu}$ and $G^{\mu\nu}$. One possibility is the tensor

$$T^{\alpha}{}_{\beta}=-G^{\alpha\gamma}F_{\beta\gamma}-\delta^{\alpha}_{\beta}\mathcal{L}+\tfrac{1}{2}(\partial_\beta A_\gamma-A_\gamma\partial_\beta)G^{\alpha\gamma}. \tag{20}$$

The first two terms parallel those in conventional electrodynamics, but the addition of the last term is necessary for energy-momentum conservation to hold. This last term is separately conserved in conventional electrodynamics and so can be removed there, but a term of this type must be present for $T^{\alpha}{}_{\beta}$ to be conserved in the presence of general Lorentz violation.

C. Covariant dispersion relation

Much of the propagation behavior of the photon is encoded in its dispersion relation, which provides spectral information for the modes. While standard methods can be used to find the dispersion relation from the equations of motion, at least at leading order in the coefficients for Lorentz violation, handling the gauge freedom typically entails the loss of observer Lorentz invariance. In this subsection, we present a technique for deriving the exact covariant dispersion relation, based on the rank-nullity properties of the equations of motion. As a concomitant, the technique provides some insight into the nature of birefringence, which arises whenever the dispersion relation has nondegenerate physical solutions.

We begin by adopting the ansatz

$$A_\mu(x)=A_\mu(p)e^{-ix\cdot p}. \tag{21}$$

This implies the equations of motion (11) can be expressed in the matrix form

$$M^{\mu\nu}A_\nu=0 \tag{22}$$

with

$$\begin{aligned}M^{\mu\nu} &= (\eta^{\mu\nu}\eta^{\alpha\beta}-\eta^{\mu\alpha}\eta^{\nu\beta}+2(\hat{k}_F)^{\mu\alpha\nu\beta})p_\alpha p_\beta\\ &\quad -2i\epsilon^{\mu\nu\alpha\beta}(\hat{k}_{AF})_\alpha p_\beta\\ &= 2\hat{\chi}^{\mu\alpha\nu\beta}p_\alpha p_\beta+2i\hat{X}^{\mu\nu\alpha}p_\alpha,\end{aligned} \tag{23}$$

where it is understood that each occurrence of ∂_α in the operators $\hat{k}_{AF}$ and $\hat{k}_F$ is replaced with $-ip_\alpha$. The matrix $M^{\mu\nu}$ is Hermitian, $M^{\mu\nu}=(M^{\nu\mu})^*$. It satisfies the conditions for charge conservation, $M^{\mu\nu}p_\mu=0$, and gauge symmetry, $M^{\mu\nu}p_\nu=0$, which imply that the determinant of $M^{\mu\nu}$ vanishes identically.

The standard method to handle the gauge freedom and the vanishing determinant involves making a definite gauge choice, thereby reducing the four-dimensional problem to a three-dimensional one. The determinant of the reduced linear equation yields the dispersion relation. Within the particular gauge choice and for a given solution to the dispersion relation, one can then solve for the polarization mode A_μ of the photon. The general solution for this mode is the sum of this solution and an arbitrary pure-gauge term $\propto p_\mu$. Typically, the gauge fixing explicitly breaks observer Lorentz invariance. The alternative method presented below focuses on the rank-nullity of the linear equation (22), which allows us to preserve Lorentz covariance throughout the calculation. We take advantage of the exterior product and its ability to determine linear independence of a set of vectors. The reader is reminded that a set of vectors $\{A^a\}$, $a=1,2,\ldots$ is linearly independent if and only if their exterior product is nonzero [51].

Starting with a set of arbitrary basis vectors $\{A^1,A^2,A^3,A^4\}$ with $A^1\wedge A^2\wedge A^3\wedge A^4\neq 0$, the image space of M is spanned by the vectors $B^a=MA^a$. The dimensionality of this space is equal to the rank of M, and it determines the dimension of the solution space of Eq. (22). In particular, gauge freedom ensures that M is rank three or lower. This implies $B^1\wedge B^2\wedge B^3\wedge B^4=0$, which is equivalent to the condition $\det M^{\mu\nu}=0$. So to find nontrivial solutions, we must impose rank two or less, which implies $B^a\wedge B^b\wedge B^c=0$ for any $a,b,c=1,2,3,4$. This is the minimum requirement, and it leads to the covariant dispersion relation.

We can translate the above discussion into conditions on M by noting that M generates for each n a linear trans-

formation between n-vectors in its domain and image spaces. The transformation for a given n is denoted $\wedge^n M$ and is specified by

$$B^{a_1} \wedge \cdots \wedge B^{a_n} = (MA^{a_1}) \wedge \cdots \wedge (MA^{a_n}) \equiv (\wedge^n M)(A^{a_1} \wedge \cdots \wedge A^{a_n}). \quad (24)$$

For each n, the linear $\wedge^n M$ transformation takes an arbitrary n-vector ω of the domain space into an n-vector $(\wedge^n M)(\omega)$ of the image space. In a coordinate basis, we get an explicit expression for the cofactor tensors $(\wedge^n M)_{\mu_1\mu_2\ldots\mu_n}{}^{\nu_1\nu_2\ldots\nu_n}$ controlling the transformation $\wedge^n M$:

$$(\wedge^n M)_{\mu_1\mu_2\ldots\mu_n}{}^{\nu_1\nu_2\ldots\nu_n} = \frac{1}{n!} M_{[\mu_1}{}^{\nu_1} M_{\mu_2}{}^{\nu_2} \cdots M_{\mu_n]}{}^{\nu_n}. \quad (25)$$

The key point for our purposes is that the rank of M is completely determined by the set of $\wedge^n M$ transformations. For any given n, the matrix M is rank n if and only if $\wedge^n M \neq 0$ and $\wedge^{n+1} M = 0$. Note that $\wedge^n M = 0$ implies $\wedge^{n+1} M = 0$.

We can now determine the size of the null space of M and hence the nature of the solution space for the equations of motion by using the rank-nullity relation. Since M is a 4×4 matrix, the rank can in principle range from four down to zero. The five possibilities can be summarized as follows. The case of rank four has $\wedge^4 M \neq 0$ and is excluded by gauge invariance, so no solutions exist. For rank three, which has $\wedge^4 M = 0$ and $\wedge^3 M \neq 0$, the nullity is one and hence there is a one-dimensional solution space. In the present context, it corresponds to pure-gauge solutions. For rank two we have $\wedge^3 M = 0$ and $\wedge^2 M \neq 0$ with a two-dimensional null space. This case yields a one-dimensional non-gauge solution space. For rank one $\wedge^2 M = 0$, $\wedge^1 M \neq 0$, and the nullity is three, so there is a two-dimensional non-gauge solution space. Finally, for the case of rank 0 we have $\wedge^1 M = M = 0$, which is trivial.

The above discussion reveals that the covariant dispersion relation ensuring at least one physical solution is

$$\wedge^3 M = 0, \quad (26)$$

in which case M is rank 2 or less. In a coordinate basis, this dispersion relation takes the tensor form

$$\frac{1}{3!} M_{[\mu_1}{}^{\nu_1} M_{\mu_2}{}^{\nu_2} M_{\mu_3]}{}^{\nu_3} = 0. \quad (27)$$

Also, if it so happens that requiring $\wedge^3 M = 0$ also leads to $\wedge^2 M = 0$, then a two-dimensional physical solution space exists. We interpret this situation as follows. Suppose we fix the three-momenta p_j, and find a frequency p_0 that solves the dispersion relation (26). If at this frequency $\wedge^2 M \neq 0$ and hence M has rank two, then there is exactly one non-gauge polarization mode A_μ associated with this solution. Other frequencies p_0 that solve the dispersion relation (26) lead to different polarizations and different phase velocities. The solution A_μ is therefore birefringent. However, if for a given frequency solution we find $\wedge^2 M = 0$ and hence M of rank one, then there are two independent polarizations that propagate with the same phase velocity. This situation represents nonbirefringence. We therefore obtain the correspondence

$$\wedge^2 M = 0 \leftrightarrow \text{no birefringence}, \quad (28)$$

which provides the explicit condition for the existence of nonbirefringent modes. The next subsection explores the issue of birefringence in more detail.

The covariant tensor dispersion relation (26) can be rewritten as a covariant scalar dispersion relation by the judicious use of gauge symmetry. To see this, adopt the special domain basis $\{A^1, A^2, A^3, p\}$. Since gauge invariance implies $Mp = 0$, the only three-vectors ω that yield nonzero values of $(\wedge^3 M)(\omega)$ must be proportional to $A^1 \wedge A^2 \wedge A^3$. Consequently, the transformation $(\wedge^3 M)(\omega)$ is one dimensional, and therefore its dual $\widetilde{\wedge^3 M}$ must also be one dimensional. The Hermiticity of M implies that there is a vector V^μ in terms of which the dual transformation $\widetilde{\wedge^3 M}$ is determined as $(\widetilde{\wedge^3 M})^{\mu\nu} = V^{\mu *} V^\nu$. Direct calculation with this result shows that $(\widetilde{\wedge^3 M})^{\mu\nu} p_\nu = (\widetilde{\wedge^3 M})^\rho{}_\rho p^\mu$, and from these relations we find $p^\rho p_\rho (\widetilde{\wedge^3 M})^{\mu\nu} = (\widetilde{\wedge^3 M})^\rho{}_\rho p^\mu p^\nu$. Finally, this expression implies that the tensor dispersion relation (26) is satisfied for any nonzero p if and only if the trace of its dual vanishes. So we arrive at the covariant dispersion relation

$$(\widetilde{\wedge^3 M})^\rho{}_\rho = 0, \quad (29)$$

which is a scalar density.

In terms of the constitutive tensors (14), the covariant scalar dispersion relation (29) can be written as

$$\begin{aligned} 0 &= -\tfrac{1}{3}\hat{\chi}^{\mu\alpha\nu\beta}((\widetilde{\wedge^2 M_e})_{\mu\alpha\nu\beta} - 3(\widetilde{\wedge^2 M_o})_{\mu\alpha\nu\beta}) \\ &= -\tfrac{1}{3}\epsilon_{\mu_1\mu_2\mu_3\mu_4}\epsilon_{\nu_1\nu_2\nu_3\nu_4} p_{\rho_1} p_{\rho_2} p_{\rho_3} p_{\rho_4} \hat{\chi}^{\mu_1\mu_2\nu_1\rho_1} \hat{\chi}^{\nu_2\rho_2\rho_3\mu_3} \\ &\quad \times \hat{\chi}^{\rho_4\mu_4\nu_3\nu_4} + 8 p_\alpha p_\beta (\hat{k}_{AF})_\mu (\hat{k}_{AF})_\nu \hat{\chi}^{\alpha\mu\beta\nu}. \end{aligned} \quad (30)$$

In this expression, the dual of $\wedge^2 M$ is defined by

$$(\widetilde{\wedge^2 M})_{\mu\alpha\nu\beta} \equiv \tfrac{1}{4}\epsilon_{\mu\alpha\rho\gamma}\epsilon_{\nu\beta\sigma\delta} M^{\rho\sigma} M^{\gamma\delta}, \quad (31)$$

while M_e and M_o are, respectively, the CPT-even and CPT-odd parts of M.

The covariant scalar dispersion relation (30) is a necessary condition for the existence of nontrivial plane-wave solutions. The first term on the right-hand side of Eq. (30) is CPT even and matches the result found in Ref. [52] in the appropriate limit. The last term contains all CPT-violating contributions. Note that this covariant scalar dispersion relation is independent of the spacetime metric $\eta_{\mu\nu}$. Note also that the momentum dependence of

the constitutive tensor $\hat{\chi}^{\mu\nu\rho\sigma}$ and of $(\hat{k}_{AF})_\mu$ implies that the dispersion relation (30) is typically a polynomial of degree greater than four in the frequency p_0. As a result, more eigenfrequencies typically exist in the presence of Lorentz violation than for the corresponding situation in conventional electrodynamics, and so more modes can propagate. However, following a reasoning similar to that leading to the equations of motion (11), we expect the solutions of interest to be small perturbations of the limiting physical solutions in conventional electrodynamics. It follows that only the corresponding subset of the solutions to the dispersion relation (30) are relevant to low-energy physics, while the others represent high-frequency modes that may play a role as Planck-scale energies are approached.

D. Birefringence

Astrophysical searches for vacuum birefringence in photon propagation provide sensitivities to Lorentz violation that are many orders of magnitude beyond those attainable via other techniques. It is therefore valuable to classify coefficients for Lorentz violation according to their birefringence effects. The analysis in the previous subsection has already provided some insight via the condition (28) for the absence of birefringence. In this subsection, we provide a decomposition of coefficients for Lorentz violation that distinguishes birefringent and nonbirefringent cases. We also offer some remarks about generic conditions for birefringence and their connection to the metric and to electromagnetic duality.

1. Coefficients for birefringence

In the minimal SME, leading-order birefringence is known to be controlled by the $d = 3$ coefficients $(k_{AF})_\mu$ and by a subset of the $d = 4$ coefficients $(k_F)^{\kappa\lambda\mu\nu}$ [7,11]. In the present context with Lorentz-violating operators of any dimension, a similar pattern holds: leading-order birefringence is associated with all the odd-d coefficients $\hat{k}_{AF}$ and with some combinations of the even-d coefficients $\hat{k}_F$. One way to verify this is via the covariant scalar dispersion relation (30).

To identify the relevant even-d coefficients, it is useful to introduce the definitions

$$\begin{aligned}
\hat{\kappa}_{e+} &= \tfrac{1}{2}(\hat{\kappa}_{DE} + \hat{\kappa}_{HB}) - \tfrac{1}{6}\mathrm{Tr}(\hat{\kappa}_{DE} + \hat{\kappa}_{HB}),\\
\hat{\kappa}_{e-} &= \tfrac{1}{2}(\hat{\kappa}_{DE} - \hat{\kappa}_{HB}) - \tfrac{1}{6}\mathrm{Tr}(\hat{\kappa}_{DE} - \hat{\kappa}_{HB}),\\
\hat{\kappa}_{o+} &= \tfrac{1}{2}(\hat{\kappa}_{DB} + \hat{\kappa}_{HE}), \qquad \hat{\kappa}_{o-} = \tfrac{1}{2}(\hat{\kappa}_{DB} - \hat{\kappa}_{HE}),\\
\hat{\kappa}_{\mathrm{tr}+} &= \tfrac{1}{6}\mathrm{Tr}(\hat{\kappa}_{DE} + \hat{\kappa}_{HB}), \qquad \hat{\kappa}_{\mathrm{tr}-} = \tfrac{1}{6}\mathrm{Tr}(\hat{\kappa}_{DE} - \hat{\kappa}_{HB}),
\end{aligned} \tag{32}$$

which give an experimentally judicious decomposition of the coefficients for Lorentz violation appearing in Eq. (18). The first four of these are traceless 3×3 matrices, with $\hat{\kappa}_{e+}$, $\hat{\kappa}_{e-}$, $\hat{\kappa}_{o-}$ symmetric and $\hat{\kappa}_{o+}$ antisymmetric. The last two are SO(3) rotation scalar combinations. Note that $\hat{\kappa}_{\mathrm{tr}+}$ can be disregarded in the minimal SME because it represents a simple Lorentz-invariant scaling factor in that context, but nonrenormalizable terms of this type can violate Lorentz symmetry and so must be included in the present context.

Among the combinations (32), only the matrices $\hat{\kappa}_{e+}$ and $\hat{\kappa}_{o-}$ cause vacuum birefringence at leading order. This result can be understood in terms of a Weyl decomposition of the constitutive tensor $\hat{\chi}^{\mu\nu\rho\sigma}$ analogous to the Weyl decomposition of the Riemann tensor,

$$\begin{aligned}
\hat{\chi}^{\mu\nu\rho\sigma} = {}& \tfrac{1}{2}(\eta^{\mu\rho}\eta^{\nu\sigma} - \eta^{\nu\rho}\eta^{\mu\sigma}) + \tfrac{1}{2}(\eta^{\mu\rho}(\hat{c}_F)^{\nu\sigma}\\
& - \eta^{\nu\rho}(\hat{c}_F)^{\mu\sigma} + \eta^{\nu\sigma}(\hat{c}_F)^{\mu\rho}\\
& - \eta^{\mu\sigma}(\hat{c}_F)^{\nu\rho}) + \hat{C}^{\mu\nu\rho\sigma}.
\end{aligned} \tag{33}$$

In this equation, the tensor $\hat{C}^{\mu\nu\rho\sigma}$ corresponds to the Weyl component and is traceless, $\hat{C}^{\mu\nu\rho\sigma}\eta_{\nu\sigma} = 0$. The term corresponding to the Ricci component involves $(\hat{c}_F)^{\alpha\beta}$, which is defined as the symmetric combination

$$(\hat{c}_F)^{\alpha\beta} \equiv (\hat{k}_F)^{\alpha\mu\beta}{}_\mu - \tfrac{1}{6}(\hat{k}_F)^{\mu\nu}{}_{\mu\nu}\eta^{\alpha\beta}. \tag{34}$$

The relations between $(\hat{c}_F)^{\alpha\beta}$, $\hat{C}^{\mu\nu\rho\sigma}$ and the $\hat{\kappa}$ matrices are

$$\begin{aligned}
(\hat{c}_F)^{00} &= \tfrac{1}{2}(3\hat{\kappa}_{\mathrm{tr}-} + \hat{\kappa}_{\mathrm{tr}+}),\\
(\hat{c}_F)^{jk} &= -(\hat{\kappa}_{e-})^{jk} + \tfrac{1}{2}((\hat{\kappa}_{\mathrm{tr}-}) - (\hat{\kappa}_{\mathrm{tr}+}))\delta^{jk},\\
(\hat{c}_F)^{0j} &= -\tfrac{1}{2}(\hat{\kappa}_{o+})^{kl}\epsilon^{jkl}, \qquad \hat{C}^{0j0k} = -\tfrac{1}{2}(\hat{\kappa}_{e+})^{jk},\\
\hat{C}^{jklm} &= \tfrac{1}{2}(\hat{\kappa}_{e+})^{np}\epsilon^{jkn}\epsilon^{lmp}, \qquad \hat{C}^{0jkl} = \tfrac{1}{2}(\hat{\kappa}_{o-})^{jm}\epsilon^{klm}.
\end{aligned} \tag{35}$$

We see that the ten independent components of $\hat{c}_F$ are equivalent to the ten independent components of $\hat{\kappa}_{e-}$, $\hat{\kappa}_{o+}$, $\hat{\kappa}_{\mathrm{tr}+}$, and $\hat{\kappa}_{\mathrm{tr}-}$, while the ten independent components of $\hat{C}$ match those of $\hat{\kappa}_{e+}$ and $\hat{\kappa}_{o-}$.

The decomposition (33) reveals that the coefficients $\hat{c}_F$ play the role of a small distortion of the spacetime metric at leading order. In this respect, they are analogous to the $c^{\alpha\beta}$ coefficients in the matter sector of the SME, which motivates the notation. As further discussed below, a small metric distortion leaves unaffected the usual degeneracy between polarizations and so cannot cause birefringence at leading order. In contrast, the nonmetric Weyl piece of Eq. (33) breaks the degeneracy and causes birefringence. Note that the effects of c-type coefficients in the minimal SME are unobservable in experiments involving only one sector, since they can be removed by a judicious coordinate choice. However, in the present context where $\hat{c}_F$ depends on energy and momentum, dispersion effects may arise that are observable.

The above decomposition and results hold for the vacuum, where the Weyl decomposition is performed using the Minkowski metric. However, the effective metric $g_{\mu\nu}$ for electrodynamics in a macroscopic medium M is no

longer Minkowski, so the above decomposition must be modified. The Weyl part $\hat{C}^M$ is required to be traceless with respect to $g_{\mu\nu}$ instead, so the assignment of $\hat{\kappa}$ matrices to $\hat{C}^M$ and $\hat{c}_F^M$ differs. The attribution of birefringence effects to a coefficient can therefore be medium dependent. It also follows that an experiment in a suitable medium can achieve sensitivities to different coefficients compared to the same experiment performed *in vacuo*.

As an example, consider a uniform isotropic medium M with refractive index n and permeability μ. Performing a decomposition of the constitutive tensor reveals that the relations between $\hat{C}^M$, $\hat{c}_F^M$, and the $\hat{\kappa}$ matrices become

$$
\begin{aligned}
(\hat{c}_F^M)^{00} &= \frac{1}{2}\sqrt{\mu}(2-n^2)\hat{\kappa}_{\mathrm{tr}+} + \frac{1}{2}\sqrt{\mu}(2+n^2)\hat{\kappa}_{\mathrm{tr}-},\\
(\hat{c}_F^M)^{jk} &= -\frac{\sqrt{\mu}(n^2+1)}{2n^2}(\hat{\kappa}_{e-})^{jk} + \frac{\sqrt{\mu}(n^2-1)}{2n^2}(\hat{\kappa}_{e+})^{jk} + \frac{1}{2}\sqrt{\mu}((\hat{\kappa}_{\mathrm{tr}-}) - (\hat{\kappa}_{\mathrm{tr}+}))\delta^{jk},\\
(\hat{c}_F^M)^{0j} &= -\frac{1}{2}\sqrt{\mu}(\hat{\kappa}_{o+})^{kl}\epsilon^{jkl}, \qquad (\hat{C}^M)^{0j0k} = -\frac{1}{4}(n^2+1)(\hat{\kappa}_{e+})^{jk} + \frac{1}{4}(n^2-1)(\hat{\kappa}_{e-})^{jk},\\
(\hat{C}^M)^{jklm} &= \frac{(n^2+1)}{4n^2}(\hat{\kappa}_{e+})^{np}\epsilon^{jkn}\epsilon^{lmp} - \frac{(n^2-1)}{4n^2}(\hat{\kappa}_{e-})^{np}\epsilon^{jkn}\epsilon^{lmp}, \qquad (\hat{C}^M)^{0jkl} = \frac{1}{2}(\hat{\kappa}_{o-})^{jm}\epsilon^{klm}.
\end{aligned}
\tag{36}
$$

For this type of medium, we see that birefringence is associated with the matrix $\hat{\kappa}_{e-}$ as well as the matrices $\hat{\kappa}_{e+}$ and $\hat{\kappa}_{o-}$. Moreover, the matrix $\hat{\kappa}_{e+}$ can now affect nonbirefringent phenomena at leading order, unlike the vacuum case. Additional coefficient mixings can be expected in anisotropic and gyroscopic media.

2. Birefringence, metric, and duality

An interesting challenge is the identification of the minimal set of requirements leading to birefringence. For simple local constitutive relations, nonbirefringence is known to be associated with a pure-metric constitutive tensor [53,54], while electromagnetic duality plays a role [55]. The idea that the essential properties of electrodynamics rely on constitutive relations rather than the underlying metric structure of the spacetime is a key aspect of the premetric approach to electrodynamics [52,56]. In this subsection, we offer some remarks on the role of the metric and of electromagnetic duality in determining birefringence conditions within the context of the general constitutive relations (14).

Our primary conjecture is that the only nonbirefringent terms arise from the non-Weyl component of $\hat{\chi}^{\mu\nu\rho\sigma}$. We therefore seek a procedure for extracting this component. The structure of the Weyl decomposition (33) suggests the possibility of introducing an effective metric $\hat{g}_{\mu\nu}$ in terms of which the Ricci component vanishes. This would imply a natural decomposition of $\hat{\chi}^{\mu\nu\rho\sigma}$ into metric and nonmetric components or, equivalently, into nonbirefringent and birefringent components.

We therefore postulate the existence of an effective metric $\hat{g}_{\mu\nu}$ satisfying the eigenproblem

$$
\tfrac{2}{3}\hat{\chi}^{\mu\nu\rho\sigma}\hat{g}_{\nu\sigma} = (\hat{g}^{-1})^{\mu\rho}, \tag{37}
$$

where the scale factor for $\hat{g}_{\mu\nu}$ is chosen so that the proportionality constant in this equation matches the value for standard electrodynamics. Note that in the present context the effective metric $\hat{g}_{\mu\rho}$ typically depends on the four-momentum and therefore cannot be interpreted as a conventional spacetime metric. The existence and uniqueness of solutions to Eq. (37) is an interesting open issue, but here we suppose all physically reasonable constitutive operators $\hat{\chi}^{\mu\nu\rho\sigma}$ lead to a solution that is unique up to a sign. For practical purposes, this issue is moot because it suffices to use Eqs. (14) and (37) to find a perturbative expansion for $\hat{g}_{\mu\nu}$.

The effective metric $\hat{g}_{\mu\nu}$ provides a unique Weyl decomposition of the constitutive tensor $\hat{\chi}^{\mu\nu\rho\sigma}$, given by

$$
\hat{\chi} = \wedge^2\hat{g}^{-1} + \hat{\chi}_w, \tag{38}
$$

where $\hat{\chi}_w$ is the trace-free Weyl component, $(\hat{\chi}_w)^{\mu\nu\rho\sigma}\hat{g}_{\nu\sigma} = 0$. Our conjecture now identifies $\hat{\chi}_w$ as the birefringent component. We can verify this in special limits. For vanishing $\hat{\chi}_w$ and no CPT violation, the dispersion relation (30) reduces to

$$
-((\hat{g}^{-1})^{\mu\nu}p_\mu p_\nu)^2/\det\hat{g} = 0, \tag{39}
$$

as expected. Also, for this case we find that the cofactor tensor $\wedge^2 M$ is proportional to $(\hat{g}^{-1})^{\mu\nu}p_\mu p_\nu$, which demonstrates the absence of birefringence. Another limit of interest involves small Lorentz violation. Solving at leading order in $\hat{k}_F$, we find

$$
\hat{g}^{\mu\nu} \simeq \eta_{\mu\nu} - (\hat{c}_F)_{\mu\nu}, \qquad (\hat{\chi}_w)^{\alpha\beta\mu\nu} \simeq \hat{C}^{\alpha\beta\mu\nu}. \tag{40}
$$

This is also consistent, since it demonstrates that $\hat{C}$ corresponds to the leading-order birefringent component and $\hat{c}_F$ to the nonbirefringent part.

In conventional electrodynamics, electromagnetic duality ensures no birefringence occurs in the vacuum. Given the two-form field strength F and the dual two-form $H = *F$, the Maxwell equations *in vacuo* take the compact form $dH = 0$, $dF = 0$. Here the $*$ operator is defined as $*_{\mu\nu}{}^{\rho\sigma} = \frac{1}{2}\epsilon_{\mu\nu}{}^{\rho\sigma}$ and obeys $** = -I$. In this language,

electromagnetic duality can be understood as the statement that if F is a solution then so is $F' = \exp(\alpha *)F = F\cos\alpha + H\sin\alpha$. This can be viewed as a rotation between F and H. The chiral components $F_\pm = \frac{1}{2}(1 \pm i*)F$ of the field strength are irreducible representations of these duality rotations and also of the Lorentz group. The relevance to our discussion is that duality symmetry excludes birefringence because it implies the space of plane-wave solutions is two dimensional. There are two independent polarizations that mix under duality transformations, and the duality symmetry ensures that both polarizations propagate with the same phase velocity, so no evolution of polarization can occur.

This conventional duality can be generalized to the effective metric $\hat{g}_{\mu\nu}$ relevant in our context. For an arbitrary effective metric, we define

$$\hat{*} = \sqrt{-\det\hat{g}} * (\wedge^2 \hat{g}^{-1}), \tag{41}$$

which is normalized to satisfy $\hat{*}\hat{*} = -I$ as usual. This operator induces a chiral structure with respect to $\hat{g}_{\mu\nu}$. The projections of the field strength F onto the chiral subspaces are now

$$F_\pm = \tfrac{1}{2}(1 \pm i\hat{*})F. \tag{42}$$

Neglecting CPT-odd terms, the dual field strength

$$H \equiv *G = *\hat{\chi}F \tag{43}$$

can also be decomposed into chiral components,

$$H_\pm = *\hat{\chi}F_\pm = \tfrac{1}{2}(1 \pm i\hat{*})H. \tag{44}$$

According to our primary conjecture, the constitutive tensor χ provides a natural decomposition of the solution space. It is therefore plausible that the absence of birefringence is associated with a duality symmetry generated by $\hat{*}$, with any nonzero Weyl piece $\hat{\chi}_w$ or nonzero CPT violation breaking this symmetry and so causing birefringence. We can explore this idea for the case of constitutive relations of the metric type, $\hat{\chi} = \wedge^2\hat{g}^{-1}$. This form of the constitutive tensor yields the closure relation $*\hat{\chi} * \hat{\chi} = 1/\det\hat{g}$. Under these circumstances, if F represents a solution to the Maxwell equations $dF = dH = 0$, then it can be shown that $F \to *\hat{\chi}F$ is also a solution. This generalizes the result for conventional duality rotations to the $\hat{*}$-chiral subspaces. It follows that every polarization is associated with a second polarization that is also a solution and hence that birefringence is absent, as expected.

A rigorous derivation of the above results is an open problem of definite interest, although it lies beyond our present scope. Note that our arguments hold inside any simply connected source-free region. We anticipate that they can also be applied to more general scenarios with inhomogeneous constituent tensors and curved spacetimes, in which duality would be defined locally. It is also plausible that duality breaking could arise via boundary conditions. This could lead, for example, to a foundational understanding of degeneracy splitting in resonant cavities. Generalizations of the framework may also merit investigation. For instance, more complicated closure relations of the form $*\hat{\chi} * \hat{\chi} = a + b * \hat{\chi}$ for scalar a and b also result in duality symmetries, and they may be related to improved decompositions of the constitutive relations. One could also consider a duality at the potential level, involving mixing of two one-forms A and B obeying $F = dA$ and $H = dB$, which can be found for any vacuum solution. Such approaches may make it possible to incorporate CPT-violating effects in this picture.

E. Effects of Lorentz violation

It is of interest to categorize the types of effects produced by Lorentz violation in various physical situations. A number of schemes are possible. In this subsection, we offer some remarks about the categorization used in later sections, which is based on identifying Lorentz-violating effects in terms of birefringence, dispersion, and anisotropy.

In the previous subsections, we have defined birefringence as the existence of only one low-energy eigenmode for a particular solution to the covariant dispersion relation (30), and we have conjectured its connection to a breakdown of duality. This definition contains more than the notion of rotation of the polarization of light in the vacuum. The breaking of eigenmode degeneracy can cause effects in circumstances other than vacuum propagation, such as the splitting of resonant frequencies in cavities. In the remainder of this work, the term birefringence is used in the sense of eigenmode nondegeneracy. In vacuum propagation, this reduces to the usual notion of rotation of polarization and can be termed vacuum birefringence.

A similar dichotomy appears in the definition of dispersion. In what follows, we adopt the term dispersive to refer to Lorentz-violating operators in the Lagrange density that appear with other than two derivatives. Only operators with mass dimension $d = 4$ are nondispersive in this sense. In the momentum-space covariant dispersion relation, these operators contribute terms that are nonquadratic in the momentum. However, this definition implies more than merely a nonlinear relationship between the frequency p_0 and the momentum $\boldsymbol{p}$ for vacuum propagation. As shown explicitly in Sec. IV E, some operators involving nonquadratic derivative terms and hence labeled as dispersive according to our usage in fact produce no leading-order dispersion in vacuum propagation, although they can produce analogous effects in other situations such as cavity resonators. Throughout this work, we use the term dispersive to mean $d \neq 4$, and we reserve the term vacuum dispersion for modifications to the usual relation $p_0 = |\boldsymbol{p}|$ for vacuum propagation.

In any physical situation, the properties of electromagnetic waves are determined by the coefficients for Lorentz violation, the medium, and the boundary conditions. Some

useful intuition can be gained by considering the interplay between these and the resulting birefringent, dispersive, and anisotropic effects.

Consider first the presence of a macroscopic medium. We have seen in the previous subsection that a coefficient controls birefringence if it is associated with *CPT* violation or if it contributes to the Weyl piece of the constitutive tensor $\hat{\chi}^{\mu\nu\rho\sigma}$. The presence of a medium can affect the Weyl decomposition, as shown in Eq. (36), so the manifestation of Lorentz-violating birefringence depends on the medium. In contrast, a coefficient controls Lorentz-violating dispersion according to the derivative structure of the corresponding operator in the Lagrange density, which is unaffected by the medium. Similarly, Lorentz-violating anisotropic effects are determined by the rotation properties of the relevant operators, and so they too are independent of the medium.

The role of the boundary conditions is different. A given choice of boundary conditions determines which coefficients for Lorentz violation are measurable. This feature is similar to a property of conventional electrodynamics. A given solution, such as a vacuum plane wave or a cavity eigenmode, is determined by both the Maxwell equations and by the boundary conditions. Changing the boundary conditions reveals distinct sets of eigensolutions with different physical properties. One cannot, for instance, expand vacuum plane waves in terms of cavity eigenmodes. Similarly, in the presence of Lorentz violation, a specific choice of boundary conditions fixes certain eigenmodes as solutions. However, only a suitable subset of the coefficients for Lorentz violation affects a given set of eigenmodes. For example, far-field boundary conditions suitable for vacuum radiation yield solutions that depend on a much reduced subset of coefficients, as is explicitly identified in Sec. IV C.

Despite their role in determining the observability of coefficients for Lorentz violation, the boundary conditions have no impact on the associated physical effects. For example, the birefringence properties of a given operator are unaffected, essentially because the duality symmetry is a local property and therefore is independent of the boundary conditions. Dispersive properties are also unaffected because they are associated with position-space derivatives on the Lorentz-violating operators and therefore are basically a local feature in position space. The associated modification of the momentum-space relation between p_0 and $\boldsymbol{p}$ reflects an impact on the eigensolution space as described above, rather than a change in the underlying dispersive properties of the operators. Similarly, the anisotropy properties of Lorentz-violating operators are fixed by the Lagrange density and are independent of the boundary conditions.

This feature of the boundary conditions has the interesting implication that a comprehensive search for Lorentz violation requires multiple observational and experimental methods, since any one method typically applies one type of boundary condition and so cannot be expected to access the whole coefficient space. It also means there are multiple approaches for categorizing the coefficients. For example, one can split the coefficient space into a subset selected by boundary conditions appropriate for vacuum propagation and its complement. This turns out to be an apposite splitting for several reasons, and we develop it in some detail beginning in Sec. IV. However, one could in principle consider alternative splittings of the coefficient space using other boundary conditions, such as ones for resonant cavities.

III. SPHERICAL DECOMPOSITION

In the previous section, we have demonstrated that the effects on photon propagation of Lorentz-violating operators of arbitrary dimension are specified by the Lagrange density (8) and are determined by the coefficients for Lorentz violation $(k_{AF}^{(d)})_\kappa{}^{\alpha_1\ldots\alpha_{(d-3)}}$ and $(k_F^{(d)})^{\kappa\lambda\mu\nu\alpha_1\ldots\alpha_{(d-4)}}$. A classification of these coefficients that characterizes the key effects of the corresponding Lorentz-violating operators is both useful and convenient for more detailed investigations. The ideal scenario is to establish a minimal collection of independent coefficients associated with operators having physical properties of direct relevance to observation and experiment.

One natural classification scheme takes advantage of the role of spatial rotations to perform an SO(3) decomposition of the coefficients for Lorentz violation. This technique has been applied to obtain first measurements of certain coefficients relevant to vacuum photon propagation from astrophysical observations of active galaxies, gamma-ray bursts, and the cosmic microwave background [22,23]. The SO(3) decomposition uses spin-weighted spherical harmonics [57,58], which are angular-momentum eigenstates and so obey relatively simple transformation rules under rotations. The method has the advantage that spin-weighted spherical harmonics are commonly used in some areas of astrophysics [59] and are well understood. A summary of some properties of spin-weighted spherical harmonics is provided in the appendix, which also derives several mathematical relations used in what follows.

In this section, we discuss the decomposition of the coefficients $\hat{k}_{AF}$ and $\hat{k}_F$ into spin-weighted components. For the analysis, the coefficient $\hat{k}_{AF}$ is separated into the pseudoscalar $(\hat{k}_{AF})_0$ and the pseudovector $\hat{\boldsymbol{k}}_{\boldsymbol{AF}}$, while $\hat{k}_F$ is separated into the tensors $\hat{\kappa}_{DE}$ and $\hat{\kappa}_{HB}$ and the pseudotensor $\hat{\kappa}_{DB}$ defined in Eq. (18). Each of these five components is expanded in a helicity basis and decomposed into spin-weighted spherical harmonics. The symmetries of $\hat{k}_{AF}$ and $\hat{k}_F$ then permit extraction of a minimal collection of spherical coefficients for Lorentz violation.

The results in this section demonstrate that the minimal collection of spherical coefficients includes nine sets of

coefficients. For convenience, we summarize the notation here. Three sets are extracted from $\hat{k}_{AF}$ and are denoted $(k_{AF}^{(d)})_{njm}^{(0B)}$, $(k_{AF}^{(d)})_{njm}^{(1B)}$, and $(\overline{k}_{AF}^{(d)})_{njm}^{(1E)}$. Six sets emerge from $\hat{k}_F$, denoted $(c_F^{(d)})_{njm}^{(0E)}$, $(k_F^{(d)})_{njm}^{(0E)}$, $(\overline{k}_F^{(d)})_{njm}^{(1E)}$, $(\overline{k}_F^{(d)})_{njm}^{(2E)}$, $(k_F^{(d)})_{njm}^{(1B)}$, and $(\overline{k}_F^{(d)})_{njm}^{(2B)}$. The symbol c specifies coefficients associated with nonbirefringent operators, while k specifies birefringent ones. A negation diacritic ¬ denotes coefficients that have no leading-order effects on the vacuum propagation of light, a property derived in Sec. IV E. The subscripts n, j, and m determine the frequency or wavelength dependence, the total angular momentum, and the z-component of the angular momentum, respectively. The allowed ranges of these three indices and the counting of the coefficients are given in Tables I, III, IV, and V. The label d gives the mass dimension of the corresponding operator for Lorentz violation, while the numerals 0,1, or 2 preceding either E or B refer to the spin weight of the operator. The superscripts E and B refer to the parity of the operator, with parity $(-1)^j$ labeled as E and parity $(-1)^{j+1}$ as B. The phases are chosen so that each spherical coefficient $\mathcal{K}_{jm}$ for Lorentz violation obeys the complex-conjugation relation

$$(\mathcal{K}_{jm})^* = (-1)^m \mathcal{K}_{j(-m)}. \tag{45}$$

Note that this implies that the pair of complex coefficients $\mathcal{K}_{jm}$ and $\mathcal{K}_{j(-m)}$ are codependent but represent two real degrees of freedom.

A. General *CPT*-odd coefficients

We begin the decomposition of $(\hat{k}_{AF})_\kappa$ by performing an expansion of the pseudoscalar component $(\hat{k}_{AF})_0$ in spherical harmonics. The first step is to separate $(\hat{k}_{AF})_0$ into pieces with definite frequency and three-momentum dependence. Denoting the frequency by $\omega = p^0$ and the components of the three-momentum $\boldsymbol{p}$ by p^k, we obtain the expression

$$(\hat{k}_{AF})_0 = \sum_d \sum_{n=0}^{d-3} (-1)^{n+(d+1)/2} \binom{d-3}{n} \times (k_{AF}^{(d)})_0{}^{0\ldots0k_1\ldots k_n} \omega^{d-3-n} p^{k_1} \ldots p^{k_n}. \tag{46}$$

Writing the magnitude of the three-momentum as $p = |\boldsymbol{p}|$, we see that each term in the sum involves a factor of $\omega^{d-3-n} p^n$. The frequency and wavelength dependence of each term is therefore controlled by the new index n. The direction dependence introduced by the components of $\boldsymbol{p}$ is characterized through the expansion in spherical harmonics below.

To determine the relevant angular-momentum eigenvalues j for the spherical-harmonic expansion, we can break the coefficients for each n into a series of three-dimensional traceless symmetric tensors of rank $n, n-2, n-4, \ldots$. This implies the range of eigenvalues $l = n, n-2, n-4, \ldots$ for the orbital angular momentum. Since the spin of $(\hat{k}_{AF})_0$ is zero, the eigenvalue j must also span this range. An alternative and more elegant approach makes use of parity. For a given n, the orbital angular momentum is limited by n. Since the spin is zero, we must have $j \leq n$. Given that $(\hat{k}_{AF})^0$ is a pseudoscalar and $\boldsymbol{p}$ is a vector, each term in the expansion must have parity $(-1)^{n+1}$ with only B-type parity occurring. This imposes the relation $(-1)^{n+1} = (-1)^{j+1}$, which implies that $j - n$ is even. The conclusion is that $j = n, n-2, n-4, \ldots \geq 0$, as before.

The resulting expansion in spherical harmonics is given by

$$(\hat{k}_{AF})_0 = \sum_{dnjm} \omega^{d-3-n} p^n{}_0 Y_{jm}(\hat{\boldsymbol{p}}) (k_{AF}^{(d)})_{njm}^{(0B)}. \tag{47}$$

The spherical coefficients for Lorentz violation $(k_{AF}^{(d)})_{njm}^{(0B)}$ are nonzero for the n and j values listed in Table I. As an example, consider $d = 5$. In this case, there are two $j = 0$ singlets, $(k_{AF}^{(5)})_{000}^{(0B)}$ and $(k_{AF}^{(5)})_{200}^{(0B)}$. There is also one $j = 1$ triplet $(k_{AF}^{(5)})_{11m}^{(0B)}$, with $m = -1, 0, 1$. Finally, there is one $j = 2$ quintuplet $(k_{AF}^{(5)})_{22m}^{(0B)}$, with $m = -2, -1, 0, 1, 2$. The total number of coefficients is $1 + 1 + 3 + 5 = 10$.

Next, we perform a spherical-harmonic expansion of the radial component $(\hat{k}_{AF})_r = \hat{\boldsymbol{p}} \cdot \hat{\boldsymbol{k}}_{\boldsymbol{AF}} = \hat{\boldsymbol{e}}_r \cdot \hat{\boldsymbol{k}}_{\boldsymbol{AF}}$. This component is also a pseudoscalar, and the decomposition follows the same basic steps as above. However, the additional $\hat{\boldsymbol{p}}$ factor implies that the total angular momentum is now limited by $j \leq n + 1$. Also, the parity of each term is given by $(-1)^n = (-1)^{j+1}$, yielding the range of j as $j = n + 1, n - 1, n - 3, \ldots \geq 0$. We therefore obtain the expansion

$$(\hat{k}_{AF})_r = \sum_{dnjm} \omega^{d-3-n} p^n{}_0 Y_{jm}(\hat{\boldsymbol{p}}) (k_{AF}^{(d)})_{njm}^{(0B')}, \tag{48}$$

involving another set of spherical coefficients $(k_{AF}^{(d)})_{njm}^{(0B')}$. However, it turns out that the symmetries of the tensors $(k_{AF}^{(d)})_\kappa{}^{\alpha_1\ldots\alpha_{(d-3)}}$ imply that these new coefficients can all be expressed as combinations of the other spherical coefficients occurring in the expansion of $(\hat{k}_{AF})_\kappa$. Before demonstrating this, we first complete the expansion of $\hat{\boldsymbol{k}}_{\boldsymbol{AF}}$.

The remaining components of $\hat{\boldsymbol{k}}_{\boldsymbol{AF}}$ have spin weight ± 1, $(\hat{k}_{AF})_\pm = \hat{\boldsymbol{e}}_\pm \cdot \hat{\boldsymbol{k}}_{\boldsymbol{AF}}$. For these cases, we again find $j \leq n + 1$, but now coefficients with both E- and B-type parities occur. The parity is $(-1)^n$, which implies $j = n+1, n-1, \ldots \geq 1$ for the B-type components and $j = n, n-2, \ldots \geq 1$ for the E-type components. Since the spin weight is ± 1, the index j for the total angular momentum is limited from below by 1. The expansions of the components $(\hat{k}_{AF})_\pm$ in terms of spin-weighted spherical harmonics take the forms

$$(\hat{k}_{AF})_{\pm} = \sum_{dnjm} \omega^{d-3-n} p^n {}_{\pm 1}Y_{jm}(\hat{\boldsymbol{p}}) \frac{1}{\sqrt{2j(j+1)}} \times (\pm(k_{AF}^{(d)})_{njm}^{(1B)} + i(\overset{\neg}{k}_{AF}^{(d)})_{njm}^{(1E)}), \tag{49}$$

where we introduce a factor of $1/\sqrt{2j(j+1)}$ for later convenience. The spherical coefficients for Lorentz violation $(k_{AF}^{(d)})_{njm}^{(1B)}$ and $(\overset{\neg}{k}_{AF}^{(d)})_{njm}^{(1E)}$ represent the remaining two independent sets. Their ranges are summarized in Table I.

The symmetries of $(k_{AF}^{(d)})_{\kappa}{}^{\alpha_1\cdots\alpha_{(d-3)}}$ described in Sec. II B imply certain constraints on the four sets of coefficients $(k_{AF}^{(d)})_{njm}^{(0B)}$, $(k_{AF}^{(d)})_{njm}^{(0B')}$, $(k_{AF}^{(d)})_{njm}^{(1B)}$, and $(\overset{\neg}{k}_{AF}^{(d)})_{njm}^{(1E)}$. To determine these constraints, the symmetries must be formulated in the momentum-space helicity basis. Recall that the tensors $(k_{AF}^{(d)})_{\kappa}{}^{\alpha_1\cdots\alpha_{(d-3)}}$ are totally symmetric in the last $d-3$ indices and that any trace involving the first index vanishes. The total-symmetry condition is implicit in the above spherical-harmonic decompositions, but the trace condition provides a nontrivial constraint.

In momentum space, the trace condition can be written as the differential equation

$$\begin{aligned} 0 &= \frac{\partial}{\partial p_{\kappa}}(\hat{k}_{AF})_{\kappa} = \frac{\partial}{\partial \omega}(\hat{k}_{AF})_0 + \boldsymbol{\nabla}\cdot\hat{\boldsymbol{k}}_{\boldsymbol{AF}} \\ &= \frac{\partial}{\partial \omega}(\hat{k}_{AF})_0 + \nabla_r(\hat{k}_{AF})_r + \nabla_+(\hat{k}_{AF})_- + \nabla_-(\hat{k}_{AF})_+ \\ &= \frac{\partial}{\partial \omega}(\hat{k}_{AF})_0 + \left(\frac{\partial}{\partial p} + \frac{2}{p}\right)(\hat{k}_{AF})_r \\ &\quad + \frac{1}{p}(J_+(\hat{k}_{AF})_- - J_-(\hat{k}_{AF})_+), \end{aligned} \tag{50}$$

where we have used the identities (A37). The combination $J_+(\hat{k}_{AF})_- - J_-(\hat{k}_{AF})_+$ is a pseudoscalar that is generated by the B component of $\hat{\boldsymbol{k}}_{\boldsymbol{AF}}$ and that contains no E component. Consequently, Eq. (50) provides a symmetry constraint involving only the B-type coefficients $(k_{AF}^{(d)})_{njm}^{(0B)}$, $(k_{AF}^{(d)})_{njm}^{(0B')}$, and $(k_{AF}^{(d)})_{njm}^{(1B)}$. Inserting the spherical-harmonic expansions into Eq. (50) and making use of the identity (A35) yields an explicit relation involving these three coefficient sets. Careful consideration of the index ranges then reveals that $(k_{AF}^{(d)})_{njm}^{(0B')}$ may be written as

$$(k_{AF}^{(d)})_{njm}^{(0B')} = \frac{-1}{n+2}((k_{AF}^{(d)})_{njm}^{(1B)} + (d-2-n)(k_{AF}^{(d)})_{(n-1)jm}^{(0B)}). \tag{51}$$

We conclude that the auxiliary coefficients $(k_{AF}^{(d)})_{njm}^{(0B')}$ are completely determined as linear combinations of the independent coefficients $(k_{AF}^{(d)})_{njm}^{(0B)}$ and $(k_{AF}^{(d)})_{njm}^{(1B)}$.

The net yield of the helicity decomposition of $(\hat{k}_{AF})_{\kappa}$ is therefore three independent sets of spherical coefficients for Lorentz violation, which are the B-type coefficients $(k_{AF}^{(d)})_{njm}^{(0B)}$ and $(k_{AF}^{(d)})_{njm}^{(1B)}$, and the E-type coefficients $(\overset{\neg}{k}_{AF}^{(d)})_{njm}^{(1E)}$. These coefficients completely characterize the CPT-odd Lorentz-violating operators of arbitrary mass dimension associated with the quadratic action for electrodynamics. All the operators are birefringent. On each set of coefficients, the label d specifies the (odd) mass dimension of the operator. The three indices n, j, and m determine the frequency or wavelength dependence, the total angular momentum, and the z-component of the angular momentum, respectively. The allowed ranges of these three indices and the counting of the coefficients are given in Table I. The superscripts E and B refer to the operator parity, while the superscript numerals 0 or 1 preceding either E or B specify the spin weight of the operator. The total number of coefficients for given odd d is $\frac{1}{2}(d+1)\times(d-1)(d-2)$, matching the group-theoretic result from Sec. II.

B. General *CPT*-even coefficients

The spherical decomposition of the CPT-even Lorentz-violating operators $(\hat{k}_F)^{\kappa\lambda\mu\nu}$ follows a procedure similar to

TABLE I. Summary of the allowed ranges of indices n and j for the independent spherical coefficients associated with CPT-odd operators. The dimension d is odd with $d \geq 3$, while $n \leq d-3$. The index m satisfies the usual restrictions $-j \leq m \leq j$, so there are $2j+1$ coefficients for each j. For a given dimension d, the number of coefficients of each type is given in the last row. Adding these gives the expected total of $\frac{1}{2}(d+1)(d-1)(d-2)$.

	$(k_{AF}^{(d)})_{njm}^{(0B)}$	$(k_{AF}^{(d)})_{njm}^{(1B)}$	$(\overset{\neg}{k}_{AF}^{(d)})_{njm}^{(1E)}$
n	j	j	j
0	0	1	
1	1	2	1
2	0 2	1 3	2
3	1 3	2 4	1 3
4	0 2 4	1 3 5	2 4
⋮	⋮ ⋱	⋮ ⋱	⋮ ⋱
$d-3$	0 2 ⋯ $d-3$	1 3 ⋯ $d-2$	2 ⋯ $d-3$
total	$\frac{1}{6}d(d-1)(d-2)$	$\frac{1}{6}(d-1)(d^2+d-3)$	$\frac{1}{6}(d+1)(d-1)(d-3)$

that for the *CPT*-odd case discussed in the previous subsection. However, instead of working directly with $(\hat{k}_F)^{\kappa\lambda\mu\nu}$, it is more convenient to decompose the three matrices $\hat{\kappa}_{DE}$, $\hat{\kappa}_{HB}$, and $\hat{\kappa}_{DB}$ given in Eq. (18), which have equivalent content.

We begin by separating the three matrices $\hat{\kappa}_{DE}$, $\hat{\kappa}_{HB}$, $\hat{\kappa}_{DB}$ into their SO(3)-irreducible trace, symmetric traceless, and antisymmetric parts. These irreducible parts can be expressed in the helicity basis via $\kappa_{ab} = \hat{\boldsymbol{e}}_a \cdot \kappa \cdot \hat{\boldsymbol{e}}_b$, where $a, b = +, r, -$. Each component can then be expanded in the appropriate spin-weighted spherical harmonics, recalling that $\hat{\kappa}_{DE}$, $\hat{\kappa}_{HB}$ are tensors while $\hat{\kappa}_{DB}$ is a pseudotensor. At this stage, we find the results can be expressed as 13 equations involving sums over 12 sets of *E*-type and eight sets of *B*-type coefficients, for a total of 20 sets of codependent coefficients. The challenge is to use these equations and the symmetries of $(\hat{k}_F)^{\kappa\tau\mu\nu}$ to identify the independent sets of coefficients among the 20 codependent ones. The 13 equations are given explicitly below. In them, all sums are restricted to even dimensions $d \geq 4$. The maximum range of the indices spans $0 \leq n \leq d-4$ for n and $0 \leq j \leq n+2$, $-j \leq m \leq j$ for the eigenvalue indices of the angular momentum. Details of the allowed index ranges for each of the 20 sets of codependent coefficients are given in Table II.

For the matrix $\hat{\kappa}_{DE}$, six sets of coefficients are needed, and the result is

$$(\hat{\kappa}_{DE})_{rr} = \sum_{dnjm} \omega^{d-4-n} p^n{}_0 Y_{jm}(\hat{\boldsymbol{p}})((\kappa_{DE}^{(d)})_{njm}^{(0E)} + (\kappa_{DE}^{(d)})_{njm}^{(0E')}), \tag{52a}$$

$$(\hat{\kappa}_{DE})_{+-} = \sum_{dnjm} \omega^{d-4-n} p^n{}_0 Y_{jm}(\hat{\boldsymbol{p}})\left(-\frac{1}{2}(\kappa_{DE}^{(d)})_{njm}^{(0E)} + (\kappa_{DE}^{(d)})_{njm}^{(0E')}\right), \tag{52b}$$

$$(\hat{\kappa}_{DE})_{\pm r} = \sum_{dnjm} \omega^{d-4-n} p^n{}_{\pm 1} Y_{jm}(\hat{\boldsymbol{p}}) \frac{1}{\sqrt{2j(j+1)}}(\pm(\kappa_{DE}^{(d)})_{njm}^{(1E)} + i(\kappa_{DE}^{(d)})_{njm}^{(1B)}), \tag{52c}$$

$$(\hat{\kappa}_{DE})_{\pm\pm} = \sum_{dnjm} \omega^{d-4-n} p^n{}_{\pm 2} Y_{jm}(\hat{\boldsymbol{p}}) \sqrt{\frac{(j-2)!}{(j+2)!}}((\kappa_{DE}^{(d)})_{njm}^{(2E)} \pm i(\kappa_{DE}^{(d)})_{njm}^{(2B)}), \tag{52d}$$

In this decomposition, the coefficients $(\kappa_{DE}^{(d)})_{njm}^{(0E')}$ emerge from the trace component of $\hat{\kappa}_{DE}$.

Another six sets of coefficients are needed for the matrix $\hat{\kappa}_{HB}$. The corresponding equations are

TABLE II. Summary of the allowed ranges of indices n and j for the 20 sets of codependent spherical coefficients associated with general *CPT*-even operators. The dimension d is even with $d \geq 4$, while $n \leq d-4$. The index m satisfies the usual restrictions $-j \leq m \leq j$, so there are $2j+1$ coefficients for each j.

	$(\kappa_{DE}^{(d)})_{njm}^{(0E)}, (\kappa_{HB}^{(d)})_{njm}^{(0E)}, (\kappa_{DB}^{(d)})_{njm}^{(0B)}$	$(\kappa_{DE}^{(d)})_{njm}^{(1E)}, (\kappa_{HB}^{(d)})_{njm}^{(1E)}, (\kappa_{DB}^{(d)})_{njm}^{(1B)}$	$(\kappa_{DE}^{(d)})_{njm}^{(2E)}, (\kappa_{HB}^{(d)})_{njm}^{(2E)}, (\kappa_{DB}^{(d)})_{njm}^{(2B)}$	$(\kappa_{DE}^{(d)})_{njm}^{(0E')}, (\kappa_{HB}^{(d)})_{njm}^{(0E')}$
n	j	j	j	j
0	0 2	2	2	0
1	1 3	1 3	3	1
2	0 2 4	2 4	2 4	0 2
3	1 3 5	1 3 5	3 5	1 3
4	0 2 4 6	2 4 6	2 4 6	0 2 4
⋮	⋮ ⋱	⋮ ⋱	⋮ ⋱	⋮ ⋱
$d-4$	0 2 ⋯ $d-2$	2 4 ⋯ $d-2$	2 4 ⋯ $d-2$	0 2 ⋯ $d-4$

	$(\kappa_{DE}^{(d)})_{njm}^{(1B)}, (\kappa_{HB}^{(d)})_{njm}^{(1B)}, (\kappa_{DB}^{(d)})_{njm}^{(1E)}, (\kappa_{DB}^{(d)})_{njm}^{(1E')}$	$(\kappa_{DE}^{(d)})_{njm}^{(2B)}, (\kappa_{HB}^{(d)})_{njm}^{(2B)}, (\kappa_{DB}^{(d)})_{njm}^{(2E)}$	$(\kappa_{DB}^{(d)})_{njm}^{(0E')}$	$(\kappa_{DB}^{(d)})_{njm}^{(1B')}$
n	j	j	j	j
0	1		1	
1	2	2	0 2	1
2	1 3	3	1 3	2
3	2 4	2 4	0 2 4	1 3
4	1 3 5	3 5	1 3 5	2 4
⋮	⋮ ⋱	⋮ ⋱	⋮ ⋱	⋮ ⋱
$d-4$	1 3 ⋯ $d-3$	3 ⋯ $d-3$	1 3 ⋯ $d-3$	2 ⋯ $d-4$

$$(\hat{\kappa}_{HB})_{rr} = \sum_{dnjm} \omega^{d-4-n} p^n{}_0 Y_{jm}(\hat{\boldsymbol{p}})((\kappa_{HB}^{(d)})_{njm}^{(0E)} + (\kappa_{HB}^{(d)})_{njm}^{(0E')}), \tag{53a}$$

$$(\hat{\kappa}_{HB})_{+-} = \sum_{dnjm} \omega^{d-4-n} p^n{}_0 Y_{jm}(\hat{\boldsymbol{p}})\left(-\frac{1}{2}(\kappa_{HB}^{(d)})_{njm}^{(0E)} + (\kappa_{HB}^{(d)})_{njm}^{(0E')}\right), \tag{53b}$$

$$(\hat{\kappa}_{HB})_{\pm r} = \sum_{dnjm} \omega^{d-4-n} p^n{}_{\pm 1} Y_{jm}(\hat{\boldsymbol{p}}) \frac{1}{\sqrt{2j(j+1)}}(\pm(\kappa_{HB}^{(d)})_{njm}^{(1E)} + i(\kappa_{HB}^{(d)})_{njm}^{(1B)}), \tag{53c}$$

$$(\hat{\kappa}_{HB})_{\pm\pm} = \sum_{dnjm} \omega^{d-4-n} p^n{}_{\pm 2} Y_{jm}(\hat{\boldsymbol{p}}) \sqrt{\frac{(j-2)!}{(j+2)!}}((\kappa_{HB}^{(d)})_{njm}^{(2E)} \pm i(\kappa_{HB}^{(d)})_{njm}^{(2B)}). \tag{53d}$$

The coefficients $(\kappa_{HB}^{(d)})_{njm}^{(0E')}$ correspond to the trace component of $\hat{\kappa}_{HB}$.

Finally, eight sets of coefficients are required in the expansion of $\hat{\kappa}_{DB}$. The results are

$$(\hat{\kappa}_{DB})_{rr} = \sum_{dnjm} \omega^{d-4-n} p^n{}_0 Y_{jm}(\hat{\boldsymbol{p}})(\kappa_{DB}^{(d)})_{njm}^{(0B)}, \tag{54a}$$

$$(\hat{\kappa}_{DB})_{\pm\mp} = \sum_{dnjm} \omega^{d-4-n} p^n{}_0 Y_{jm}(\hat{\boldsymbol{p}})\left(-\frac{1}{2}(\kappa_{DB}^{(d)})_{njm}^{(0B)} \mp i(\kappa_{DB}^{(d)})_{njm}^{(0E')}\right), \tag{54b}$$

$$(\hat{\kappa}_{DB})_{r\pm} = \sum_{dnjm} \omega^{d-4-n} p^n{}_{\pm 1} Y_{jm}(\hat{\boldsymbol{p}}) \frac{1}{\sqrt{2j(j+1)}}(\pm(\kappa_{DB}^{(d)})_{njm}^{(1B)} + i(\kappa_{DB}^{(d)})_{njm}^{(1E)} \pm (\kappa_{DB}^{(d)})_{njm}^{(1B')} - i(\kappa_{DB}^{(d)})_{njm}^{(1E')}), \tag{54c}$$

$$(\hat{\kappa}_{DB})_{\pm r} = \sum_{dnjm} \omega^{d-4-n} p^n{}_{\pm 1} Y_{jm}(\hat{\boldsymbol{p}}) \frac{1}{\sqrt{2j(j+1)}}(\pm(\kappa_{DB}^{(d)})_{njm}^{(1B)} + i(\kappa_{DB}^{(d)})_{njm}^{(1E)} \mp (\kappa_{DB}^{(d)})_{njm}^{(1B')} + i(\kappa_{DB}^{(d)})_{njm}^{(1E')}), \tag{54d}$$

$$(\hat{\kappa}_{DB})_{\pm\pm} = \sum_{dnjm} \omega^{d-4-n} p^n{}_{\pm 2} Y_{jm}(\hat{\boldsymbol{p}}) \sqrt{\frac{(j-2)!}{(j+2)!}}((\kappa_{DB}^{(d)})_{njm}^{(2B)} \pm i(\kappa_{DB}^{(d)})_{njm}^{(2E)}), \tag{54e}$$

The sets of coefficients $(\kappa_{DB}^{(d)})_{njm}^{(1B')}$, $(\kappa_{DB}^{(d)})_{njm}^{(1E')}$, and $(\kappa_{DB}^{(d)})_{njm}^{(0E')}$ are associated with the antisymmetric part of $\hat{\kappa}_{DE}$, which corresponds to $\hat{\kappa}_{o+}$ in Eq. (32).

The next step is to use the symmetries of the tensors $(k_F^{(d)})^{\kappa\lambda\mu\nu\alpha_1\ldots\alpha_{(d-4)}}$ to determine the independent sets of coefficients. These symmetries are described in Sec. II, following Eq. (6). As in the *CPT*-odd case, the independent coefficients can be identified by expressing the symmetries as differential equations in momentum space. It turns out that all the symmetries of $k_F^{(d)}$ are implicit in the above 13 equations, except for the condition of vanishing antisymmetrization on any three indices of $(k_F^{(d)})^{\kappa\lambda\mu\nu\alpha_1\ldots\alpha_{(d-4)}}$. In momentum space, this symmetry can be imposed by requiring

$$0 = \partial^{[\rho}(\hat{k}_F)^{\mu\nu]\kappa\lambda}, \tag{55}$$

where $\partial^\kappa = \partial/\partial p_\kappa$. In terms of $\hat{\kappa}$ matrices, this requirement becomes the four conditions

$$\begin{aligned} &\nabla_b(\hat{\kappa}_{HB})^{ab} = 0, \qquad \nabla_b(\hat{\kappa}_{DB})^{ab} = 0, \\ &\frac{\partial}{\partial\omega}(\hat{\kappa}_{DB})^{ab} = \varepsilon^{bcd}\nabla_c(\hat{\kappa}_{DE})_d{}^a, \\ &\frac{\partial}{\partial\omega}(\hat{\kappa}_{HB})^{ab} = -\varepsilon^{bcd}\nabla_c(\hat{\kappa}_{DB})_d{}^a \end{aligned} \tag{56}$$

in the notation of the appendix. Note the similarity to the Maxwell equations.

The symmetry constraints (56) lead to relations among the 20 codependent coefficients in the expansions (52)–(54). The procedure for determining these relations involves expressing the differential equations (56) in terms of the operators $\partial/\partial\omega$, $\partial/\partial p$, and $J_\pm$, and then inserting the expansions. Following this procedure, we find that Eq. (56) provides nine constraints on the eight *B*-type coefficients and 11 constraints on the 12 *E*-type coefficients. However, these constraints are not all independent.

TABLE III. Summary of the allowed ranges of indices n and j for the independent *B*-type spherical coefficients associated with *CPT*-even birefringent operators. The dimension d is even with $d \geq 4$, while $n \leq d-4$. The index m satisfies the usual restrictions $-j \leq m \leq j$, so there are $2j+1$ coefficients for each j. For a given dimension d, the number of coefficients of each type is given in the last row.

	$(k_F^{(d)})_{njm}^{(1B)}$	$(\bar{k}_F^{(d)})_{njm}^{(2B)}$
n	j	j
0	2	
1	1 3	2
2	2 4	3
3	1 3 5	2 4
4	2 4 6	3 5
⋮	⋮ ⋱	⋮ ⋱
$d-4$	2 4 ⋯ $d-2$	3 ⋯ $d-3$
total	$\frac{1}{6}(d^3-4d-18)$	$\frac{1}{6}(d+3)(d-2)(d-4)$

Some calculation with the nine constraints on the B-type coefficients shows that there exist only two linearly independent sets of B-type coefficients for Lorentz violation, which we denote by $(k_F^{(d)})^{(1B)}_{njm}$ and $(\overset{\neg}{k}_F^{(d)})^{(2B)}_{njm}$. The index ranges for these two sets are summarized in Table III. All the corresponding Lorentz-violating operators produce birefringent effects. In terms of these two sets, the eight codependent B-type coefficients appearing in the expansions (52)–(54) are given by

$$(\kappa_{DE}^{(d)})^{(1B)}_{njm} = (d-3-n)n(k_F^{(d)})^{(1B)}_{(n-1)jm}, \tag{57a}$$

$$(\kappa_{DE}^{(d)})^{(2B)}_{njm} = -(d-3-n)(j+2)(j-1)(k_F^{(d)})^{(1B)}_{(n-1)jm} - (d-3-n)(d-2-n)(\overset{\neg}{k}_F^{(d)})^{(2B)}_{(n-2)jm}, \tag{57b}$$

$$(\kappa_{HB}^{(d)})^{(1B)}_{njm} = (n+2)(\overset{\neg}{k}_F^{(d)})^{(2B)}_{njm}, \tag{57c}$$

$$(\kappa_{HB}^{(d)})^{(2B)}_{njm} = -(n+2)(n+3)(\overset{\neg}{k}_F^{(d)})^{(2B)}_{njm}, \tag{57d}$$

$$(\kappa_{DB}^{(d)})^{(0B)}_{njm} = (n+1)(k_F^{(d)})^{(1B)}_{njm}, \tag{57e}$$

$$(\kappa_{DB}^{(d)})^{(1B)}_{njm} = -\tfrac{1}{2}(n(n+3)+j(j+1))(k_F^{(d)})^{(1B)}_{njm} - \tfrac{1}{2}(d-3-n)(\overset{\neg}{k}_F^{(d)})^{(2B)}_{(n-1)jm}, \tag{57f}$$

$$(\kappa_{DB}^{(d)})^{(1B')}_{njm} = -\tfrac{1}{2}((n+2)(n+3)-j(j+1))(k_F^{(d)})^{(1B)}_{njm} + \tfrac{1}{2}(d-3-n)(\overset{\neg}{k}_F^{(d)})^{(2B)}_{(n-1)jm}, \tag{57g}$$

$$(\kappa_{DB}^{(d)})^{(2B)}_{njm} = \tfrac{1}{2}(n+3)(j+2)(j-1)(k_F^{(d)})^{(1B)}_{njm} + (d-3-n)(n+2)(\overset{\neg}{k}_F^{(d)})^{(2B)}_{(n-1)jm}. \tag{57h}$$

The same procedure applied to the 11 constraints on the E-type coefficients reveals that there are four linearly independent sets of E-type coefficients for Lorentz violation. In this case, however, some components of the corresponding operators are birefringent while others are nonbirefringent. For ease of application in searches for Lorentz violation, it would be useful to have a decomposition that separates birefringent and nonbirefringent components. At leading order, this separation is achieved by the Weyl decomposition (33). Unfortunately, the representations from the Weyl decomposition are incompatible with the E-type coefficient representations contained in the symmetry constraints (55). Although the latter indeed include some operators that are purely birefringent and others that are purely nonbirefringent, there are typically also birefringent operators with coefficients that contribute to the nonbirefringent matrices $\hat{\kappa}_{e-}$, $\hat{\kappa}_{o+}$, $\hat{\kappa}_{\mathrm{tr}+}$, and $\hat{\kappa}_{\mathrm{tr}-}$. Among the four independent sets of E-type coefficients for Lorentz violation, there are thus ones that contribute to $(\hat{c}_F)^{\mu}$, ones that contribute to $\hat{C}^{\kappa\lambda\mu\nu}$, and ones that contribute to both. However, we do find that only a small fraction of the coefficients contribute solely to $\hat{C}^{\kappa\lambda\mu\nu}$. Consequently, it is reasonable to seek a decomposition separating the nonbirefringent terms appearing only in $(\hat{c}_F)^{\mu}$ from the birefringent terms contributing to $\hat{C}^{\kappa\lambda\mu\nu}$ and possibly also to $(\hat{c}_F)^{\mu\nu}$.

We first consider the nonbirefringent case. With zero leading-order birefringence, Lorentz violation associated with the quadratic action for electrodynamics is completely characterized by $(\hat{c}_F)^{\mu\nu}$ via

$$(\hat{k}_F)^{\mu\nu\rho\sigma} \to \tfrac{1}{2}(\eta^{\mu\rho}(\hat{c}_F)^{\nu\sigma} - \eta^{\nu\rho}(\hat{c}_F)^{\mu\sigma} + \eta^{\nu\rho}(\hat{c}_F)^{\mu\rho} - \eta^{\mu\sigma}(\hat{c}_F)^{\nu\rho}). \tag{58}$$

The symmetry constraints (55) applied to this expression yield the equation $0 = \partial^{[\rho}(\hat{c}_F)^{\mu]\nu}$ in the nonbirefringent case. The form of this constraint suggests solving via a scalar potential $\hat{\Phi}_F$, where

$$(\hat{c}_F)^{\mu\nu} \to \partial^{\mu}\partial^{\nu}\hat{\Phi}_F, \tag{59}$$

where the derivatives act in momentum space. This result holds in the nonbirefringent case but is false in general. Expanding the potential $\hat{\Phi}_F$ in spherical harmonics,

$$\hat{\Phi}_F = \sum_{dnjm} \omega^{d-2-n} p^n{}_0 Y_{jm}(\hat{\boldsymbol{p}})(c_F^{(d)})^{(0E)}_{njm}, \tag{60}$$

we arrive at the minimal set $(c_F^{(d)})^{(0E)}_{njm}$ of nonbirefringent spherical coefficients for Lorentz violation. This expansion

TABLE IV. Summary of the allowed ranges of indices n and j for the independent spherical coefficients associated with CPT-even nonbirefringent operators. The dimension d is even with $d \geq 4$, while $n \leq d-4$. The index m satisfies the usual restrictions $-j \leq m \leq j$, so there are $2j+1$ coefficients for each j. For a given dimension d, the number of coefficients is given in the last row.

	$(c_F^{(d)})^{(0E)}_{njm}$						
n	j						
0	0						
1		1					
2	0		2				
3		1		3			
4	0		2		4		
⋮	⋮					⋱	
$d-2$	0		2		4	$\cdots$	$d-2$
total	$\tfrac{1}{6}(d+1)d(d-1)$						

reveals that no B-type spherical coefficients appear in the absence of leading-order birefringence. The index ranges and component counting for the coefficients $(c_F^{(d)})^{(0E)}_{njm}$ are summarized in Table IV.

Using the expansion (60), the coefficients $(\hat{c}_F)^{\mu\nu}$ can be expressed in terms of the spherical coefficients $(c_F^{(d)})^{(0E)}_{njm}$. We can also find the contributions to the matrix components in the expansions (52)–(54) in the absence of birefringence. Some of these components vanish and others become equal, yielding

$$(\kappa_{DB}^{(d)})^{(1E)}_{njm} \to 0, \quad (\kappa_{DB}^{(d)})^{(2E)}_{njm} \to 0, \quad (\kappa_{DE}^{(d)})^{(0E)}_{njm} \leftrightarrow -(\kappa_{HB}^{(d)})^{(0E)}_{njm},$$
$$(\kappa_{DE}^{(d)})^{(1E)}_{njm} \leftrightarrow -(\kappa_{HB}^{(d)})^{(1E)}_{njm} \quad (\kappa_{DE}^{(d)})^{(2E)}_{njm} \leftrightarrow -(\kappa_{HB}^{(d)})^{(2E)}_{njm}. \quad (61)$$

These conditions lead to vanishing $\hat{\kappa}_{e+}$ and $\hat{\kappa}_{o-}$, as required by nonbirefringence. The nonzero contributions are given by

$$(\kappa_{DE}^{(d)})^{(0E')}_{njm} \supseteq \frac{-(n+2)(n+3)+j(j+1)}{3}(c_F^{(d)})^{(0E)}_{(n+2)jm} + (d-3-n)(d-2-n)(c_F^{(d)})^{(0E)}_{njm}, \quad (62a)$$
$$(\kappa_{DE}^{(d)})^{(0E)}_{njm} \supseteq \frac{-2n(n+2)-j(j+1)}{3}(c_F^{(d)})^{(0E)}_{(n+2)jm}, \quad (62b)$$
$$(\kappa_{DE}^{(d)})^{(1E)}_{njm} \supseteq (n+1)j(j+1)(c_F^{(d)})^{(0E)}_{(n+2)jm}, \quad (62c)$$
$$(\kappa_{DE}^{(d)})^{(2E)}_{njm} \supseteq \frac{-(j+2)(j+1)j(j-1)}{2}(c_F^{(d)})^{(0E)}_{(n+2)jm}, \quad (62d)$$
$$(\kappa_{HB}^{(d)})^{(0E')}_{njm} \supseteq \frac{-2(n+2)(n+3)+2j(j+1)}{3}(c_F^{(d)})^{(0E)}_{(n+2)jm}, \quad (62e)$$
$$(\kappa_{HB}^{(d)})^{(0E)}_{njm} \supseteq \frac{2n(n+2)+j(j+1)}{3}(c_F^{(d)})^{(0E)}_{(n+2)jm}, \quad (62f)$$
$$(\kappa_{HB}^{(d)})^{(1E)}_{njm} \supseteq -(n+1)j(j+1)(c_F^{(d)})^{(0E)}_{(n+2)jm}, \quad (62g)$$
$$(\kappa_{HB}^{(d)})^{(2E)}_{njm} \supseteq \frac{(j+2)(j+1)j(j-1)}{2}(c_F^{(d)})^{(0E)}_{(n+2)jm}, \quad (62h)$$
$$(\kappa_{DB}^{(d)})^{(0E')}_{njm} \supseteq (d-3-n)(n+1)(c_F^{(d)})^{(0E)}_{(n+1)jm}, \quad (62i)$$
$$(\kappa_{DB}^{(d)})^{(1E')}_{njm} \supseteq -(d-3-n)j(j+1)(c_F^{(d)})^{(0E)}_{(n+1)jm}. \quad (62j)$$

The above analysis completely characterizes the nonbirefringent Lorentz-violating operators associated with the quadratic action for electrodynamics.

In the presence of birefringence, three additional independent sets of E-type coefficients appear. We can therefore seek four mutually independent sets of spherical coefficients, with one given by $(c_F^{(d)})^{(0E)}_{njm}$ and the remaining three covering the birefringent portion of coefficient space. It turns out that the three new sets of coefficients for birefringence have spin weights zero, one, and two, and we denote them by $(k_F^{(d)})^{(0E)}_{njm}$, $(\overset{\neg}{k}_F^{(d)})^{(1E)}_{njm}$, and $(\overset{=}{k}_F^{(d)})^{(2E)}_{njm}$. The index ranges and component counting for these three sets are summarized in Table V.

Imposing the symmetry conditions (56), a lengthy calculation yields explicit expressions in terms of $(k_F^{(d)})^{(0E)}_{njm}$, $(\overset{\neg}{k}_F^{(d)})^{(1E)}_{njm}$, and $(\overset{=}{k}_F^{(d)})^{(2E)}_{njm}$ for the 12 sets of codependent E-type coefficients appearing in the expansions (52)–(54). We find contributions to the codependent coefficients arising from the trace components of $\hat{\kappa}_{DE}$ and $\hat{\kappa}_{HB}$ given by

$$(\kappa_{DE}^{(d)})^{(0E')}_{njm} \supseteq \frac{(n+2)(n+3)-j(j+1)}{3}(k_F^{(d)})^{(0E)}_{njm} + (d-3-n)(d-2-n)(k_F^{(d)})^{(0E)}_{(n-2)jm}$$
$$- \frac{2(d-3-n)((n+1)(n+2)+(j+2)(j-1))}{3}(\overset{\neg}{k}_F^{(d)})^{(1E)}_{(n-1)jm} - \frac{2(d-3-n)(d-2-n)}{3}(\overset{=}{k}_F^{(d)})^{(2E)}_{(n-2)jm}, \quad (63a)$$
$$(\kappa_{HB}^{(d)})^{(0E')}_{njm} \supseteq \frac{-2((n+2)(n+3)-j(j+1))}{3}(k_F^{(d)})^{(0E)}_{njm}. \quad (63b)$$

The contributions to the remaining codependent coefficients in $\hat{\kappa}_{DE}$ are

$$(\kappa_{DE}^{(d)})_{njm}^{(0E)} \supseteq \frac{2n(n+2)+j(j+1)}{3}(k_F^{(d)})_{njm}^{(0E)} + \frac{2(d-3-n)(4(n+1)(n+2)+(j+2)(j-1))}{3}(\overline{k}_F^{(d)})_{(n-1)jm}^{(1E)} + \frac{2(d-3-n)(d-2-n)}{3}(\overline{k}_F^{(d)})_{(n-2)jm}^{(2E)}, \tag{64a}$$

$$(\kappa_{DE}^{(d)})_{njm}^{(1E)} \supseteq -(n+1)j(j+1)(k_F^{(d)})_{njm}^{(0E)} - 2(d-3-n)((n+1)(n+2)+(j+2)(j-1))(n+1)(\overline{k}_F^{(d)})_{(n-1)jm}^{(1E)} - 2(d-3-n)(d-2-n)(n+1)(\overline{k}_F^{(d)})_{(n-2)jm}^{(2E)}, \tag{64b}$$

$$(\kappa_{DE}^{(d)})_{njm}^{(2E)} \supseteq \frac{(j+2)(j+1)j(j-1)}{2}(k_F^{(d)})_{njm}^{(0E)} + (d-3-n)(j+2)(j-1)(2(n+2)^2+(j+2)(j-1))(\overline{k}_F^{(d)})_{(n-1)jm}^{(1E)} + (d-3-n)(d-2-n)(2(n+2)^2+(j+2)(j-1))(\overline{k}_F^{(d)})_{(n-2)jm}^{(2E)}, \tag{64c}$$

while the contributions to the remaining codependent coefficients in $\hat{\kappa}_{HB}$ are

$$(\kappa_{HB}^{(d)})_{njm}^{(0E)} \supseteq \frac{2n(n+2)+j(j+1)}{3}(k_F^{(d)})_{njm}^{(0E)} + 2(n+3)(n+4)(\overline{k}_F^{(d)})_{njm}^{(2E)}, \tag{65a}$$

$$(\kappa_{HB}^{(d)})_{njm}^{(1E)} \supseteq -(n+1)j(j+1)(k_F^{(d)})_{njm}^{(0E)} - 2(n+3)^2(n+4)(\overline{k}_F^{(d)})_{njm}^{(2E)}, \tag{65b}$$

$$(\kappa_{HB}^{(d)})_{njm}^{(2E)} \supseteq \frac{(j+2)(j+1)j(j-1)}{2}(k_F^{(d)})_{njm}^{(0E)} + (2(n+3)^2-j(j+1))(n+3)(n+4)(\overline{k}_F^{(d)})_{njm}^{(2E)}. \tag{65c}$$

Finally, the contributions to $\hat{\kappa}_{DB}$ are

$$(\kappa_{DB}^{(d)})_{njm}^{(0E')} \supseteq (d-3-n)(n+1)(k_F^{(d)})_{(n-1)jm}^{(0E)} - (n+2)(n+3)(n+4)(\overline{k}_F^{(d)})_{njm}^{(1E)}, \tag{66a}$$

$$(\kappa_{DB}^{(d)})_{njm}^{(1E')} \supseteq -(d-3-n)j(j+1)(k_F^{(d)})_{(n-1)jm}^{(0E)} + (n+2)^2(n+3)(n+4)(\overline{k}_F^{(d)})_{njm}^{(1E)}, \tag{66b}$$

$$(\kappa_{DB}^{(d)})_{njm}^{(1E)} \supseteq -n(n+2)(n+3)(n+4)(\overline{k}_F^{(d)})_{njm}^{(1E)} - 2(d-3-n)(n+2)(n+3)(\overline{k}_F^{(d)})_{(n-1)jm}^{(2E)}, \tag{66c}$$

$$(\kappa_{DB}^{(d)})_{njm}^{(2E)} \supseteq (j+2)(j-1)(n+2)(n+3)(n+4)(\overline{k}_F^{(d)})_{njm}^{(1E)} + 2(d-3-n)(n+2)(n+3)^2(\overline{k}_F^{(d)})_{(n-1)jm}^{(2E)}. \tag{66d}$$

The above 12 equations completely characterize the birefringent *CPT*-even Lorentz-violating operators associated with the quadratic action for electrodynamics.

To summarize this subsection, we find that the coefficients controlling the *CPT*-even Lorentz-violating operators separate into one set of nonbirefringent *E*-type spherical coefficients, three sets of birefringent *E*-type spherical coefficients, and two sets of birefringent *B*-type spherical coefficients. The component counting for each of these sets can be found in Tables III, IV, and V. Adding the totals from each table, we find a net total of $(d+1)d(d-3)$ independent spherical coefficients at each even dimension

TABLE V. Summary of the allowed ranges of indices n and j for the independent *E*-type spherical coefficients associated with *CPT*-even birefringent operators. The dimension d is even with $d \geq 4$, while $n \leq d-4$. The index m satisfies the usual restrictions $-j \leq m \leq j$, so there are $2j+1$ coefficients for each j. For a given dimension d, the number of coefficients of each type is given in the last row.

	$(k_F^{(d)})_{njm}^{(0E)}$	$(\overline{k}_F^{(d)})_{njm}^{(1E)}$	$(\overline{k}_F^{(d)})_{njm}^{(2E)}$
n	j	j	j
0	2		
1	1 3	2	
2	0 2 4	1 3	2
3	1 3 5	2 4	3
4	0 2 4 6	1 3 5	2 4
⋮	⋮ ⋱	⋮ ⋱	⋮ ⋱
$d-4$	0 2 ⋯ $d-2$	1 3 ⋯ $d-3$	2 4 ⋯ $d-4$
total	$\frac{1}{6}(d^3-d-30)$	$\frac{1}{6}(d-4)(d^2+d+3)$	$\frac{1}{6}(d-4)(d^2-2d-9)$

d. As expected, this matches the group-theoretic result obtained in Sec. II. Some properties of all these coefficients are summarized in Table XVII of Sec. VIII.

IV. SPECIAL MODELS

For a given observational or experimental procedure, particular sensitivity may be achieved to specific combinations of spherical coefficients. Also, the nine basic sets of spherical coefficients contain a large number of independent components, which suggests that some types of analyses may be challenging to perform in the general context. It is therefore useful to identify special models that are limiting cases and are relevant to specific measurements.

In this section, we first present several convenient limiting cases. Five basic types of model are considered. One is the minimal SME, which restricts attention to renormalizable terms. Another is the isotropic limit, in which rotational invariance is preserved in a preferred frame. A third is the vacuum model, which encompasses the subset of effects detectable in searches using dispersion or birefringence from astrophysical sources. The fourth is the nonbirefringent nondispersive model, for which the Lorentz-violating photon propagation exhibits several parallels to the conventional case. The fifth is the vacuum-orthogonal model, which is the complement of the vacuum model and contains coefficients that can be detected only in laboratory experiments. In a final subsection, we identify particular subsets of the spherical SME coefficients that correspond to some special cases appearing in the literature.

A. Minimal SME

The first limiting case we consider is the pure-photon sector of the minimal SME, obtained by restricting attention to Lorentz-violating operators of renormalizable dimension $d \leq 4$. Numerous measurements of the corresponding coefficients have been performed to date [6], with most analyses using Cartesian components rather than spherical ones. Discussions of the minimal SME can be found in the literature [7,11], so we restrict the focus of this subsection to establishing the relationship between Cartesian and spherical coefficients. Working in a fixed inertial frame with Cartesian coordinates (t, x, y, z), we determine the linear combinations of spherical coefficients that correspond to the Cartesian coefficients.

For the Lorentz-violating operators with $d = 3$, which are CPT odd, there are four Cartesian components of $(k_{AF}^{(3)})^{\kappa}$. They are linear combinations of the four spherical coefficients $(k_{AF}^{(3)})_{000}^{(0B)}$ and $(k_{AF}^{(3)})_{01m}^{(1B)}$, where $m = 0, \pm 1$. In terms of a 4×4 matrix S, we can write the relationship generically as

$$\mathcal{K}_{\text{Cartesian}} = \frac{1}{\sqrt{4\pi}} S \cdot \mathcal{K}_{\text{spherical}}, \tag{67}$$

TABLE VI. Matrix elements relating Cartesian to spherical coefficients in the CPT-odd part of the photon sector in the minimal SME. Note that an overall factor of $\sqrt{1/4\pi}$ is omitted.

	$(k_{AF}^{(3)})_{000}^{(0B)}$ $-k_{(V)00}^{(3)}$	$(k_{AF}^{(3)})_{011}^{(1B)}$ $2k_{(V)11}^{(3)}$	$(k_{AF}^{(3)})_{010}^{(1B)}$ $2k_{(V)10}^{(3)}$	$(k_{AF}^{(3)})_{01(-1)}^{(1B)}$ $2k_{(V)1(-1)}^{(3)}$
$(k_{AF}^{(3)})^t$	1	0	0	0
$(k_{AF}^{(3)})^x$	0	$\sqrt{\frac{3}{8}}$	0	$-\sqrt{\frac{3}{8}}$
$(k_{AF}^{(3)})^y$	0	$i\sqrt{\frac{3}{8}}$	0	$i\sqrt{\frac{3}{8}}$
$(k_{AF}^{(3)})^z$	0	0	$-\sqrt{\frac{3}{4}}$	0

where $\mathcal{K}_{\text{Cartesian}}$ and $\mathcal{K}_{\text{spherical}}$ are four-dimensional column matrices containing the Cartesian and spherical components, respectively. Table VI gives the elements of the matrix S. This table also displays the correspondence between the four spherical coefficients $(k_{AF}^{(3)})_{000}^{(0B)}$, $(k_{AF}^{(3)})_{01m}^{(1B)}$ and the four vacuum coefficients $k_{(V)jm}^{(3)}$, which are defined in Eq. (84d) below in the context of the vacuum model discussed in Sec. IV C.

As an example from Table VI, consider the Cartesian coefficient $(\hat{k}_{AF})^x$. In terms of spherical coefficients, the table gives

$$\begin{aligned}(\hat{k}_{AF})^x &= \frac{1}{\sqrt{4\pi}}\left(\sqrt{\frac{3}{8}}(k_{AF}^{(3)})_{011}^{(1B)} - \sqrt{\frac{3}{8}}(k_{AF}^{(3)})_{01(-1)}^{(1B)}\right) \\ &= \frac{1}{\sqrt{4\pi}}\left(\sqrt{\frac{3}{2}}k_{(V)11}^{(3)} - \sqrt{\frac{3}{2}}k_{(V)1(-1)}^{(3)}\right).\end{aligned} \tag{68}$$

Note that the spherical coefficients are complex in general, but the property $(k_{AF}^{(3)})_{011}^{(0B)} = -[(k_{AF}^{(3)})_{01(-1)}^{(0B)}]^*$ contained in the phase condition (45) ensures a total of four real degrees of freedom. Indeed, the components $(\hat{k}_{AF})^x$ and $(\hat{k}_{AF})^y$ correspond, respectively, to the real and imaginary parts of the spherical coefficient $(k_{AF}^{(3)})_{011}^{(0B)}$.

For the renormalizable CPT-even Lorentz-violating operators, all of which have $d = 4$, the operator $\hat{k}_F$ contains 20 real independent constants. From Tables III, IV, and V, we see that these include two scalar singlets $(c_F^{(4)})_{000}^{(0E)}$ and $(c_F^{(4)})_{200}^{(0E)}$, one triplet $(c_F^{(4)})_{11m}^{(0E)}$, and three quintuplets $(c_F^{(4)})_{22m}^{(0E)}$, $(k_F^{(4)})_{22m}^{(0E)}$, $(k_F^{(4)})_{22m}^{(1B)}$. In terms of the $\hat{\kappa}$ matrices of Eq. (18), the two singlets can be viewed as corresponding to the two trace components, while the triplet corresponds to the antisymmetric part of $\hat{\kappa}_{DB}$. The three quintuplets match to the traceless parts of $\hat{\kappa}_{DE}$ and $\hat{\kappa}_{HB}$ and the symmetric part of $\hat{\kappa}_{DB}$.

We can again write the relationship between Cartesian and spherical coefficients using the generic form (67). The elements of the matrix S connecting the parity-even coefficients $\hat{\kappa}_{DE}$ and $\hat{\kappa}_{HB}$ and the spherical coefficients are given in Table VII. The elements of S for the parity-odd coefficients $\hat{\kappa}_{DB}$ are given in Table VIII. These tables also relate the 20 spherical coefficients with $d = 4$ to the rele-

TABLE VII. Matrix elements relating Cartesian to spherical coefficients in the *CPT*-even and parity-even part of the photon sector in the minimal SME. We have assumed $(c_F^{(4)})^{(0E)}_{000} = 3(c_F^{(4)})^{(0E)}_{200}$. Note that an overall factor of $\sqrt{1/4\pi}$ is omitted.

	$(c_F^{(4)})^{(0E)}_{200}$	$(c_F^{(4)})^{(0E)}_{222}$	$(c_F^{(4)})^{(0E)}_{221}$	$(c_F^{(4)})^{(0E)}_{220}$	$(c_F^{(4)})^{(0E)}_{22-1}$	$(c_F^{(4)})^{(0E)}_{22-2}$	$(k_F^{(4)})^{(0E)}_{022}$	$(k_F^{(4)})^{(0E)}_{021}$	$(k_F^{(4)})^{(0E)}_{020}$	$(k_F^{(4)})^{(0E)}_{02-1}$	$(k_F^{(4)})^{(0E)}_{02-2}$
	$\frac{1}{4}c^{(4)}_{(I)00}$	$c^{(4)}_{(I)22}$	$c^{(4)}_{(I)21}$	$c^{(4)}_{(I)20}$	$c^{(4)}_{(I)2-1}$	$c^{(4)}_{(I)2-2}$	$\frac{-k^{(4)}_{(E)22}}{\sqrt{6}}$	$\frac{-k^{(4)}_{(E)21}}{\sqrt{6}}$	$\frac{-k^{(4)}_{(E)20}}{\sqrt{6}}$	$\frac{-k^{(4)}_{(E)2-1}}{\sqrt{6}}$	$\frac{-k^{(4)}_{(E)2-2}}{\sqrt{6}}$
$(\kappa^{(4)}_{DE})^{xx}$	4	$-\sqrt{\frac{15}{2}}$	0	$\sqrt{5}$	0	$-\sqrt{\frac{15}{2}}$	$\sqrt{\frac{15}{2}}$	0	$-\sqrt{5}$	0	$\sqrt{\frac{15}{2}}$
$(\kappa^{(4)}_{DE})^{xy}$	0	$-i\sqrt{\frac{15}{2}}$	0	0	0	$i\sqrt{\frac{15}{2}}$	$i\sqrt{\frac{15}{2}}$	0	0	0	$-i\sqrt{\frac{15}{2}}$
$(\kappa^{(4)}_{DE})^{xz}$	0	0	$\sqrt{\frac{15}{2}}$	0	$-\sqrt{\frac{15}{2}}$	0	0	$-\sqrt{\frac{15}{2}}$	0	$\sqrt{\frac{15}{2}}$	0
$(\kappa^{(4)}_{DE})^{yy}$	4	$\sqrt{\frac{15}{2}}$	0	$\sqrt{5}$	0	$\sqrt{\frac{15}{2}}$	$-\sqrt{\frac{15}{2}}$	0	$-\sqrt{5}$	0	$-\sqrt{\frac{15}{2}}$
$(\kappa^{(4)}_{DE})^{yz}$	0	0	$i\sqrt{\frac{15}{2}}$	0	$i\sqrt{\frac{15}{2}}$	0	0	$-i\sqrt{\frac{15}{2}}$	0	$-i\sqrt{\frac{15}{2}}$	0
$(\kappa^{(4)}_{DE})^{zz}$	4	0	0	$-2\sqrt{5}$	0	0	0	0	$2\sqrt{5}$	0	0
$(\kappa^{(4)}_{HB})^{xx}$	-4	$\sqrt{\frac{15}{2}}$	0	$-\sqrt{5}$	0	$\sqrt{\frac{15}{2}}$	$\sqrt{\frac{15}{2}}$	0	$-\sqrt{5}$	0	$\sqrt{\frac{15}{2}}$
$(\kappa^{(4)}_{HB})^{xy}$	0	$i\sqrt{\frac{15}{2}}$	0	0	0	$-i\sqrt{\frac{15}{2}}$	$i\sqrt{\frac{15}{2}}$	0	0	0	$-i\sqrt{\frac{15}{2}}$
$(\kappa^{(4)}_{HB})^{xz}$	0	0	$-\sqrt{\frac{15}{2}}$	0	$\sqrt{\frac{15}{2}}$	0	0	$-\sqrt{\frac{15}{2}}$	0	$\sqrt{\frac{15}{2}}$	0
$(\kappa^{(4)}_{HB})^{yy}$	-4	$-\sqrt{\frac{15}{2}}$	0	$-\sqrt{5}$	0	$-\sqrt{\frac{15}{2}}$	$-\sqrt{\frac{15}{2}}$	0	$-\sqrt{5}$	0	$-\sqrt{\frac{15}{2}}$
$(\kappa^{(4)}_{HB})^{yz}$	0	0	$-i\sqrt{\frac{15}{2}}$	0	$-i\sqrt{\frac{15}{2}}$	0	0	$-i\sqrt{\frac{15}{2}}$	0	$-i\sqrt{\frac{15}{2}}$	0
$(\kappa^{(4)}_{HB})^{zz}$	-4	0	0	$2\sqrt{5}$	0	0	0	0	$2\sqrt{5}$	0	0

vant 20 vacuum coefficients $c^{(4)}_{(I)jm}$, $k^{(4)}_{(E)jm}$, $k^{(4)}_{(B)jm}$, which are defined in Eqs. (84a)–(84c) in the context of the vacuum model presented in Sec. IV C.

In the photon sector of the minimal SME, the nonbirefringent operators are controlled by the ten spherical coefficients $(c_F^{(4)})^{(0E)}_{njm}$, as shown in Sec. III B. Nine combinations of these have been measured in laboratory-based experiments. The remaining coefficient combination,

$$\hat{\kappa}_{\mathrm{tr}+} = \frac{1}{\sqrt{4\pi}}[(c_F^{(4)})^{(0E)}_{000} - 3(c_F^{(4)})^{(0E)}_{200}], \tag{69}$$

is Lorentz invariant and leads to a rescaling of the electric and magnetic fields. This combination is therefore typically taken to vanish, which implies the condition

$$(c_F^{(4)})^{(0E)}_{000} = 3(c_F^{(4)})^{(0E)}_{200}. \tag{70}$$

This property has been assumed in constructing the entries for Table VII.

Using the matrix elements in Tables VI, VII, and VIII, it is comparatively straightforward to convert between Cartesian and spherical representations of the photon-sector coefficients in the minimal SME. Note, however, that the spherical coefficients represent angular-momentum eigenstates and therefore have simpler rota-

TABLE VIII. Matrix elements relating Cartesian to spherical coefficients in the *CPT*-even and parity-odd part of the photon sector in the minimal SME. Note that an overall factor of $\sqrt{1/4\pi}$ is omitted.

	$(c_F^{(4)})^{(0E)}_{111}$	$(c_F^{(4)})^{(0E)}_{110}$	$(c_F^{(4)})^{(0E)}_{11-1}$	$(k_F^{(4)})^{(1B)}_{222}$	$(k_F^{(4)})^{(1B)}_{221}$	$(k_F^{(4)})^{(1B)}_{220}$	$(k_F^{(4)})^{(1B)}_{22-1}$	$(k_F^{(4)})^{(1B)}_{22-2}$
	$-2c^{(4)}_{(I)11}$	$-2c^{(4)}_{(I)10}$	$-2c^{(4)}_{(I)1-1}$	$-\sqrt{\frac{2}{3}}k^{(4)}_{(B)22}$	$-\sqrt{\frac{2}{3}}k^{(4)}_{(B)21}$	$-\sqrt{\frac{2}{3}}k^{(4)}_{(B)20}$	$-\sqrt{\frac{2}{3}}k^{(4)}_{(B)2-1}$	$-\sqrt{\frac{2}{3}}k^{(4)}_{(B)2-2}$
$(\kappa^{(4)}_{DB})^{xx}$	0	0	0	$\sqrt{\frac{15}{8}}$	0	$-\frac{\sqrt{5}}{2}$	0	$\sqrt{\frac{15}{8}}$
$(\kappa^{(4)}_{DB})^{xy}$	0	$\sqrt{3}$	0	$i\sqrt{\frac{15}{8}}$	0	0	0	$-i\sqrt{\frac{15}{8}}$
$(\kappa^{(4)}_{DB})^{xz}$	$i\sqrt{\frac{3}{2}}$	0	$i\sqrt{\frac{3}{2}}$	0	$-\sqrt{\frac{15}{8}}$	0	$\sqrt{\frac{15}{8}}$	0
$(\kappa^{(4)}_{DB})^{yx}$	0	$-\sqrt{3}$	0	$i\sqrt{\frac{15}{8}}$	0	0	0	$-i\sqrt{\frac{15}{8}}$
$(\kappa^{(4)}_{DB})^{yy}$	0	0	0	$-\sqrt{\frac{15}{8}}$	0	$-\frac{\sqrt{5}}{2}$	0	$-\sqrt{\frac{15}{8}}$
$(\kappa^{(4)}_{DB})^{yz}$	$-\sqrt{\frac{3}{2}}$	0	$\sqrt{\frac{3}{2}}$	0	$-i\sqrt{\frac{15}{8}}$	0	$-i\sqrt{\frac{15}{8}}$	0
$(\kappa^{(4)}_{DB})^{zx}$	$-i\sqrt{\frac{3}{2}}$	0	$-i\sqrt{\frac{3}{2}}$	0	$-\sqrt{\frac{15}{8}}$	0	$\sqrt{\frac{15}{8}}$	0
$(\kappa^{(4)}_{DB})^{zy}$	$\sqrt{\frac{3}{2}}$	0	$-\sqrt{\frac{3}{2}}$	0	$-i\sqrt{\frac{15}{8}}$	0	$-i\sqrt{\frac{15}{8}}$	0

tional properties. The behavior of the spherical coefficients under rotations is discussed in Sec. V.

B. Isotropic models

In any given inertial frame, a small subset of Lorentz-violating operators preserve rotational invariance. Restricting attention to these operators defines an interesting limiting case of the general theory. In these models, sometimes called ''fried-chicken'' models due to their popularity and simplicity, the isotropic inertial frame must be specified because observer boosts to other frames destroy the rotational invariance. One natural choice for the preferred frame is the frame of the CMB, but other choices are possible. Note, however, that isotropy in the CMB frame implies anisotropy in a Sun-centered frame and in laboratory experiments.

Within our analysis, imposing rotational invariance is immediate. The general isotropic model is obtained by imposing the condition that all spherical coefficients vanish in the preferred frame, except those with $j = 0$. This condition drastically reduces the number of available coefficients. The only nonzero coefficients are

$$(\mathring{c}_F^{(d)})_n = (c_F^{(d)})_{n00}^{(0E)}, \qquad (\mathring{k}_F^{(d)})_n = (k_F^{(d)})_{n00}^{(0E)}, \qquad (\mathring{k}_{AF}^{(d)})_n = (k_{AF}^{(d)})_{n00}^{(0B)}. \tag{71}$$

Following standard convention [38], these isotropic coefficients are identified by a ring diacritic. Note that the coefficient $(\mathring{c}_F^{(d)})_n$ controls isotropic nonbirefringent Lorentz-violating operators in the preferred frame, while the others control leading-order birefringent effects.

In the general isotropic model, the nonzero components of $\hat{k}_{AF}$ are

$$(\hat{k}_{AF})_0 = \sum_{dn} \frac{\omega^{d-3-n} p^n}{\sqrt{4\pi}} (\mathring{k}_{AF}^{(d)})_n, \tag{72a}$$

$$(\hat{k}_{AF})_r = -\sum_{dn} \frac{\omega^{d-3-n} p^n}{\sqrt{4\pi}} \frac{(d-2-n)}{n+2} (\mathring{k}_{AF}^{(d)})_{(n-1)}. \tag{72b}$$

For the $\hat{\kappa}$ matrices, we find the expressions

$$(\hat{\kappa}_{DE})_{rr} = \sum_{dn} \frac{\omega^{d-4-n} p^n}{\sqrt{4\pi}} [-(n+1)(n+2)((\mathring{c}_F^{(d)})_{(n+2)} - (\mathring{k}_F^{(d)})_n) + (d-3-n)(d-2-n)((\mathring{c}_F^{(d)})_n + (\mathring{k}_F^{(d)})_{(n-2)})], \tag{73a}$$

$$(\hat{\kappa}_{DE})_{+-} = \sum_{dn} \frac{\omega^{d-4-n} p^n}{\sqrt{4\pi}} [(-1)(n+2)((\mathring{c}_F^{(d)})_{(n+2)} - (\mathring{k}_F^{(d)})_n) + (d-3-n)(d-2-n)((\mathring{c}_F^{(d)})_n + (\mathring{k}_F^{(d)})_{(n-2)})], \tag{73b}$$

$$(\hat{\kappa}_{HB})_{rr} = \sum_{dn} \frac{\omega^{d-4-n} p^n}{\sqrt{4\pi}} (-2)(n+2)((\mathring{c}_F^{(d)})_{(n+2)} + (\mathring{k}_F^{(d)})_n), \tag{73c}$$

$$(\hat{\kappa}_{HB})_{+-} = \sum_{dn} \frac{\omega^{d-4-n} p^n}{\sqrt{4\pi}} (-1)(n+2)^2((\mathring{c}_F^{(d)})_{(n+2)} + (\mathring{k}_F^{(d)})_n), \tag{73d}$$

$$(\hat{\kappa}_{DB})_{\pm\mp} = \sum_{dn} \frac{\omega^{d-4-n} p^n}{\sqrt{4\pi}} (\mp i)(d-3-n)(n+1)((\mathring{c}_F^{(d)})_{(n+1)} + (\mathring{k}_F^{(d)})_{(n-1)}). \tag{73e}$$

The index ranges and component counting for the isotropic coefficients can be determined from the $j = 0$ columns of Tables I, III, IV, and V. For a given even dimension d, there are $d/2$ coefficients $(\mathring{c}_F^{(d)})_n$ and $(d-4)/2$ coefficients $(\mathring{k}_F^{(d)})_n$, for a total of $(d-2)$ independent components. For odd d, there are $(d-1)/2$ coefficients $(\mathring{k}_{AF}^{(d)})_n$. A summary of the properties of these coefficients is provided as part of Table XVIII in Sec. VIII.

C. Vacuum models

For observations of light from distant sources, far-field solutions apply. The electromagnetic fields are well approximated by vacuum plane waves with $\omega = p$. Although Lorentz-violating operators typically generate a nontrivial dispersion relation with $\omega \neq p$, we can impose $\omega = p$ in the operators $\hat{k}_F$ and $\hat{k}_{AF}$ to obtain leading-order results. The resulting vacuum coefficients for Lorentz violation comprise the set of linear combinations of spherical coefficients relevant for photon propagation in the vacuum. They are of direct interest for studies of light from astrophysical sources, and they can also be important in Earth-based tests.

Imposing $\omega = p$ in the expansions (9) and (10) for $\hat{k}_{AF}$ and $\hat{k}_F$ dramatically simplifies the spherical-harmonic structure. It turns out that the relevant combinations of coefficients are those associated with the Stokes parameters of the eigenmodes for vacuum photon propagation, because these eigenmodes characterize the effects of Lorentz violation on the overall photon polarization [11]. To find the eigenmodes, we first need plane-wave solutions of the modified Maxwell equations (11).

At leading order, the covariant dispersion relation Eq. (30) becomes

$$(p^\mu p_\mu - (\hat{c}_F)^{\mu\nu} p_\mu p_\nu)^2 - 2(\hat{\chi}_w)^{\alpha\beta\gamma\delta} \times (\hat{\chi}_w)_{\alpha\mu\gamma\nu} p_\beta p_\delta p^\mu p^\nu - 4(p^\mu (\hat{k}_{AF})_\mu)^2 \simeq 0. \tag{74}$$

The two solutions at leading order can be written as

$$p^0 \simeq (1 - \mathfrak{s}^0 \pm \sqrt{(\mathfrak{s}^1)^2 + (\mathfrak{s}^2)^2 + (\mathfrak{s}^3)^2})p, \tag{75}$$

where the three rotationally invariant dimensionless combinations

$$\begin{aligned} \mathfrak{s}^0 &= \tfrac{1}{2}(\hat{c}_F)^{\mu\nu} p_\mu p_\nu/\omega^2, \\ (\mathfrak{s}^1)^2 + (\mathfrak{s}^2)^2 &= \tfrac{1}{2}(\hat{\chi}_w)^{\alpha\beta\gamma\delta}(\hat{\chi}_w)_{\alpha\mu\gamma\nu} p_\beta p_\delta p^\mu p^\nu/\omega^4, \\ \mathfrak{s}^3 &= -p^\mu(\hat{k}_{AF})_\mu/\omega^2 \end{aligned} \tag{76}$$

contain coefficients for nonbirefringent *CPT*-even, birefringent *CPT*-even, and birefringent *CPT*-odd effects, respectively. The three combinations $\mathfrak{s}^1$, $\mathfrak{s}^2$, $\mathfrak{s}^3$ turn out to determine the Stokes parameters of the two eigenmodes. The momentum structure of Eq. (76) reveals that the vacuum coefficients for odd d are simply obtained as the totally symmetric and traceless part of $(k_{AF}^{(d)})^{\kappa\alpha_1\cdots\alpha_{(d-3)}}$. For even d, a similar result holds for the vacuum coefficients $(\hat{c}_F)^{\mu\nu}$ controlling nonbirefringent effects.

The procedure for finding the Stokes parameters $(s^1, s^2, s^3) = (Q, U, V)$ associated with the two solutions in Eq. (75) follows the same basic steps as in Ref. [11]. Using the plane-wave equation (22), we find a solution with unique polarization for each of the signs in Eq. (75). It is advantageous to work in the temporal gauge, for which $A_0 = 0$ and $\boldsymbol{E} \propto \boldsymbol{A}$. We can then construct the specific Stokes parameters for each eigenmode. Adopting the orthonormal spherical coordinate system described in Appendix A 2, we define a general Stokes vector $\boldsymbol{s}$ and its corresponding three Stokes parameters by

$$\boldsymbol{s} = \begin{pmatrix} s^1 \\ s^2 \\ s^3 \end{pmatrix} = \begin{pmatrix} |E^\theta|^2 - |E^\phi|^2 \\ 2\,\mathrm{Re}\, E^{\theta *} E^\phi \\ 2\,\mathrm{Im}\, E^{\theta *} E^\phi \end{pmatrix}. \tag{77}$$

This Stokes vector completely characterizes the polarization of an electromagnetic wave. It is also useful to define a fourth Stokes parameter:

$$s^0 = |E^\theta|^2 + |E^\phi|^2, \tag{78}$$

which corresponds to the intensity I.

Due to their orthogonality, the specific Stokes vectors for the two plane-wave solutions differ by a sign. It therefore suffices to construct a single specific Stokes vector $\boldsymbol{\mathfrak{s}}$, which can be associated with the faster of the two birefringent modes. In spherical coordinates, this vector is given by

$$\boldsymbol{\mathfrak{s}} = \begin{pmatrix} \mathfrak{s}^1 \\ \mathfrak{s}^2 \\ \mathfrak{s}^3 \end{pmatrix} \simeq \begin{pmatrix} -\tfrac{1}{2}((\hat{\kappa}_{e+})^{\theta\theta} - (\hat{\kappa}_{e+})^{\phi\phi}) - (\hat{\kappa}_{o-})^{\theta\phi} \\ -(\hat{\kappa}_{e+})^{\theta\phi} + \tfrac{1}{2}((\hat{\kappa}_{o-})^{\theta\theta} - (\hat{\kappa}_{o-})^{\phi\phi}) \\ -((\hat{k}_{AF})^0 - (\hat{k}_{AF})^r)/\omega \end{pmatrix}, \tag{79}$$

where we have adopted a convenient normalization. At leading order, the components of $\boldsymbol{\mathfrak{s}}$ are consistent with the combinations (76). In spherical coordinates, the fourth combination is

$$\begin{aligned} \mathfrak{s}^0 &\simeq -\tfrac{1}{2}(\hat{\kappa}_{e-})^{rr} + (\hat{\kappa}_{\mathrm{tr}-}) + (\hat{\kappa}_{o+})^{\theta\phi} \\ &= \tfrac{1}{2}(\hat{\kappa}_{DE} - \hat{\kappa}_{HB} + i\hat{\kappa}_{DB} + i\hat{\kappa}_{HE})_{+-} \end{aligned} \tag{80}$$

at leading order. This combination is analogous to the scalar Stokes parameter s^0.

The combinations $\mathfrak{s}^0$ and $\mathfrak{s}^3$ are invariant under rotations about the direction $\hat{\boldsymbol{p}}$ of the photon three-momentum, like the general Stokes parameters. They therefore have zero spin weight. The remaining combinations $\mathfrak{s}^1$ and $\mathfrak{s}^2$ transform under rotations as a rank-2 traceless tensor in the tangent space of the sphere and so are combinations of components with spin weight ± 2. As a result, the expansion in spin-weighted spherical harmonics of the Stokes parameters for Lorentz-violating photon propagation takes the form [22,23]

$$\begin{aligned} \mathfrak{s}^0 &= \sum_{djm} \omega^{d-4}(-1)^j {}_0Y_{jm}(\hat{\boldsymbol{p}}) c_{(I)jm}^{(d)}, \\ \mathfrak{s}^1 \pm i\mathfrak{s}^2 &= \sum_{djm} \omega^{d-4}(-1)^j {}_{\pm 2}Y_{jm}(\hat{\boldsymbol{p}})(k_{(E)jm}^{(d)} \mp i k_{(B)jm}^{(d)}), \\ \mathfrak{s}^3 &= \sum_{djm} \omega^{d-4}(-1)^j {}_0Y_{jm}(\hat{\boldsymbol{p}}) k_{(V)jm}^{(d)}. \end{aligned} \tag{81}$$

This result is independent of the index n because at leading order we can take $\omega = p$ in Eq. (76). We remark that the notation $c_{(I)jm}^{(d)}$ adopted here for one of the sets of vacuum coefficients differs from that of Ref. [23], where the quantity

$$k_{(I)jm}^{(d)} \equiv c_{(I)jm}^{(d)} \tag{82}$$

is used instead. The improved present notation $c_{(I)jm}^{(d)}$ reflects the absence of birefringence from the corresponding Lorentz-violating operators. Also, the factors of $(-1)^j$ in Eq. (81) have been introduced for convenience and to match the definitions in Ref. [23]. The point is that vacuum models are well suited for studies involving radiation from astrophysical sources, for which the source direction $\hat{\boldsymbol{n}}$ is normally specified rather than the propagation direction $\hat{\boldsymbol{p}} = -\hat{\boldsymbol{n}}$. For these studies, it is therefore more natural to work with spin weight defined with respect to $\hat{\boldsymbol{n}}$ instead of $\hat{\boldsymbol{p}}$. The correspondence

$$(-1)^j {}_sY_{jm}(\hat{\boldsymbol{p}}) = {}_{-s}Y_{jm}(\hat{\boldsymbol{n}}), \tag{83}$$

which follows from Eq. (A7), can be used to transform between the two pictures.

The net result of the above discussion is that the vacuum behavior is controlled by four sets of vacuum coefficients $c_{(I)jm}^{(d)}$, $k_{(E)jm}^{(d)}$, $k_{(B)jm}^{(d)}$, and $k_{(V)jm}^{(d)}$. These are related to the general coefficients for Lorentz violation by taking the limit $\omega = p$ in the various expansions provided in Sec. III. Via this limit, we find the results

$$c^{(d)}_{(I)jm} = \sum_n \frac{1}{2}(-1)^j\left(-\frac{1}{2}(\kappa^{(d)}_{DE})^{(0E)}_{njm} + \frac{1}{2}(\kappa^{(d)}_{HB})^{(0E)}_{njm} + (\kappa^{(d)}_{DE})^{(0E')}_{njm} - (\kappa^{(d)}_{HB})^{(0E')}_{njm} + 2(\kappa^{(d)}_{DB})^{(0E')}_{njm}\right), \tag{84a}$$

$$k^{(d)}_{(E)jm} = \sum_n \frac{1}{2}(-1)^{j+1}\sqrt{\frac{(j-2)!}{(j+2)!}}((\kappa^{(d)}_{DE})^{(2E)}_{njm} + (\kappa^{(d)}_{HB})^{(2E)}_{njm} + 2(\kappa^{(d)}_{DB})^{(2E)}_{njm}), \tag{84b}$$

$$k^{(d)}_{(B)jm} = \sum_n \frac{1}{2}(-1)^{j}\sqrt{\frac{(j-2)!}{(j+2)!}}((\kappa^{(d)}_{DE})^{(2B)}_{njm} + (\kappa^{(d)}_{HB})^{(2B)}_{njm} - 2(\kappa^{(d)}_{DB})^{(2B)}_{njm}), \tag{84c}$$

$$k^{(d)}_{(V)jm} = \sum_n (-1)^{j+1}\left(\frac{d}{n+3}(k^{(d)}_{AF})^{(0B)}_{njm} + \frac{1}{n+2}(k^{(d)}_{AF})^{(1B)}_{njm}\right). \tag{84d}$$

As expected, no frequency or wavelength dependence appears in these expressions. These equations reveal that the vacuum coefficients are linear combinations of the general coefficients involving identical d, j, m indices but different n values.

The index ranges for the vacuum coefficients $c^{(d)}_{(I)jm}$, $k^{(d)}_{(E)jm}$, $k^{(d)}_{(B)jm}$, and $k^{(d)}_{(V)jm}$ can be found using general symmetry arguments or the relations (84). For even d, there are $(d-1)^2$ coefficients $c^{(d)}_{(I)jm}$, $(d-1)^2-4$ coefficients $k^{(d)}_{(E)jm}$, and $(d-1)^2-4$ coefficients $k^{(d)}_{(B)jm}$, giving a total of $3(d-1)^2-8$ independent components associated with CPT-even Lorentz violation in vacuum propagation. For odd d, the coefficients $k^{(d)}_{(V)jm}$ for CPT-odd Lorentz violation have $(d-1)^2$ independent components. Some properties of these coefficients are summarized as part of Table XVIII in Sec. VIII.

The phenomenological effects controlled by each set of vacuum coefficients are different. The coefficients $k^{(d)}_{(E)jm}$ and $k^{(d)}_{(B)jm}$ are associated with CPT-even operators that lead to birefringence, with the propagating modes being linearly polarized. The coefficients $k^{(d)}_{(V)jm}$ control CPT-odd birefringence, and the corresponding eigenmodes are circularly polarized. In contrast, the CPT-even operators associated with the coefficients $c^{(d)}_{(I)jm}$ are nonbirefringent. These physical differences suggest it may be of value to introduce special vacuum models as particular limiting cases. For example, a nonbirefringent vacuum model involving only nonzero coefficients $c^{(d)}_{(I)jm}$ can be countenanced. This model has Lorentz-violating operators only in even dimensions $d = 4, 6, 8, \ldots$, with the number of independent coefficients being $9, 25, 49\ldots$, respectively. Another model of interest can be obtained as a hybrid of the general vacuum model and the isotropic limit, by introducing a preferred frame in which attention is restricted only to $j = 0$ coefficients. This vacuum isotropic model involves only the coefficients $c^{(d)}_{(I)00}$ and $k^{(d)}_{(V)00}$. It therefore contains exactly one Lorentz-violating operator for each value of d.

D. Camouflage models

The vacuum models considered in the previous subsection are well suited for astrophysical observations. In this and the following subsections, we consider instead the subset of spherical coefficients that are challenging to detect via studies of astrophysical birefringence or dispersion but that produce observable effects in laboratory experiments. We begin here by focusing on Lorentz-violating models without leading-order birefringent or vacuum-dispersive effects, which we call camouflage models. The next subsection generalizes this treatment to identify explicitly all vacuum-orthogonal coefficients, including ones that control nonvacuum birefringence. The key idea motivating these constructions is that studies of astrophysical birefringence yield among the best sensitivities to Lorentz violation in any sector, due to the accumulation of polarization changes that occur over the cosmological propagation times. This also applies to studies of astrophysical dispersion, albeit typically at lesser sensitivity. As a result, searches for Lorentz violation can naturally be split into ones sensitive to operators generating vacuum birefringence or vacuum dispersion and ones with sensitivity to other operators.

We begin by restricting attention to operators without leading-order birefringence, which are associated with the spherical coefficients $(c^{(d)}_F)^{(0E)}_{njm}$. Some key results for this case are discussed in Sec. III B above. Following Eq. (58), the Lagrange density reduces to

$$\mathcal{L} = -\tfrac{1}{4}F_{\mu\nu}F^{\mu\nu} - \tfrac{1}{2}F_{\mu\rho}(\hat{c}_F)^{\mu\nu}F_{\nu}{}^{\rho}. \tag{85}$$

Note that CPT invariance holds because $\hat{k}_{AF} = 0$, and that only even-dimensional operators with E-type parity contribute.

Using Eqs. (52) and (62), we can write the $\hat{\kappa}$ matrices in terms of the coefficients $(c^{(d)}_F)^{(0E)}_{njm}$ by taking the equality in (62). However, it is often more convenient to use the explicit expansion (59) and (60) via the generating function $\hat{\Phi}$. The results are summarized as

$$\frac{1}{2}(3\hat{\kappa}_{\mathrm{tr}-} + \hat{\kappa}_{\mathrm{tr}+}) = \sum_{dnjm} \omega^{d-4-n} p^n{}_0 Y_{jm}(\hat{\boldsymbol{p}})(d-2-n)(d-3-n)(c_F^{(d)})^{(0E)}_{njm}, \tag{86a}$$

$$\frac{3}{2}(\hat{\kappa}_{\mathrm{tr}-} - \hat{\kappa}_{\mathrm{tr}+}) = \sum_{dnjm} \omega^{d-4-n} p^n{}_0 Y_{jm}(\hat{\boldsymbol{p}})((n+2)(n+3) - j(j+1))(c_F^{(d)})^{(0E)}_{(n+2)jm}, \tag{86b}$$

$$(\hat{\kappa}_{e-})_{rr} = -2(\hat{\kappa}_{e+})_{+-} = \sum_{dnjm} \omega^{d-4-n} p^n{}_0 Y_{jm}(\hat{\boldsymbol{p}}) \frac{-(2n(n+2) + j(j+1))}{3} (c_F^{(d)})^{(0E)}_{(n+2)jm}, \tag{86c}$$

$$(\hat{\kappa}_{e-})_{\pm r} = (\hat{\kappa}_{e-})_{r\pm} = \sum_{dnjm} \omega^{d-4-n} p^n{}_{\pm 1} Y_{jm}(\hat{\boldsymbol{p}})(\pm 1)(n+1)\sqrt{\frac{j(j+1)}{2}} (c_F^{(d)})^{(0E)}_{(n+2)jm}, \tag{86d}$$

$$(\hat{\kappa}_{e-})_{\pm\pm} = \sum_{dnjm} \omega^{d-4-n} p^n{}_{\pm 2} Y_{jm}(\hat{\boldsymbol{p}}) \frac{-1}{2} \sqrt{\frac{(j+2)!}{(j-1)!}} (c_F^{(d)})^{(0E)}_{(n+2)jm}, \tag{86e}$$

$$(\hat{\kappa}_{o+})_{+-} = -(\hat{\kappa}_{o+})_{-+} = \sum_{dnjm} \omega^{d-4-n} p^n{}_0 Y_{jm}(\hat{\boldsymbol{p}})(-i)(d-3-n)(n+1)(c_F^{(d)})^{(0E)}_{(n+1)jm}, \tag{86f}$$

$$(\hat{\kappa}_{o+})_{\pm r} = -(\hat{\kappa}_{o+})_{r\pm} = \sum_{dnjm} \omega^{d-4-n} p^n{}_{\pm 1} Y_{jm}(\hat{\boldsymbol{p}})(-i)(d-3-n)\sqrt{\frac{j(j+1)}{2}} (c_F^{(d)})^{(0E)}_{(n+1)jm}. \tag{86g}$$

Recall that the matrix $\hat{\kappa}_{e-}$ is traceless and symmetric, while $\hat{\kappa}_{o+}$ is antisymmetric. For no leading-order birefringence, the relations

$$\begin{aligned} \hat{\kappa}_{DE} &= \hat{\kappa}_{e-} + \hat{\kappa}_{\mathrm{tr}-} + \hat{\kappa}_{\mathrm{tr}+}, \\ \hat{\kappa}_{HB} &= -\hat{\kappa}_{e-} - \hat{\kappa}_{\mathrm{tr}-} + \hat{\kappa}_{\mathrm{tr}+}, \qquad \hat{\kappa}_{DB} = \hat{\kappa}_{o+} \end{aligned} \tag{87}$$

also hold.

The next step is to consider dispersive effects. For dimensions $d > 4$, only a subset of independent combinations of the coefficients $(c_F^{(d)})^{(0E)}_{njm}$ are associated with leading-order vacuum dispersion. The nondispersive operators are precisely the ones of interest that define the camouflage models. At leading order, the condition that ensures no vacuum dispersion is

$$0 = p_\mu p_\nu (\hat{c}_F)^{\mu\nu}|_{p^2=0}. \tag{88}$$

This is satisfied if the generating function $\hat{\Phi}_F$ in Eq. (60) is of the form $\hat{\Phi}_F = p^2 \tilde{\Phi}_F$. We can therefore define the camouflage coefficients $(\bar{c}_F^{(d)})^{(0E)}_{njm}$ through the expansion

$$\tilde{\Phi}_F = \sum_{dnjm} \omega^{d-4-n} p^n{}_0 Y_{jm}(\hat{\boldsymbol{p}}) (\bar{c}_F^{(d)})^{(0E)}_{njm}. \tag{89}$$

This result leads to the comparatively simple relation

$$(c_F^{(d)})^{(0E)}_{njm} = (\bar{c}_F^{(d)})^{(0E)}_{njm} - (\bar{c}_F^{(d)})^{(0E)}_{(n-2)jm} \tag{90}$$

in the limit of no leading-order birefringence or vacuum dispersion.

The index ranges for the camouflage coefficients $(\bar{c}_F^{(d)})^{(0E)}_{njm}$ are given in Table IX. For each even dimension d, there are $(d-1)(d-2)(d-3)/6$ independent components. They represent combinations of the $(d+1)\times d(d-1)/6$ coefficients $(c_F^{(d)})^{(0E)}_{njm}$ that are complementary to the $(d-1)^2$ vacuum coefficients $c^{(d)}_{(I)jm}$ introduced in Sec. IV C. Note that a subset of the camouflage operators are rotation invariant, so a hybrid camouflage isotropic model exists that has $(d-2)/2$ independent coefficients for each even d.

The camouflage coefficients $(\bar{c}_F^{(d)})^{(0E)}_{njm}$ are challenging to detect via astrophysical observations of birefringence or dispersion because their effects arise only at higher order. Along with the minimal-SME coefficients $(c_F^{(4)})^{(0E)}_{njm}$, they are best sought via alternative methods such as laboratory experiments. A class of experiments sensitive to the effects of these coefficients is discussed in Sec. VII.

TABLE IX. Summary of the allowed ranges of indices n and j for the independent camouflage coefficients. The dimension d is even with $d \geq 4$, while $n \leq d-4$. The index m satisfies the usual restrictions $-j \leq m \leq j$, so there are $2j+1$ coefficients for each j. For a given dimension d, the total number of coefficients is given in the last row.

	$(\bar{c}_F^{(d)})^{(0E)}_{njm}$								
n	j								
0	0								
1		1							
2	0		2						
3		1		3					
4	0		2		4				
⋮	⋮					⋱			
$d-4$	0		2		4	$\cdots$			$d-4$
total	$\frac{1}{6}(d-1)(d-2)(d-3)$								

E. Vacuum-orthogonal models

In Sec. IV C, we identified the subset of spherical coefficients relevant for photon propagation in the vacuum. These are the vacuum coefficients $c^{(d)}_{(I)jm}$, $k^{(d)}_{(E)jm}$, $k^{(d)}_{(B)jm}$, and $k^{(d)}_{(V)jm}$. The number of independent vacuum coefficients grows as d^2 for large d, whereas the total number of coefficients grows as d^3. Consequently, the vacuum coefficients comprise a comparatively small portion of the total coefficient space. In this subsection, we construct a complete set of independent coefficients spanning the complementary part of the coefficient space. We refer to these as the vacuum-orthogonal coefficients. At leading order, the corresponding vacuum-orthogonal operators induce neither dispersion nor birefringence for photon propagation in the vacuum. Instead, these Lorentz-violating effects can become relevant whenever the boundary conditions or the properties of macroscopic media differ from those for vacuum propagation.

To extract the vacuum-orthogonal coefficients, we begin by considering the E-type vacuum coefficients $c^{(d)}_{(I)jm}$ and $k^{(d)}_{(E)jm}$. Expanding Eqs. (84a) and (84b) in terms of the general spherical coefficients, we find that each is a combination of $(c_F^{(d)})^{(0E)}_{njm}$, $(k_F^{(d)})^{(0E)}_{njm}$, $(\overline{k}_F^{(d)})^{(1E)}_{njm}$, and $(\overline{k}_F^{(d)})^{(2E)}_{njm}$. Careful consideration shows that the restriction $k^{(d)}_{(E)jm} = 0$ can be achieved by writing $(k_F^{(d)})^{(0E)}_{njm}$ as combinations of $(\overline{k}_F^{(d)})^{(1E)}_{njm}$ and $(\overline{k}_F^{(d)})^{(2E)}_{njm}$ and a new set of vacuum-orthogonal coefficients $(\overline{k}_F^{(d)})^{(0E)}_{njm}$. The net result is the replacement of $(k_F^{(d)})^{(0E)}_{njm}$ with $(\overline{k}_F^{(d)})^{(0E)}_{njm}$ in the nine sets of general coefficients, implemented via the substitution

$$(k_F^{(d)})^{(0E)}_{njm} \to (\overline{k}_F^{(d)})^{(0E)}_{njm} - (\overline{k}_F^{(d)})^{(0E)}_{(n+2)jm} - a_1(\overline{k}_F^{(d)})^{(1E)}_{(n+1)jm} - a_2(\overline{k}_F^{(d)})^{(2E)}_{njm}, \tag{91}$$

where the numerical factors a_1 and a_2 are

$$a_1 = \frac{(d-5-n)(2(n+4)^2+(j+2)(j-1))+2(n+3)(n+4)(n+5)}{j(j+1)},$$
$$a_2 = \frac{1}{(j+2)(j+1)j(j-1)}[(d-5-n)(d-4-n)(2(n+4)^2+(j+2)(j-1)) + 4(d-4-n)(n+3)(n+4)^2+(2(n+3)^2-j(j+1))(n+3)(n+4)]. \tag{92}$$

The result (91) represents combinations of E-type coefficients that are complementary to the vacuum coefficients $k^{(d)}_{(E)jm}$. The index ranges and counting for the vacuum-orthogonal coefficients $(\overline{k}_F^{(d)})^{(0E)}_{njm}$ are given in Table X.

TABLE X. Summary of the allowed ranges of indices n and j for the E-type vacuum-orthogonal coefficients $(\overline{k}_F^{(d)})^{(0E)}_{njm}$ associated with CPT-even nonbirefringent operators. The dimension d is even with $d \geq 4$, while $n \leq d-4$. The index m satisfies the usual restrictions $-j \leq m \leq j$, so there are $2j+1$ coefficients for each j. For a given dimension d, the number of coefficients is given in the last row.

	$(\overline{k}_F^{(d)})^{(0E)}_{njm}$									
n	j									
0										
1		1								
2	0		2							
3		1		3						
4	0		2		4					
⋮	⋮					⋱				
$d-4$	0		2		4		$\cdots$			$d-4$
total	$\frac{1}{6}(d-1)(d-2)(d-3)-1$									

The result (91) represents combinations of E-type coefficients that are complementary to the vacuum coefficients $k^{(d)}_{(E)jm}$. The index ranges and counting for the vacuum-orthogonal coefficients $(\overline{k}_F^{(d)})^{(0E)}_{njm}$ are given in Table X.

The restriction $c^{(d)}_{(I)jm} = 0$ yields a similar result for the coefficients $(c_F^{(d)})^{(0E)}_{njm}$,

$$(c_F^{(d)})^{(0E)}_{njm} \to (\overline{c}_F^{(d)})^{(0E)}_{njm} - (\overline{c}_F^{(d)})^{(0E)}_{(n-2)jm} - b_1(k_F^{(d)})^{(0E)}_{(n-2)jm} + b_2(\overline{k}_F^{(d)})^{(1E)}_{(n-1)jm} + b_3(\overline{k}_F^{(d)})^{(2E)}_{njm}. \tag{93}$$

where the numerical factors b_1, b_2, and b_3 are

$$b_1 = \frac{(d-3-n)(d-2-n)+2(d-2-n)n+n(n+1)-j(j+1)}{(d-3)(d-2)},$$
$$b_2 = \frac{(d-3-n)(2(n+1)(n+2)+(j+2)(j-1))+2(n+1)(n+2)(n+3)}{(d-3)(d-2)}, \tag{94}$$
$$b_3 = \frac{(d-5-n)(d-4-n)-(n+3)(n+4)}{(d-3)(d-2)}.$$

The coefficients $(\overline{c}_F^{(d)})^{(0E)}_{njm}$ appearing in Eq. (93) are the camouflage coefficients introduced in the previous subsection. Their index ranges and counting are given in Table IX. Note that $(k_F^{(d)})^{(0E)}_{njm}$ appears in Eq. (93), so the expression (91) is needed to fully reduce $(c_F^{(d)})^{(0E)}_{njm}$. Note also that Eq. (93) generalizes Eq. (90) to include coefficients for birefringent operators that leave unaffected vacuum propagation at leading order. This shows explicitly that these operators contribute both to birefringent and to nonbirefringent effects, an effect discussed in Sec. III B.

Determining the combinations of spherical coefficients that are complementary to the vacuum coefficient $k^{(d)}_{(B)jm}$ is more straightforward. We can write

$$k^{(d)}_{(B)jm} = \sum_n \frac{(-1)^{j+1}(d-1)}{2}\sqrt{\frac{(j-2)!}{(j+2)!}}((d-2)(\overline{k}_F^{(d)})^{(2B)}_{njm} + (j+2)(j-1)(k_F^{(d)})^{(1B)}_{njm}). \tag{95}$$

Taking into account the index ranges of $(k_F^{(d)})^{(1B)}_{njm}$ and $(\overline{k}_F^{(d)})^{(2B)}_{njm}$, we find that a suitable set of coefficients compatible with the restriction $k^{(d)}_{(B)jm} = 0$ is obtained by replacing $(k_F^{(d)})^{(1B)}_{njm}$ with a new set $(\overline{k}_F^{(d)})^{(1B)}_{njm}$ of vacuum-orthogonal coefficients. The combination leading to vanishing $k^{(d)}_{(B)jm}$ is given by

$$(k_F^{(d)})^{(1B)}_{njm} \to (\overline{k}_F^{(d)})^{(1B)}_{njm} - (\overline{k}_F^{(d)})^{(1B)}_{(n+2)jm} - \frac{(d-2)}{(j+2)(j-1)}(\overline{k}_F^{(d)})^{(2B)}_{(n+1)jm}. \tag{96}$$

The index ranges and counting for the coefficients $(\overline{k}_F^{(d)})^{(1B)}_{njm}$ are given in Table XI. Note that the coefficients $(\overline{k}_F^{(d)})^{(1B)}_{njm}$ and $(\overline{k}_F^{(d)})^{(2B)}_{njm}$ are absent from Eq. (93), so the corresponding operators have no nonbirefringent effects.

Finally, we construct the combinations of spherical coefficients that are complementary to $k^{(d)}_{(V)jm}$. Although the vacuum coefficients $k^{(d)}_{(V)jm}$ have the comparatively simple form (84d), finding combinations that cover the coefficient space under the restriction $k^{(d)}_{(V)jm} = 0$ involves some calculation. It turns out to involve two new sets $(\overline{k}_{AF}^{(d)})^{(0B)}_{njm}$, $(\overline{k}_{AF}^{(d)})^{(1B)}_{njm}$ of vacuum-orthogonal coefficients, which appear via the substitutions

$$(k_{AF}^{(d)})^{(0B)}_{njm} \to \frac{(d-2-n)(n+3)}{d(d-2-n+j)}((\overline{k}_{AF}^{(d)})^{(0B)}_{njm} - (\overline{k}_{AF}^{(d)})^{(0B)}_{(n-2)jm}) - \frac{1}{n+1}(\overline{k}_{AF}^{(d)})^{(1B)}_{(n-1)jm}, \tag{97}$$

TABLE XI. Summary of the allowed ranges of indices n and j for the B-type vacuum-orthogonal coefficients $(\overline{k}_F^{(d)})^{(1B)}_{njm}$ associated with CPT-even nonbirefringent operators. The dimension d is even with $d \geq 4$, while $n \leq d-4$. The index m satisfies the usual restrictions $-j \leq m \leq j$, so there are $2j+1$ coefficients for each j. For a given dimension d, the number of coefficients is given in the last row.

	$(\overline{k}_F^{(d)})^{(1B)}_{njm}$								
n	j								
0									
1	1								
2		2							
3	1		3						
4		2		4					
⋮	⋮				⋱				
$d-4$		2		4		$\cdots$			$d-4$
total	$\frac{1}{6}d(d-2)(d-4)$								

$$(k_{AF}^{(d)})^{(1B)}_{njm} \to \frac{j(n+2)}{d-3-n+j}((\overline{k}_{AF}^{(d)})^{(0B)}_{(n+1)jm} - (\overline{k}_{AF}^{(d)})^{(0B)}_{(n-1)jm}) + \frac{d}{n+4}(\overline{k}_{AF}^{(d)})^{(1B)}_{njm}. \tag{98}$$

The index ranges and the numbers of independent components for the vacuum-orthogonal coefficients $(\overline{k}_{AF}^{(d)})^{(0B)}_{njm}$ and $(\overline{k}_{AF}^{(d)})^{(1B)}_{njm}$ are shown in Table XII.

To summarize, in this subsection we have completed the decomposition of the original nine sets of general spherical coefficients into those that generate leading-order effects in the vacuum propagation of light and those that comprise the complementary subset. The four sets of vacuum coefficients are $c^{(d)}_{(I)jm}$, $k^{(d)}_{(E)jm}$, $k^{(d)}_{(B)jm}$, and $k^{(d)}_{(V)jm}$. They are discussed in Sec. IV C. The complement consists of the nine

TABLE XII. Summary of the allowed ranges of indices n and j for the vacuum-orthogonal coefficients $(\overline{k}_{AF}^{(d)})^{(0B)}_{njm}$ and $(\overline{k}_{AF}^{(d)})^{(1B)}_{njm}$ associated with CPT-odd nonbirefringent operators. The dimension d is even with $d \geq 4$, while $n \leq d-4$. The index m satisfies the usual restrictions $-j \leq m \leq j$, so there are $2j+1$ coefficients for each j. For a given dimension d, the number of coefficients is given in the last row.

	$(\overline{k}_{AF}^{(d)})^{(0B)}_{njm}$								$(\overline{k}_{AF}^{(d)})^{(1B)}_{njm}$							
n	j								j							
0	0								1							
1		1								2						
2	0		2						1		3					
3		1		3						2		4				
4	0		2		4				1		3		5			
⋮	⋮				⋱				⋮				⋱			
$d-4$		1		3		$\cdots$		$d-4$		2		4		$\cdots$		$d-3$
total	$\frac{1}{6}(d-1)(d-2)(d-3)$								$\frac{1}{6}(d+1)(d-1)(d-3)$							

reduced sets of vacuum-orthogonal coefficients $(\bar{c}_F^{(d)})^{(0E)}_{njm}$, $(\bar{k}_F^{(d)})^{(0E)}_{njm}$, $(\bar{k}_F^{(d)})^{(1E)}_{njm}$, $(\bar{k}_F^{(d)})^{(2E)}_{njm}$, $(\bar{k}_F^{(d)})^{(1B)}_{njm}$, $(\bar{k}_F^{(d)})^{(2B)}_{njm}$, $(\bar{k}_{AF}^{(d)})^{(0B)}_{njm}$, $(\bar{k}_{AF}^{(d)})^{(1B)}_{njm}$, and $(\bar{k}_{AF}^{(d)})^{(1E)}_{njm}$. Note that these are nonzero only for $d > 4$. This decomposition is summarized as part of Table XVIII in Sec. VIII.

Except for the camouflage coefficients $(\bar{c}_F^{(d)})^{(0E)}_{njm}$ discussed in the previous subsection, all the vacuum-orthogonal coefficients control birefringence effects that cannot be detected at leading order via vacuum propagation. To measure these coefficients, alternative methods such as laboratory experiments are therefore desirable. In contrast, all four sets of vacuum coefficients are detectable in astrophysical tests involving birefringence or dispersion, with the exception of the special $d = 4$ coefficients $c^{(4)}_{(I)jm}$. The latter have been extensively studied through a variety of different methods [12–17].

Note also that various hybrid models involving the vacuum-orthogonal coefficients can be countenanced. For example, a general vacuum-orthogonal isotropic model is obtained upon further restricting attention to the isotropic coefficients $(\bar{c}_F^{(d)})^{(0E)}_{n00}$, $(\bar{k}_F^{(d)})^{(0E)}_{n00}$, and $(\bar{k}_{AF}^{(d)})^{(0B)}_{n00}$. This model has $(d-2)/2$ nonbirefringent and $(d-4)/2$ birefringent operators for even d, along with $(d-3)/2$ birefringent operators for odd d.

F. Connections to other formalisms

Several specialized models involving particular Lorentz-violating photon operators with $d > 4$ have been considered in the literature. The generality of the SME implies that any realistic model for the photon propagator compatible with standard field theory is encompassed via special values of the coefficients $\hat{k}_F$ and $\hat{k}_{AF}$. In this subsection, we outline some of these connections. For a selection of specific models defined via field theory, we provide explicit limiting values of the SME coefficients for Lorentz violation that reproduce the models. We also offer here some remarks about the relationship between the SME and the kinematical approach to Lorentz violation, which is based on altering the transformation laws. Comments on the links between the photon sector of the SME and Lorentz-violating modifications of the photon dispersion relation outside the context of standard field theory can be found in Sec. VI A.

1. Field-theoretic models

We begin by discussing models defined via a Lagrange density in field theory. Several specialized models exist that involve photon fields with a small number of specific Lorentz-violating operators of mass dimensions $d = 5$ and in some cases also $d = 6$. We provide here brief comments identifying the match between these models and the SME coefficients for Lorentz violation.

One such model is presented by Gambini and Pullin [60]. Lorentz violation in this model is controlled by the parameter χl_P. To see the connection to the SME, we can make the field redefinition

$$\boldsymbol{E} + 2\chi l_P \boldsymbol{\nabla} \times \boldsymbol{E} \to \boldsymbol{E}. \tag{99}$$

This model then is equivalent to taking the special limit of the SME with the nonzero coefficients being $(k^{(5)}_{AF})^{0jk}$ and $(k^{(6)}_F)^{jklmpq}$, given by

$$\begin{aligned}(k^{(5)}_{AF})^{0jk} &= 2\chi l_P \delta^{jk},\\ (k^{(6)}_F)^{jklmpq} &= -4\chi^2 l_P^2 (\epsilon^{jkn}\epsilon^{nlm}\delta^{pq} - \tfrac{1}{4}\epsilon^{jk(p}\epsilon^{q)lm}).\end{aligned} \tag{100}$$

This model involves only isotropic Lorentz violations, so it is a special limit of the isotropic models discussed in Sec. IV B. In terms of the coefficients for Lorentz violation defined in Eq. (71), the match

$$\begin{aligned}(\mathring{k}^{(5)}_{AF})_2 &= -2\sqrt{4\pi}\chi l_P,\\ (\mathring{c}^{(6)}_F)_2 &= (\mathring{k}^{(6)}_F)_2 = -\sqrt{4\pi}\chi^2 l_P^2/5\end{aligned} \tag{101}$$

provides a complete specification of this model within the SME. It involves three nonzero isotropic coefficients containing a single degree of freedom. A nonlinear generalization of this model is obtained in Ref. [61], in which the propagator component is a special limit of the isotropic models discussed in Sec. IV B with 3 degrees of freedom.

Another specialized model incorporating photon-sector Lorentz violation is introduced by Myers and Pospelov [62]. This model has a unit timelike background vector n^μ that defines a preferred frame and a parameter ξ/M_P setting the scale of the Lorentz violation. Only one $d = 5$ Lorentz-violating operator affects the photon propagator. In terms of SME coefficients, the model is obtained by taking the nonzero coefficients for Lorentz violation to be

$$(k^{(5)}_{AF})^{\kappa\mu\nu} = -\frac{\xi}{M_P}\left(n^\kappa n^\mu n^\nu - \frac{1}{5}n^2 n^{(\mu}\eta^{\nu)\kappa}\right). \tag{102}$$

In the preferred frame, the vector takes the form $n^\mu = (1, 0, 0, 0)$. This model can therefore also be defined uniquely in terms of isotropic Lorentz violation and understood as a special limit of the isotropic models discussed in Sec. IV B. It is equivalent to taking as nonzero only the coefficient $(\mathring{k}^{(5)}_{AF})_0$, with the specific choice

$$(\mathring{k}^{(5)}_{AF})_0 = \frac{3\xi\sqrt{4\pi}}{5M_P}. \tag{103}$$

A model focusing on a Lagrange density that is explicitly gauge invariant and involves Lorentz-violating operators with $d = 5$ is considered by Bolokhov and Pospelov [63]. By construction, the component of the model relevant to the photon propagator is restricted to Lorentz violation affecting leading-order vacuum propagation. It consists of

$d = 5$ operators governed by a totally symmetric and traceless parameter $C^{\mu\nu\rho}$. This parameter has 16 independent components, corresponding to the 16 vacuum coefficients $k^{(5)}_{(V)jm}$ among the 36 independent coefficients $(k^{(5)}_{AF})^{\mu\nu\rho}$ for Lorentz violation at $d = 5$ in the SME. In terms of the latter coefficients, the model is fixed by

$$k^{(5)}_{(V)jm} \sim (k^{(5)}_{AF})^{\mu\nu\rho}|_{\substack{\text{symmetric}\\ \text{traceless}}} = -2C^{\mu\nu\rho}, \tag{104}$$

where the correspondence on the left-hand side is determined by matching Eqs. (76) and (81), and the restriction to the 16 relevant coefficients in $(k^{(5)}_{AF})^{\mu\nu\rho}$ is obtained by imposing total symmetry and tracelessness. The 20 SME coefficients at $d = 5$ that are absent from this model are the vacuum-orthogonal coefficients $(\overline{k}^{(5)}_{AF})^{(0B)}_{njm}$, $(\overline{k}^{(5)}_{AF})^{(1B)}_{njm}$, and $(\overline{k}^{(5)}_{AF})^{(1E)}_{njm}$, which leave unaffected leading-order vacuum propagation but nonetheless produce leading-order effects in suitable laboratory experiments.

The series structure of the SME Lagrange density (8) implies that models defined via nonpolynomial but analytic functionals of field operators can be matched to the SME by Taylor expansion. This includes models with apparent singularities, provided the expansion is taken about a nonsingular point. In the latter case, distinct analytic continuations may correspond to different values of SME coefficients, which may lead to unusual dynamical effects.

As an illustration, consider the class of Lorentz-violating models called very special relativity (VSR) [64], in which the Lorentz group is broken explicitly to the four-parameter subgroup SIM(2). It is useful to introduce the operator $N^\mu = n^\mu/(n\cdot\partial)$, where n^μ is a unit null vector that establishes a preferred lightlike direction. It follows that the combination $N\cdot T$ involving a tensor field operator T is SIM(2) covariant but violates Lorentz covariance. We can construct a generic on-shell linear VSR electrodynamics preserving gauge invariance by specifying field equations of the form

$$\partial_\mu F^{\mu\nu} + K_\mu(N)F^{\mu\nu} = 0, \tag{105}$$

where $K^\mu(N)$ is a nontrival four-vector function of N^μ that can also depend on the metric, the Levi-Civita tensor, and derivatives. Note that it is problematic to obtain a gauge-invariant action for these equations.

To investigate the correspondence to the SME, it is convenient to work in momentum space, where the operator $iN^\mu = n^\mu/(n\cdot p)$ is singular whenever $n\cdot p = 0$. Matching the momentum-space version of the VSR electrodynamics (105) to the momentum-space version of the SME equations of motion (11) therefore involves expanding $K_\mu(iN)F^{\mu\nu}(p)$ about a nonsingular point Q in momentum space. Assigning coordinates p^μ_Q to Q, we find the expansion converges either for $0 < n\cdot p < 2n\cdot p_Q$ or for $2n\cdot p_Q < n\cdot p < 0$, corresponding to two different analytic continuations of K_μ. Each expansion can be matched to a set of SME coefficients, but the two sets of coefficients differ. This implies the VSR electrodynamics (105) is represented by two different limits of the SME, according to the value of the photon momentum relative to the preferred lightlike direction.

2. Robertson-Mansouri-Sexl model

In a different vein, some authors adopt a kinematical approach to Lorentz violation that is based on modifications of the transformation laws. An older test model of this type that is encompassed by the SME approach is the kinematical formalism of Robertson, Mansouri, and Sexl (RMS) [65,66]. This approach assumes that there is a preferred universal inertial frame U in which light propagates conventionally as measured using a definite set of rods and clocks. In other frames, which include any inertial frame E relevant for experiment, light can behave anisotropically with respect to the boosted rods and clocks. The RMS approach assumes that the lengths of rods and the ticking rates of clocks are invariant in inertial frames related to U by RMS coordinate transformations $T^\mu{}_\nu$. These are deformations of the Lorentz transformations involving three functions of the boost $\boldsymbol{v}$, conventionally denoted as $a(\boldsymbol{v})$, $b(\boldsymbol{v})$, $d(\boldsymbol{v})$.

The RMS formalism can be translated into the SME framework. Consider first the preferred universal frame U. Since light is conventional in U by definition, the Maxwell action must be valid in this frame, so that

$$\mathcal{L}^{\text{photon}}_{\text{RMS,U}} = -\tfrac{1}{4}\eta^{\mu\rho}\eta^{\nu\sigma}F_{\mu\nu}F_{\rho\sigma}. \tag{106}$$

This Lagrange density is Lorentz invariant, so all Lorentz violation in this frame resides in the physics describing the chosen rods and clocks. For the photons, we can match the RMS formalism to the SME by imposing the condition

$$\mathcal{L}^{\text{photon}}_{\text{SME,U}} = \mathcal{L}^{\text{photon}}_{\text{RMS,U}}, \tag{107}$$

which eliminates all Lorentz-violating effects in the photon sector of the SME as seen in U.

For the RMS rods and clocks, any realistic set is made of constituent particles and fields. Since the SME describes general Lorentz violation for all particles and fields, it follows that the properties of any definite set of rods and clocks can be derived from the full SME action, at least in principle. This action contains infinitely many coefficients for Lorentz violation outside the photon sector, so there is plenty of room for anomalous behavior. However, to preserve the observed isotropy of light in U required by the RMS formalism for any possible choice of rods and clocks, only violations of Lorentz invariance in U that produce isotropic effects on the rods and clocks should be countenanced. We conclude that the match between the RMS formalism and the SME in the frame U requires restricting the SME to a subset of coefficients outside the photon sector. For definiteness in what follows, we denote these

SME coefficients collectively by $\{k\}$. Note that $\{k\}$ can include anisotropic coefficients, provided they have no anisotropic effects on the chosen rods and clocks.

Next, consider an experimentally relevant frame E that is moving with velocity $\boldsymbol{v}$ relative to U. In the RMS formalism, the properties of light in E are obtained by performing a RMS coordinate transformation using $T^{\mu}{}_{\nu}$. This leads to a modified Maxwell action with

$$\mathcal{L}^{\text{photon}}_{\text{RMS,E}} = -\tfrac{1}{4}\sqrt{|g_{\text{RMS}}|}(g^{-1}_{\text{RMS}})^{\mu\rho}(g^{-1}_{\text{RMS}})^{\nu\sigma}F_{\mu\nu}F_{\rho\sigma}, \quad (108)$$

where

$$(g_{\text{RMS}})_{\mu\nu} = \eta_{\rho\sigma}(T^{-1})^{\rho}{}_{\mu}(T^{-1})^{\sigma}{}_{\nu} \quad (109)$$

is an effective metric that depends on the three functions a, b, d. Note that physically different choices for the rods and clocks in the frame U imply different invariant RMS transformations and hence different a, b, d.

In contrast, the SME properties of light and the boosted rods and clocks in the frame E are obtained by performing a particle Lorentz transformation with the velocity $\boldsymbol{v}$. Since $\mathcal{L}^{\text{photon}}_{\text{SME,U}}$ is invariant under particle Lorentz transformations, light in the SME must obey conventional electrodynamics in the frame E too. However, the rods and clocks involve Lorentz-violating operators that change under the particle Lorentz transformation. This produces a deformation of the standard rods and clocks in E that depends on the SME coefficients $\{k\}$.

We thus find that the RMS formalism and the SME naturally generate two different coordinate systems for describing physics in the frame E. To relate the two, we can redefine the length and time intervals specified by the boosted SME rods and clocks to match numerically those of the boosted RMS rods and clocks, and we can choose the SME synchronization to match the RMS one. The redefinition can be implemented by scaling the spacetime coordinates. In the photon sector of the SME, the scaling produces an effective metric $(g_{\text{SME,eff}})_{\mu\nu}$ that depends on the coefficients $\{k\}$. Since measurements made with rods and clocks using either coordinate system now agree, this metric must match the RMS metric (109) in the frame E. This yields the result

$$(g_{\text{SME,eff}})_{\mu\nu}(\{k\}) = (g_{\text{RMS}})_{\mu\nu}(a, b, d), \quad (110)$$

which provides a direct correspondence between the SME coefficients and the RMS functions.

The above match shows that the RMS formalism can be understood as a special limit of the SME in which normal light behavior together with Lorentz violation affecting rods and clocks isotropically are assumed in the frame U. This limit excludes infinitely many Lorentz-violating effects. Since the RMS formalism is a special-relativistic test model, the gravitational sector of the SME must also be disregarded. Note that the three functions a, b, d can be expanded in powers of the velocity to yield a triple infinity of constant parameters, which can be absorbed into the multiple infinity of coefficients $\{k\}$. In the idealized case of rods and clocks formed from a scalar particle with only one isotropic dimension-zero coefficient k for Lorentz violation in the frame U, explicit expressions for the three RMS functions in terms of k are given in Sec. III C of Ref. [11].

Another point of interest is that physically different rods and clocks are associated with different functions a, b, d, and so involve different combinations of the coefficients $\{k\}$. Within the RMS formalism, measurements of a, b, d in a given experiment cannot meaningfully be compared to those in another experiment unless physically identical rods and clocks are used in both. Note that the rods and clocks must also be in the same physical state, since state changes in the presence of Lorentz violation can deform physical properties. This major disadvantage of the RMS formalism is circumvented by the SME. The SME coefficients for Lorentz violation are specific to particles and interactions and can therefore be reported in an experiment-independent way in a conveniently chosen frame, which conventionally is taken as the Sun-centered frame described in Sec. V.

To illustrate the above reasoning with an explicit example, we can consider a scenario in which the photons, the chosen rods, and the chosen clocks each have properties governed by different effective metrics. Following the RMS assumptions, the effective metric $(g_{\text{photon,U}})_{\mu\nu}$ for photons in the frame U must be taken as the Minkowski metric, while the effective metric $(g_{\text{rod,U}})_{\mu\nu}$ for the rods and the effective metric $(g_{\text{clock,U}})_{\mu\nu}$ for the clocks characterize the Lorentz-violating physics in U. We examine here a simple model for which

$$(g_{\text{photon,U}})_{\mu\nu} = \eta_{\mu\nu}, \qquad (g_{\text{rod,U}})_{\mu\nu} = \eta_{\mu\nu} - (c_{\text{rod,U}})_{\mu\nu},$$
$$(g_{\text{clock,U}})_{\mu\nu} = \eta_{\mu\nu} - (c_{\text{clock,U}})_{\mu\nu}. \quad (111)$$

The quantities $(c_{\text{rod,U}})_{\mu\nu}$ and $(c_{\text{clock,U}})_{\mu\nu}$ can be viewed as effective coefficients for Lorentz violation defined in the frame U. Depending on the nature of the chosen rods and clocks, these coefficients can be identified either directly with specific SME coefficients or indirectly as suitable combinations of SME coefficients. We also assume the conditions

$$\begin{aligned}(c_{\text{rod,U}})_{j0} &= (c_{\text{rod,U}})_{0k} = 0,\\ (c_{\text{rod,U}})_{jk} &= \tfrac{1}{3}(c_{\text{rod,U}})_{00}\delta_{jk},\\ (c_{\text{clock,U}})_{j0} &= (c_{\text{clock,U}})_{0k} = 0,\\ (c_{\text{clock,U}})_{jk} &= \tfrac{1}{3}(c_{\text{clock,U}})_{00}\delta_{jk},\end{aligned} \quad (112)$$

which ensure isotropic properties of the rods and clocks in U, as required by the RMS formalism. For simplicity, the coefficients are taken to be independent of spacetime position or, equivalently, independent of frequency and momentum. This simple model therefore has only 2 degrees of freedom controlling Lorentz violation.

Suppose for definiteness that the experimentally relevant frame E is moving with velocity $\boldsymbol{v} = (v, 0, 0)$ relative to U. Following the general reasoning above, we can obtain the SME description of the model in E by performing a standard particle Lorentz transformation Λ from U to E. The resulting effective metrics in E are given by expressions of the form

$$g_{\mathrm{E}} = \Lambda^{-1T} g_{\mathrm{U}} \Lambda^{-1}. \tag{113}$$

In the frame E, light remains conventional but the rods and clocks are distorted. To match to the RMS formalism, we must therefore seek alternative coordinates in E in which the rods are isotropic and of the same length as in U, and in which the clocks tick at the original rate in U. The appropriate coordinate transformation C leaves the origin of E in place but acts on the effective metrics as

$$g_{\mathrm{E}} \to C^{-1T} g_{\mathrm{E}} C^{-1} \equiv C^{-1T} \Lambda^{-1T} g_{\mathrm{U}} \Lambda^{-1} C^{-1}. \tag{114}$$

Since the components $(g_{\mathrm{rod}})_{jk}$ determine the rod length and the component $(g_{\mathrm{clock}})_{00}$ determines the clock ticking rate, and since both these quantities are assumed invariant in the RMS formalism, the required transformation C is fixed by demanding that

$$\begin{aligned} [C^{-1T}\Lambda^{-1T}(g_{\mathrm{rod,U}})\Lambda^{-1}C^{-1}]_{jk} &= (g_{\mathrm{rod,U}})_{jk}, \\ [C^{-1T}\Lambda^{-1T}(g_{\mathrm{clock,U}})\Lambda^{-1}C^{-1}]_{00} &= (g_{\mathrm{clock,U}})_{00}. \end{aligned} \tag{115}$$

With the usual definition $\gamma \equiv 1/\sqrt{1-v^2}$, we find that the nonzero elements of C take the form

$$\begin{aligned} C^0{}_0 &= \sqrt{\frac{1-(c_{\mathrm{clock,U}})_{00}\gamma^2(1+\frac{1}{3}v^2)}{1-(c_{\mathrm{clock,U}})_{00}}}, \\ C^1{}_1 &= \sqrt{\frac{1+(c_{\mathrm{rod,U}})_{00}\gamma^2(\frac{1}{3}+v^2)}{1+\frac{1}{3}(c_{\mathrm{rod,U}})_{00}}}, \\ C^2{}_2 &= C^3{}_3 = 1, \end{aligned} \tag{116}$$

which amounts to performing different dilations of time and of space in the direction of the boost.

With this information in hand, we can construct the RMS transformation $T \equiv C\Lambda$ from U to E. This provides the direct correspondence between the SME coefficients and the RMS functions a, b, d for this simple model. We obtain

$$\begin{aligned} a &= \frac{1}{\gamma}\sqrt{\frac{1-(c_{\mathrm{clock,U}})_{00}\gamma^2(1+\frac{1}{3}v^2)}{1-(c_{\mathrm{clock,U}})_{00}}}, \\ b &= \gamma\sqrt{\frac{1+(c_{\mathrm{rod,U}})_{00}\gamma^2(\frac{1}{3}+v^2)}{1+\frac{1}{3}(c_{\mathrm{rod,U}})_{00}}}, \\ d &= 1, \qquad \epsilon = \frac{-a\gamma^2 v}{b}, \end{aligned} \tag{117}$$

where ϵ is the RMS synchronization function in Einstein synchronization. Unlike the elementary single-coefficient example given in Ref. [11], the present model has $a \neq 1/b$. It also has $d = 1$, but allowing frequency dependence in $(c_{\mathrm{rod,U}})_{00}$ can generate $d \neq 1$ via the mixing of frequency with momentum resulting from the Λ boost and its consequent effects on C. A frequency or momentum dependence may arise directly from the inclusion of matter-sector operators of nonrenormalizable dimension [44], or indirectly from combinations of SME coefficients of renormalizable dimension when the motions of the component particles in the rod are incorporated.

Expanding the above results for a, b, d to leading order in v^2 and to leading order in coefficients for Lorentz violation yields

$$\begin{aligned} a &\approx 1 + \alpha v^2, \qquad \alpha = -\tfrac{1}{2} - \tfrac{5}{12}(c_{\mathrm{clock,U}})_{00}, \\ b &\approx 1 + \beta v^2, \qquad \beta = \tfrac{1}{2} + \tfrac{7}{12}(c_{\mathrm{rod,U}})_{00}, \\ d &\approx 1 + \delta v^2, \qquad \delta = 0. \end{aligned} \tag{118}$$

The combination of the RMS parameters α, β, δ that can be tested in Michelson-Morley experiments is known to be [66]

$$\beta + \delta - \tfrac{1}{2} = \tfrac{7}{12}(c_{\mathrm{rod,U}})_{00}, \tag{119}$$

and the combination tested in Kennedy-Thorndike experiments is

$$\alpha - \beta + 1 = -\tfrac{7}{12}(c_{\mathrm{rod,U}})_{00} - \tfrac{5}{12}(c_{\mathrm{clock,U}})_{00}, \tag{120}$$

while Ives-Stilwell experiments are sensitive to α. Evidently, two of the three types of experiments are required to disentangle all effects, even for this simple model. Various special cases can be considered. For example, if either $(c_{\mathrm{rod,U}})_{00}$ or $(c_{\mathrm{clock,U}})_{00}$ vanishes, then either Michelson-Morley or Ives-Stilwell experiments have no signal. If $(c_{\mathrm{rod,U}})_{00} = (c_{\mathrm{clock,U}})_{00}$, all experiments have interdependent signals.

The example verifies that the RMS formalism concerns Lorentz-violation residing in the matter sector rather than in the photon sector. Note that different choices of rods and clocks generically involve different values of $(c_{\mathrm{rod,U}})_{00}$ and $(c_{\mathrm{clock,U}})_{00}$ and therefore are associated with distinct Lorentz-violating effects, confirming that results from RMS experiments performed using different rods and clocks cannot meaningfully be compared. Note also that $(c_{\mathrm{rod,U}})_{00}$ and $(c_{\mathrm{clock,U}})_{00}$ are defined in the frame U, which typically differs from the canonical Sun-centered frame S in which SME coefficients are reported. A conventional particle Lorentz boost from U to S can be implemented to identify the relevant coefficient combinations in S. Interpreting experiments in the RMS formalism requires a choice of U, which is often taken as the frame of the cosmic microwave background, in which case the relevant boost to S is of order 10^{-3} and so to a good approximation $(c_{\mathrm{rod,U}})_{00} = (c_{\mathrm{rod,S}})_{TT}$ and $(c_{\mathrm{clock,U}})_{00} = (c_{\mathrm{clock,S}})_{TT}$. Alternatively, the frame U can simply be chosen to be

the frame S, since to date no compelling evidence for anisotropic Lorentz violation in S has been identified. Other choices are also possible. The requirement that U be specified to fix the RMS formalism is a disadvantage that is avoided in the SME, where any universal frame U is acceptable and moreover the existence of U is unnecessary for interpreting experimental data.

3. Deformed special relativities

Another kinematical approach involves requiring the invariance of all physics under some specified modification of the Lorentz transformations. Recent efforts along these lines are generically called deformed special relativity (DSR), or in some cases doubly special relativity or kappa-deformed relativity [67]. They posit that all physics is invariant under a set of deformed nonlinear Lorentz transformations, usually one that introduces a maximum energy scale. A generic DSR model is defined by replacing the four-momentum p_μ with a modified four-momentum π_μ, typically with a Planck-scale suppression factor for the deformation [68]. The momentum-space Lorentz transformations act conventionally on π_μ. This induces unconventional DSR transformations on p_μ, which are required to leave invariant the physics of the model.

Since the SME contains arbitrary polynomial Lorentz-violating operators at all mass dimensions, it must be possible to express any nonsingular DSR model involving realistic fields in the SME framework. The deformations normally are assumed to preserve rotation invariance, in which case the match to the SME involves the isotropic coefficients discussed in Sec. IV B. Within the context of the present work, we can investigate this correspondence explicitly in the photon sector.

Consider a generic DSR model in which the replacement of the four-momentum p_μ is specified by the nonlinear transformation

$$p_\mu \to \pi_\mu = M_\mu{}^\nu(p)p_\nu \tag{121}$$

acting in momentum space, where $M_\mu{}^\nu(p)$ is a nonsingular matrix that is a deformation of the identity. By definition, the Lorentz transformations $\Lambda_\alpha{}^\beta$ in momentum space act on π_μ as usual, $\pi_\mu \to \pi'_\mu = \Lambda_\mu{}^\nu \pi_\nu$. It follows that the expressions

$$p_\mu \to p'_\mu = S_\mu{}^\nu p_\nu, \qquad S_\mu{}^\nu = (M^{-1}\Lambda M)_\mu{}^\nu \tag{122}$$

specify the nonlinear DSR transformations $S_\mu{}^\nu$ of p_μ.

In the photon sector, we can determine the DSR-covariant dispersion relation for the photon by applying the replacement (121) to the standard Maxwell dispersion relation $p_\mu \eta^{\mu\nu} p_\nu = 0$. This gives

$$p_\mu (g_{\rm DSR}^{-1})^{\mu\nu} p_\nu = 0, \tag{123}$$

where the effective metric

$$(g_{\rm DSR})_{\mu\nu} = \eta_{\rho\sigma}(M^{-1})_\mu{}^\rho (M^{-1})_\nu{}^\sigma \tag{124}$$

is defined in momentum space. By construction, the dispersion relation (123) is invariant under the DSR transformations $S_\mu{}^\nu$ in Eq. (122).

In the SME context, the DSR dispersion relation (123) is recovered as a limiting case of the scalar covariant dispersion relation (30). The match arises in the special limit with $(\hat{k}_{AF})_\mu = 0$ and with the momentum-space operator $(\hat{k}_F)^{\mu\nu\rho\sigma}$ given by

$$(\hat{k}_F)^{\mu\nu\rho\sigma} = \sqrt{g_{\rm DSR}}(g_{\rm DSR}^{-1})^{\mu\rho}(g_{\rm DSR}^{-1})^{\nu\sigma} - \tfrac{1}{2}(\eta^{\mu\rho}\eta^{\nu\sigma} - \eta^{\nu\rho}\eta^{\mu\sigma}). \tag{125}$$

We see that the nonlinear transformation $M_\mu{}^\nu(p)$ generates a subset of the Lorentz-violating operators in the SME, typically in the form of an infinite series.

An alternative derivation yielding the same result can be performed at the level of field theory. We can construct the DSR-invariant modified action for this generic model by taking the Maxwell action in momentum space and implementing the replacement (121). The transformation of the photon field under $S_\mu{}^\nu$ is taken as

$$A_\mu(p) \to A'_\mu(p') = S_\mu{}^\nu(p) A_\nu(p), \tag{126}$$

corresponding to the replacement $A_\mu \to M_\mu{}^\nu A_\nu$. This gives the momentum-space Lagrange density

$$\mathcal{L}^{\rm photon}_{\rm DSR}(p) = -\tfrac{1}{4}\sqrt{|g_{\rm DSR}|}(g_{\rm DSR}^{-1})^{\mu\rho}(g_{\rm DSR}^{-1})^{\nu\sigma} F_{\mu\nu}F_{\rho\sigma}, \tag{127}$$

where the effective metric $(g_{\rm DSR})_{\mu\nu}$ in momentum space is given by Eq. (124). By construction, the Lagrange density (127) is invariant under the DSR transformations $S_\mu{}^\nu$ in Eq. (122). In the SME context, this same Lagrange density is obtained as the special limit of the SME photon sector of the form

$$\mathcal{L}^{\rm photon}_{\rm SME}|_{\rm DSR} \equiv \mathcal{L}^{\rm photon}_{\rm DSR} = -\tfrac{1}{4}F^{\mu\nu}F_{\mu\nu} - \tfrac{1}{4}F_{\mu\nu}(\hat{k}_F)^{\mu\nu\rho\sigma}F_{\rho\sigma}, \tag{128}$$

where the momentum-space operator $(\hat{k}_F)^{\mu\nu\rho\sigma}$ is given by Eq. (125). This SME construction applies for a generic DSR model, and it confirms that the nonlinear transformation $M_\mu{}^\nu(p)$ produces a series of SME coefficients for Lorentz violation.

Although the model (128) transforms nontrivially under conventional particle Lorentz transformations, observable physical effects cannot arise. This is because in any frame the inverse momentum replacement can be applied to all particles and fields to recover an action of the usual Lorentz-invariant form in terms of the momentum π^μ, and any experiment naturally identifies this momentum as the physical one. The situation in this respect differs from that of the RMS formalism, where only the rods and

clocks are assumed invariant under modified Lorentz transformations while light behaves differently, so physical effects can arise. It also differs from the SME, where distinct particles and fields can break Lorentz symmetry in different ways and only a subset of coefficients are unobservable. The absence of observable effects when the conventional momentum is adopted is a known characteristic of DSR models [69], which follows from their definition as nonlinear momentum-space representations of the usual Lorentz transformations.

More generally, the above considerations reveal that modifications of the dynamics are unphysical whenever they arise from a universal and reversible momentum substitution. Observable effects might in principle be possible in special models if singularities in the physics obstruct the recovery of the usual four-momentum via the inverse momentum replacement, although the requirement of physical singularities seems unappealing. However, an alternative approach does exist. Observable effects in models with deformed Lorentz transformations can be obtained by imposing the deformed invariance only on a subset of particles or fields, while either conventional Lorentz invariance or a different deformed invariance holds for others. This idea has not been investigated in the literature, perhaps because the idea of two or more mutually incompatible invariances in nature runs counter to the DSR philosophy. Note that any such models are subsets of the SME, so constraints from SME coefficients apply.

As one simple exotic example of a model with multiple invariances, one can consider ''spinning'' special relativity in which the deformed symmetry differs for fermions and bosons. The quadratic action for a fermion would then be invariant under one transformation, while that for a boson would have a different invariance. The deformed transformations can also be chosen to depend explicitly on the representation, so that multiple invariances would be involved in the various pieces of the quadratic action. Different versions of this idea could be considered. For instance, ''flavorful'' and ''colorful'' special relativities could be constructed by choosing the deformations to vary with the particle species, or more specifically with the representation of the internal symmetry group. In any case, the full action generically breaks the individual invariances, thereby leading to detectable signals. As before, any subgroup of the deformed transformations that leaves invariant the full action is associated with unobservable effects.

V. REFERENCE FRAMES AND ROTATIONS

For comparative purposes, it is useful to adopt a standard inertial frame in reporting measurements of coefficients for Lorentz violation. The canonical frame used in the literature is a Sun-centered celestial equatorial frame [11,34]. Cartesian coordinates in this frame are denoted (T, X, Y, Z). The Z axis lies along the rotation axis of the Earth, while the X-Y plane coincides with the Earth's equatorial plane. The X axis is directed from the Earth to the Sun at the vernal equinox. One advantage of this conventional choice is that transforming between the Sun-centered frame and a laboratory frame is comparatively simple.

In a typical application, a measurement of coefficients for Lorentz violation is made in a laboratory frame of reference. However, the rotation and revolution of the Earth imply this frame is noninertial, so the coefficients for Lorentz violation in the laboratory vary with time. These varying coefficients are related to the constant ones in the Sun-centered frame by an observer Lorentz transformation, which predominantly involves rotations. In this section, we construct the relevant rotation transformations to an arbitrary laboratory reference frame, including one based on a rotating turntable. We apply the results to obtain the transformation of spherical coefficients for Lorentz violation between the laboratory and Sun-centered frames. Since the spherical coefficients represent a decomposition based on angular momentum, their transformation is comparatively straightforward. Moreover, the spin weight is unaffected by rotations because helicity commutes with the angular momentum $\boldsymbol{J}$. The only index that changes under rotations is therefore the J_z eigenvalue m.

A. Rotation matrices

To construct the rotation transformations, we adopt Euler angles α, β, and γ that relate two arbitrary Cartesian frames with coordinates (x, y, z) and (x', y', z') through the rotation

$$R = e^{-i\alpha J_z} e^{-i\beta J_y} e^{-i\gamma J_z}. \tag{129}$$

This rotation can be visualized by starting with the two frames coinciding, rotating the second frame by γ about the z axis, then by β about the y axis, and finally by α about the z axis again. Acting on coordinates, this combination of rotations can be shown to be implemented by the matrix equation

$$\begin{pmatrix} x' \\ y' \\ z' \end{pmatrix} = \begin{pmatrix} \cos\gamma & \sin\gamma & 0 \\ -\sin\gamma & \cos\gamma & 0 \\ 0 & 0 & 1 \end{pmatrix} \begin{pmatrix} \cos\beta & 0 & -\sin\beta \\ 0 & 1 & 0 \\ \sin\beta & 0 & \cos\beta \end{pmatrix} \times \begin{pmatrix} \cos\alpha & \sin\alpha & 0 \\ -\sin\alpha & \cos\alpha & 0 \\ 0 & 0 & 1 \end{pmatrix} \begin{pmatrix} x \\ y \\ z \end{pmatrix}. \tag{130}$$

Note that this result implies that the net rotation can alternatively be viewed as a rotation by α about z, followed by a rotation by β about the rotated y axis, and then by a rotation by γ about the rotated z axis.

To determine the rotation rules for spherical harmonics, consider a spin-weighted function ${}_sf$ expanded in both coordinate systems:

$$ {}_sf = \sum_{jm} f_{jm}\, {}_sY_{jm}(\Omega) = \sum_{jm} f'_{jm}\, {}_sY_{jm}(\Omega'). \tag{131} $$

The spherical harmonics are related by

$$ {}_sY_{jm}(\Omega') = R_s Y_{jm}(\Omega), \tag{132} $$

which implies the transformation

$$ \begin{aligned} f_{jm} &= \sum_{m'} D^{(j)}_{mm'}(\alpha, \beta, \gamma) f'_{jm'}, \\ f'_{jm} &= \sum_{m'} D^{(j)}_{mm'}(-\gamma, -\beta, -\alpha) f_{jm'}. \end{aligned} \tag{133} $$

In these expressions, the quantities

$$ D^{(j)}_{mm'}(\alpha, \beta, \gamma) = \int {}_sY^*_{jm} e^{-i\alpha J_z} e^{-i\beta J_y} e^{-i\gamma J_z}\, {}_sY_{jm'} d\Omega \tag{134} $$

are the Wigner rotation matrices [70]. It can be shown that these matrices are independent of s, which is to be expected because $\boldsymbol{J}$ commutes with the helicity operator. Consequently, all spherical coefficients are rotated using the same set of matrices, regardless of their spin weight.

The Wigner matrices are often written in the form

$$ D^{(j)}_{mm'}(\alpha, \beta, \gamma) = e^{-i\alpha m} e^{-i\gamma m'} d^{(j)}_{mm'}(\beta), \tag{135} $$

where $d^{(j)}_{mm'}(\beta) = D^{(j)}_{mm'}(0, \beta, 0)$ are called the little Wigner matrices. The phases in this equation correspond to the two rotations about the z axis, while $d^{(j)}_{mm'}$ accounts for the rotation about y. Explicitly, the little-matrix elements are given by

$$ \begin{aligned} d^{(j)}_{mm'}(\beta) = \sum_k (-1)^{k+m+m'} & \\ \times \frac{\sqrt{(j+m)!(j-m)!(j+m')!(j-m')!}}{(j-m-k)!(m-m'+k)!(j+m'-k)!k!} & \\ \times \left(\cos\frac{\beta}{2}\right)^{2j} \left(\tan\frac{\beta}{2}\right)^{2k+m-m'}, & \end{aligned} \tag{136} $$

where the sum is restricted to all k for which the arguments of the factorials are non-negative.

B. Laboratory frame

We next apply the Wigner matrices to relate the coefficients for Lorentz violation in the laboratory frame to those in the Sun-centered frame. For this purpose, it is useful to work with a canonical laboratory frame [11]. Cartesian coordinates in this frame are denoted (x, y, z). The z direction is directed towards the zenith, and the x axis lies at an angle ϕ measured east of south. The colatitude of the laboratory is denoted χ. The orientation of the laboratory with respect to the Sun-centered coordinates (X, Y, Z) is determined by the local sidereal time $T_\oplus$. Since the Z axis points towards the celestial north pole while the X and Y axes lie in the equatorial plane with right ascension 0° and 90°, respectively, it follows that the laboratory z axis points toward right ascension $\omega_\oplus T_\oplus$, where $\omega_\oplus \simeq 2\pi/(23\ \text{hr}\ 56\ \text{min})$ is the Earth's sidereal frequency.

With these conventions, the angles ϕ, χ, and $\omega_\oplus T_\oplus$ represent three Euler angles giving the relevant net rotation between frames. From the perspective of the Sun-centered frame, the laboratory frame is obtained by rotating by ϕ about Z, then by χ about Y, and lastly by $\omega_\oplus T_\oplus$ about Z. The Euler angles relating the Sun-centered frame to the laboratory frame are therefore

$$ \alpha = \omega_\oplus T_\oplus, \qquad \beta = \chi, \qquad \gamma = \phi. \tag{137} $$

It follows that the explicit rotation relating the two sets of coordinates is

$$ \begin{aligned} \begin{pmatrix} x \\ y \\ z \end{pmatrix} = & \begin{pmatrix} \cos\phi & \sin\phi & 0 \\ -\sin\phi & \cos\phi & 0 \\ 0 & 0 & 1 \end{pmatrix} \begin{pmatrix} \cos\chi & 0 & -\sin\chi \\ 0 & 1 & 0 \\ \sin\chi & 0 & \cos\chi \end{pmatrix} \\ & \times \begin{pmatrix} \cos\omega_\oplus T_\oplus & \sin\omega_\oplus T_\oplus & 0 \\ -\sin\omega_\oplus T_\oplus & \cos\omega_\oplus T_\oplus & 0 \\ 0 & 0 & 1 \end{pmatrix} \begin{pmatrix} X \\ Y \\ Z \end{pmatrix}. \end{aligned} \tag{138} $$

The spherical coefficients in the laboratory frame can now be expressed as Sun-frame coefficients through the relation

$$ \begin{aligned} \mathcal{K}^{\text{lab}}_{jm} &= \sum_{m'} D^{(j)}_{mm'}(-\phi, -\chi, -\omega_\oplus T_\oplus) \mathcal{K}^{\text{Sun}}_{jm'} \\ &= \sum_{m'} e^{im\phi} e^{im'\omega_\oplus T_\oplus} d^{(j)}_{mm'}(-\chi) \mathcal{K}^{\text{Sun}}_{jm'}, \end{aligned} \tag{139} $$

where $\mathcal{K}^{\text{lab}}_{jm}$ and $\mathcal{K}^{\text{Sun}}_{jm}$ represent arbitrary spherical coefficients for Lorentz violation in the laboratory and Sun-centered frames, respectively.

The result (139) is auspicious. A key signal in many experiments is the sidereal variation introduced by the rotation of the Earth. Here, this rotation is expressed in a simple form involving time-dependent phases $e^{im\omega_\oplus T_\oplus}$. Only the colatitude χ appears in the little Wigner matrices $d^{(j)}_{m'm}(-\chi)$, which are time independent. Consequently, for typical applications these time-independent factors need be calculated only once for a given experiment at fixed χ.

Some experiments involve turntables rotating about the vertical axis. This situation can be incorporated into the above rotation by fixing the laboratory frame with respect to the turntable. This implies the azimuthal angle acquires a time dependence of the form $\phi = \omega_{\text{tt}} T_{\text{tt}}$, where ω_{tt} is the turntable rotation frequency and T_{tt} is measured from a time when the x axis points south. Again, the time dependence enters through simple phases.

As a simple example, consider the rotations of vector coefficients in an experiment involving a turntable. Calculating the Wigner matrices for $j = 1$, we find that the rotation between spherical coefficients in the laboratory and Sun-centered frames is given by

$$\begin{pmatrix} \mathcal{K}^{\rm lab}_{11} \\ \mathcal{K}^{\rm lab}_{10} \\ \mathcal{K}^{\rm lab}_{1(-1)} \end{pmatrix} = \begin{pmatrix} e^{i\omega_{tt}T_{tt}} & 0 & 0 \\ 0 & 1 & 0 \\ 0 & 0 & e^{-i\omega_{tt}T_{tt}} \end{pmatrix} \times \begin{pmatrix} \cos^2\frac{\chi}{2} & -\frac{1}{\sqrt{2}}\sin\chi & \sin^2\frac{\chi}{2} \\ \frac{1}{\sqrt{2}}\sin\chi & \cos\chi & -\frac{1}{\sqrt{2}}\sin\chi \\ \sin^2\frac{\chi}{2} & \frac{1}{\sqrt{2}}\sin\chi & \cos^2\frac{\chi}{2} \end{pmatrix} \times \begin{pmatrix} e^{i\omega_\oplus T_\oplus} & 0 & 0 \\ 0 & 1 & 0 \\ 0 & 0 & e^{-i\omega_\oplus T_\oplus} \end{pmatrix} \begin{pmatrix} \mathcal{K}^{\rm Sun}_{11} \\ \mathcal{K}^{\rm Sun}_{10} \\ \mathcal{K}^{\rm Sun}_{1(-1)} \end{pmatrix} \tag{140}$$

in matrix form.

In some situations, it may be convenient to define a third frame that is fixed with respect to the apparatus. The advantage of this third frame is that it may be chosen to simplify calculations. For example, a laboratory apparatus often has a symmetry axis, so adopting a third apparatus frame with one coordinate axis along the symmetry direction may be convenient. To incorporate this in the above formalism, it suffices to identify a suitable apparatus frame and to determine the corresponding Euler angles relating it to the laboratory frame. The laboratory-frame and apparatus-frame spherical coefficients are then related through Eq. (133). Thus, if the apparatus-frame coordinates (x', y', z') are related to laboratory-frame coordinates by

$$\begin{pmatrix} x' \\ y' \\ z' \end{pmatrix} = \begin{pmatrix} \cos\gamma & \sin\gamma & 0 \\ -\sin\gamma & \cos\gamma & 0 \\ 0 & 0 & 1 \end{pmatrix} \begin{pmatrix} \cos\beta & 0 & -\sin\beta \\ 0 & 1 & 0 \\ \sin\beta & 0 & \cos\beta \end{pmatrix} \times \begin{pmatrix} \cos\alpha & \sin\alpha & 0 \\ -\sin\alpha & \cos\alpha & 0 \\ 0 & 0 & 1 \end{pmatrix} \begin{pmatrix} x \\ y \\ z \end{pmatrix}, \tag{141}$$

where α, β, γ are appropriate Euler angles, then the apparatus-frame spherical coefficients can be written in terms of the laboratory-frame spherical coefficients through

$$\mathcal{K}^{\rm app}_{jm} = \sum_{m'} D^{(j)}_{mm'}(-\gamma, -\beta, -\alpha)\mathcal{K}^{\rm lab}_{jm'}. \tag{142}$$

Assuming the orientation of the system is fixed in the laboratory frame, the Wigner matrices for this rotation are constant.

As a simple illustration, consider a system with symmetry axis oriented along the x axis of the laboratory frame. In this case, it may be beneficial to choose an apparatus frame having angular-momentum projection axis z' aligned with the symmetry axis. This can be achieved by taking $x' = -z$, $y' = y$, and $z' = x$. A suitable choice of Euler angles is then given by $\alpha = 0$, $\beta = 90°$, and $\gamma = 0$.

VI. ASTROPHYSICAL TESTS

In this section, we discuss searches for Lorentz violation involving observation of radiation from sources at cosmological distances. Due to the large baselines involved, searches for birefringent and dispersive effects can in principle achieve high sensitivities to almost all the vacuum coefficients $c^{(d)}_{(I)jm}$, $k^{(d)}_{(E)jm}$, $k^{(d)}_{(B)jm}$, and $k^{(d)}_{(V)jm}$ introduced in Sec. IV C.

Where relevant, vacuum birefringence provides considerably greater sensitivity than vacuum dispersion, as is shown below. It is therefore natural to separate the relevant Lorentz-violating operators into two classes. The first class is controlled by the vacuum coefficients $k^{(d)}_{(E)jm}$, $k^{(d)}_{(B)jm}$, $k^{(d)}_{(V)jm}$ and produces leading-order birefringence. The second consists of vacuum operators causing dispersion without leading-order birefringence and is associated with the coefficients $c^{(d)}_{(I)jm}$ for $d > 4$. Observations of dispersion are therefore well suited to measurements of $c^{(d)}_{(I)jm}$, while studies of birefringence are appropriate for measurements of the remaining coefficients.

We begin in Sec. VI A with a discussion of dispersion tests. The basic theory and results are summarized, and new constraints are obtained using recent results. In Sec. VI B, we consider birefringence tests. A general treatment is first outlined, and then applications to point sources and to the CMB are presented. We obtain new constraints from gamma-ray bursts on coefficients of mass dimensions five, seven, and nine, and we discuss some general features of the effects of Lorentz violation on the CMB.

A. Dispersion tests

Frequency-dependent photon velocities arise from Lorentz-violating operators with $d \neq 4$, which cause wave dispersion. Astrophysical searches for vacuum dispersion seek these differences in the velocity of light at different wavelengths. Typical searches involve explosive or pulsed sources of radiation, such as gamma-ray bursts, pulsars, or blazars, that produce light over a wide range of wavelengths in a short period of time. Assuming the temporal structure of the emission is sufficiently well understood, observed but unexpected arrival-time differences can be interpreted as wavelength dependences in the velocity. Even if detailed frequency information is unavailable, limits can still be obtained from the pulse width because dispersion results in a spreading of wave packets.

A number of astrophysical searches for a modified photon dispersion relation have been performed. Most of these studies assume isotropic Lorentz violation. To make the connection between these approaches and the SME, we momentarily restrict our attention to the vacuum isotropic model discussed in Sec. IV C, which is the relevant limit for astrophysical studies of isotropic violations. Recall that this model has exactly one nonzero spherical coefficient

for Lorentz violation at each d, consisting of $c^{(d)}_{(I)00}$ for even d and $k^{(d)}_{(V)00}$ for odd d. In the isotropic limit, the velocity defect arising from Eq. (75) is given by

$$\delta v \simeq \frac{1}{\sqrt{4\pi}} \sum_d E^{d-4}(-c^{(d)}_{(I)00} \pm k^{(d)}_{(V)00}), \tag{143}$$

in terms of the photon energy E. The coefficients $c^{(d)}_{(I)00}$ are associated with CPT-even operators producing dispersion but no leading-order birefringence, while nonzero coefficients $k^{(d)}_{(V)00}$ imply birefringence and corresponding changes in polarization. Among the studies involving modified dispersion relations with isotropic Lorentz violation, it follows that only those with odd d and birefringence or even d and no birefringence are consistent with linear effective field theory in flat spacetime [71].

Isotropic Lorentz-violating effects in modified dispersion relations are sometimes described using a velocity deviation of the form $\delta v = \pm \xi_1 E$, where ξ_1 is a constant [62,72]. This model is phenomenologically equivalent to the single SME coefficient $k^{(5)}_{(V)00} = \sqrt{4\pi}\xi_1$. However, because this particular combination causes birefringence, its best constraints currently come from polarimetry observations, which are discussed in the next subsection. An isotropic higher-order correction of the form $\delta v = \xi_2 E^2$ has also been considered [73]. This case corresponds to the $d = 6$ coefficient $c^{(6)}_{(I)00} = -\sqrt{4\pi}\xi_2$. Bounds on this term from the active galaxy Markarian 501 are currently of order 10^{-21} GeV^{-2} [23], though some evidence for nonzero dispersion from this source exists [74]. Other cases that are sometimes considered involve an isotropic nonbirefringent linear defect $\delta v = \xi_1 E$ [75] or an isotropic birefringent defect $\delta v = \pm \xi_2 E^2$, where the sign indicates helicity [76]. Both these cases are inconsistent with the present general analysis and may be problematic.

In principle, searches for Lorentz violation via dispersion are sensitive to all coefficients with $d \neq 4$. However, considerably greater sensitivities to coefficients associated with birefringence are typically accessible via polarimetry. This can be understood as follows. In a vacuum dispersion study involving a source at baseline distance L, the quantity of interest is the change $\delta t \simeq \delta v L$ in arrival time of the signal, which implies a sensitivity to δv given by $\delta t/L$. In contrast, for a polarimetric study of the same astrophysical source, the quantity of interest is the phase difference $\delta\phi \simeq E\delta v L$ of the eigenmodes, which yields sensitivity $\delta\phi/LE$. Comparing these two results, we see that dispersive sensitivity depends on the difference in arrival time, while polarimetric sensitivity depends on the periodicity $\propto 1/E$ of the source radiation. Consequently, to achieve similar sensitivity, an astrophysical dispersion test requires a time resolution comparable to the inverse frequency of the photons, which is infeasible.

We can therefore conclude that astrophysical dispersion studies are best suited to searches for the nonbirefringent vacuum coefficients $c^{(d)}_{(I)jm}$. Note, however, that birefringence also causes a spreading of wave packets, due to the differences in velocity of the two birefringent eigenmodes. Moreover, all birefringent operators with $d \neq 4$ are also dispersive. A definitive interpretation of an observed arrival-time difference as a dispersive nonbirefringent effect associated with the vacuum coefficients $c^{(d)}_{(I)jm}$ therefore requires a polarimetric study of the signal or elimination of possible contributions from the other vacuum coefficients via independent studies.

Setting all other coefficients to zero, the velocity defect including anisotropies is given by

$$\delta v \simeq -\mathfrak{s}^0 = -\sum_{djm} E^{d-4}\, {}_0Y_{jm}(\hat{\boldsymbol{n}}) c^{(d)}_{(I)jm}. \tag{144}$$

Note that this involves only even-dimensional Lorentz-violating operators and that the $d = 4$ case involves no dispersion. For operators with $d > 4$, the sensitivities increase with energy and so high-frequency sources can be expected to yield the sharpest results. Note also that limiting attention to isotropic dispersion disregards a total of $(d^2 - 2d - 2)$ independent types of vacuum Lorentz violation at each d.

The difference in velocity between photons of different energies leads to an arrival-time difference given by [23]

$$\begin{aligned} t_2 - t_1 &\approx \int_0^z \frac{v_1 - v_2}{H_z} dz \\ &\approx (E_2^{d-4} - E_1^{d-4}) \int_0^z \frac{(1+z)^{d-4}}{H_z} dz \sum_{jm} {}_0Y_{jm} c^{(d)}_{(I)jm}, \end{aligned} \tag{145}$$

where the source redshift is z and t_1, t_2 are the propagation times for photons with observed energies E_1, E_2 and velocities v_1, v_2. Also,

$$\begin{aligned} H_z = H_0[&\Omega_r(1+z)^4 + \Omega_m(1+z)^3 \\ &+ \Omega_k(1+z)^2 + \Omega_\Lambda]^{1/2} \end{aligned} \tag{146}$$

is the Hubble expansion rate at z, expressed in terms of the present-day Hubble constant $H_0 \simeq 71\ \mathrm{km\,s^{-1}\,Mpc^{-1}}$, radiation density $\Omega_r \simeq 0.015$, matter density $\Omega_m \simeq 0.27$, vacuum density $\Omega_\Lambda \simeq 0.73$, and curvature density $\Omega_k = 1 - \Omega_r - \Omega_m - \Omega_\Lambda$. In Ref. [23], these expressions are used to place direction-dependent bounds on combinations of the coefficients $c^{(6)}_{(I)jm}$ and $c^{(8)}_{(I)jm}$, using observations of GRB 021206 [77] and of the blazar Markarian 501 [74]. These results are summarized in Table XIII.

As an illustration, consider the recent measurements made by the Fermi Observatory on the source GRB 080916C [78]. This exceptionally energetic source produced a burst of photons with observed energies ranging to $13.22^{+0.70}_{-1.54}$ GeV, all of which arrived within 16.54 s of

TABLE XIII. Constraints on spherical coefficients from astrophysical dispersion studies. The first five rows give constraints on the vacuum coefficients with $d = 6, 8$. The next five rows give the constraints on coefficients in the isotropic limit, for which there is exactly one nonzero coefficient for each d. Except for the limits from GRB 080916C and PKS 2155-304, which are obtained in the text, all results in the table are taken from the analysis of Ref. [23], which used data from Refs. [74,77]. The bounds shown are at the 95% confidence level.

Model	Coefficients	Result	System
Vacuum	$\lvert\sum_{jm\,0} Y_{jm}(99.7°, 240°) c^{(6)}_{(I)jm}\rvert$	$<1 \times 10^{-16}$ GeV^{-2}	GRB 021206
	$\sum_{jm\,0} Y_{jm}(50.2°, 253°) c^{(6)}_{(I)jm}$	$3^{+1}_{-2} \times 10^{-22}$ GeV^{-2}	Markarian 501
	$\sum_{jm\,0} Y_{jm}(147°, 120°) c^{(6)}_{(I)jm}$	$<3.2 \times 10^{-20}$ GeV^{-2}	GRB 080916C
	$\lvert\sum_{jm\,0} Y_{jm}(330°, -30°) c^{(6)}_{(I)jm}\rvert$	$<7.4 \times 10^{-22}$ GeV^{-2}	PKS 2155-304
	$\lvert\sum_{jm\,0} Y_{jm}(99.7°, 240°) c^{(8)}_{(I)jm}\rvert$	$<3 \times 10^{-13}$ GeV^{-4}	GRB 021206
	$\sum_{jm\,0} Y_{jm}(147°, 120°) c^{(8)}_{(I)jm}$	$<2.6 \times 10^{-23}$ GeV^{-4}	GRB 080916C
Vacuum isotropic	$\lvert c^{(6)}_{(I)00}\rvert$	$<4 \times 10^{-16}$ GeV^{-2}	GRB 021206
	$c^{(6)}_{(I)00}$	$10^{+4}_{-7} \times 10^{-22}$ GeV^{-2}	Markarian 501
	$c^{(6)}_{(I)00}$	$<1.1 \times 10^{-19}$ GeV^{-2}	GRB 080916C
	$\lvert c^{(6)}_{(I)00}\rvert$	$<2.6 \times 10^{-21}$ GeV^{-2}	PKS 2155-304
	$\lvert c^{(8)}_{(I)00}\rvert$	$<9 \times 10^{-13}$ GeV^{-4}	GRB 021206
	$c^{(8)}_{(I)00}$	$<9.2 \times 10^{-23}$ GeV^{-4}	GRB 080916C

the initial detection of low-energy photons. The high photon energies and the large redshift of $z = 4.35 \pm 0.15$ make this burst a sensitive probe of Lorentz violation. A conservative bound on the vacuum coefficients for Lorentz violation can be obtained using the 2σ lower limits for the energy and redshift. Performing the integral (145) for $d = 6$ and assuming the lower energy is negligible, we find the constraint

$$\sum_{jm} {}_0Y_{jm}(147°, 120°) c^{(6)}_{(I)jm} < 3.2 \times 10^{-20}\ \text{GeV}^{-2} \quad (147)$$

on a direction-dependent combination of operators for Lorentz violation of mass dimension $d = 6$. Taking instead operators of mass dimension $d = 8$, we obtain the constraint

$$\sum_{jm} {}_0Y_{jm}(147°, 120°) c^{(8)}_{(I)jm} < 2.6 \times 10^{-23}\ \text{GeV}^{-4}. \quad (148)$$

Note that these are one-sided bounds that suppose the higher-energy photons propagate more slowly and that disregard possible burst-timing structure from the source. Under the assumption that the observed time difference is due to Lorentz-violating effects, a careful study of the leading edge of the high-energy photons might also permit the derivation of a lower positive bound for each of the above coefficient combinations.

Another example is provided by the recent data obtained for the active galaxy PKS 2155-304 by the High Energy Stereoscopic System (HESS) [79]. This source has redshift $z = 0.116$ and a light curve spanning an energy range of a few TeV, with time delays of a few tens of seconds. The reported analysis places a constraint of 41 s TeV^{-2} at the 95% confidence level on dispersion effects quadratic in the energy. Performing the integral (145) as before and identifying the reported constraint with $(t_2 - t_1)/(E_2^2 - E_1^2)$ implies a conservative bound on a direction-dependent combination of vacuum coefficients for Lorentz violation with $d = 6$. We obtain

$$\left|\sum_{jm} {}_0Y_{jm}(330°, -30°) c^{(6)}_{(I)jm}\right| < 7.4 \times 10^{-22}\ \text{GeV}^{-2} \quad (149)$$

at the 95% confidence level. A more complete study of the existing data from this source could yield additional constraints involving operators of mass dimension $d \geq 8$.

The above analyses demonstrate that a single point source provides sensitivity to only a limited number of direction-dependent combinations of coefficients for Lorentz violation. Multiple sources are needed to access all coefficients for a given value of d. For example, there are 25 coefficients $c^{(6)}_{(I)jm}$ and 49 coefficients $c^{(8)}_{(I)jm}$, and so even when birefringence is neglected we see that a corresponding number of sources at different locations on the sky is required to constrain fully these coefficients and the corresponding types of Lorentz violation. Data from gamma-ray bursts and other burst sources obtained by existing telescopes, including Fermi, HESS, the Major Atmospheric Gamma-ray Imaging Cherenkov Telescope (MAGIC) [74], and the Very Energetic Radiation Imaging Telescope Array System (VERITAS) [80], or by future

telescopes such as the Advanced Gamma-ray Imaging System (AGIS) [81], the Cherenkov Telescope Array (CTA) [82], and the High Altitude Water Cherenkov Experiment (HAWC) [83], could be combined to measure completely the coefficients $c^{(d)}_{(I)jm}$ for various fixed values of $d \geq 6$.

In contrast, in the limit of rotation invariance we recover the vacuum isotropic model, which reduces the number of coefficients to one for each d. This implies that a single source suffices to place constraints when only one value of d is considered at a time. For example, in the vacuum isotropic model a single constraint $<10^{-22}$ GeV^{-2} in any location on the sky suffices to exclude the suggestion of a signal for $d = 6$ Lorentz violation from Markarian 501, whereas the general SME treatment requires at least 25 independent sources at this constraint level. For the limiting case of the vacuum isotropic model, the above bounds from Fermi reduce to the one-sided constraints

$$c^{(6)}_{(I)00} < 1.1 \times 10^{-19}\ \text{GeV}^{-2}, \tag{150}$$

and

$$c^{(8)}_{(I)00} < 9.2 \times 10^{-23}\ \text{GeV}^{-4}, \tag{151}$$

while the one from HESS reduces to

$$|c^{(6)}_{(I)00}| < 2.6 \times 10^{-21}\ \text{GeV}^{-2}. \tag{152}$$

Both the isotropic and the anisotropic constraints obtained from GRB 080916C and PKS 2155-304 are also included in Table XIII.

B. Birefringence tests

In birefringent scenarios, the two eigenmodes propagate at slightly different velocities. This implies that the superposition of the modes is altered as light propagates in free space. Since the two modes differ in polarization, the change in superposition causes a change in the net polarization of the radiation. This provides a signature of Lorentz violation. In the present subsection, we outline the theory of these polarization changes and discuss birefringence tests based on polarimetry using both point sources and the CMB.

1. Theory

The direction of a Stokes vector $\boldsymbol{s} = (s^1, s^2, s^3)^T$ in the abstract Stokes-parameter space uniquely characterizes the polarization of the associated plane wave [84]. A Stokes vector in the s^1-s^2 plane corresponds to linear polarization, while a Stokes vector along the s^3 axis represents circular polarization. Other directions represent general elliptical polarizations.

In this picture, birefringence can be understood as a rotation of the Stokes vector $\boldsymbol{s} = (s^1, s^2, s^3)^T$ about the birefringence axis $\boldsymbol{\varsigma} = (\varsigma^1, \varsigma^2, \varsigma^3)^T$. The birefringence axis represents the polarization of the eigenmodes and is determined by the properties of the medium. The total angle of rotation is equivalent to the change in the relative phase between the two eigenmodes. With the normalization adopted in Eq. (81), we can write this rotation in differential form:

$$d\boldsymbol{s}/dt = 2E\boldsymbol{\varsigma} \times \boldsymbol{s} = -i\Sigma \cdot \boldsymbol{s}, \tag{153}$$

where E is the photon energy and $\Sigma^{jk} = -2iE\epsilon^{jkl}\varsigma^l$ represents the rotation generators.

Some basic features of birefringence in the context of Lorentz violation can be extracted from this picture [11]. If CPT is conserved, then $\boldsymbol{\varsigma}$ lies in the s^1-s^2 plane, and so the birefringent eigenmodes are linearly polarized. Linearly polarized radiation therefore typically rotates out of the s^1-s^2 plane and becomes elliptically polarized. Similarly, circularly polarized radiation rotates away from the s^3 axis, becomes elliptical, and may eventually rotate through a linear polarization. In contrast, if CPT is violated, then the birefringent eigenmodes are circularly polarized with one being left-handed and the other right-handed. The rotation axis $\boldsymbol{\varsigma}$ is therefore aligned with the s^3 axis in this case. As a result, linear polarizations remain linear, but a change in the linear-polarization angle occurs. However, circular polarizations remain circular because they are eigenmodes of the propagation.

In a typical application, one considers a distant source of polarized light and integrates the rotation (153) from emission to detection. This yields changes in polarization that can depend on both energy and direction of propagation. To search for birefringence, we can either model the polarization at the source and seek discrepancies in the observed polarization, or we can test for unexpected energy dependence in the polarization parameters.

Since we are characterizing Lorentz violation using spin-weighted spherical coefficients, it is convenient to reformulate the rotation of the Stokes vector in terms of spin-weighted Stokes parameters. We can decompose the components of the Stokes vector according to their spin weight with respect to the line of sight $\hat{\boldsymbol{n}}$. This yields $s_{(0)} = s^3$ as a Stokes parameter of spin weight 0 and $s_{(\pm 2)} = s^1 \mp is^2$ as two Stokes parameters having spin weight ± 2.

In the Stokes basis with $\boldsymbol{s} = (s_{(+2)}, s_{(0)}, s_{(-2)})^T$, the rotation generators are given in matrix form as

$$\Sigma = 2E \begin{pmatrix} \varsigma_{(0)} & -\varsigma_{(+2)} & 0 \\ -\frac{1}{2}\varsigma_{(-2)} & 0 & \frac{1}{2}\varsigma_{(+2)} \\ 0 & \varsigma_{(-2)} & -\varsigma_{(0)} \end{pmatrix}. \tag{154}$$

Here, $\boldsymbol{\varsigma} = (\varsigma_{(+2)}, \varsigma_{(0)}, \varsigma_{(-2)})^T$ is the birefringence axis in this basis, with components given by

$$\begin{aligned} \varsigma_{(\pm 2)} &= \sum_{djm} E^{d-4}\, {}_{\pm 2}Y_{jm}(\hat{\boldsymbol{n}})(k^{(d)}_{(E)jm} \pm ik^{(d)}_{(B)jm}), \\ \varsigma_{(0)} &= \sum_{djm} E^{d-4}\, {}_{0}Y_{jm}(\hat{\boldsymbol{n}})k^{(d)}_{(V)jm}. \end{aligned} \tag{155}$$

Since the rotation of the Stokes vector is determined by the combination $E\mathfrak{s}$, the effects of birefringence enter with an energy dependence of E^{d-3}. This implies that an increased sensitivity to coefficients with $d > 3$ can be achieved by using higher-energy photons. We also see that unconventional energy dependence is a signal for Lorentz violation. Only the $d = 3$ case leads to energy-independent birefringence.

For many astrophysical sources, cosmological expansion is significant during the time of flight and must be incorporated in the analysis. We implement this by expressing the differential rotation in terms of redshift:

$$d\boldsymbol{s} = \frac{i\Sigma_z \cdot \boldsymbol{s}}{(1+z)H_z}dz, \tag{156}$$

where Σ_z represents the rotation matrix at the blueshifted energy $(1+z)E$ and source direction $\hat{\boldsymbol{n}}$. To obtain the net polarization change, we then integrate this expression from source redshift z to 0.

Some searches for Lorentz violation investigate Lorentz-violating operators of a specified mass dimension d. With this assumption, the calculation of the net rotation is simplified because the energy integral is independent of the matrix multiplication. In the CPT-odd case with a single odd value of d, the rotations of the Stokes vector about the s^3 axis lead to a change in the linear-polarization angle ψ without affecting the degree of linear or circular polarization. The rotation is diagonal in the spin-weighted basis, and we obtain the simple result

$$s_{(\pm 2)} = e^{\mp i 2\delta\Psi_z} s_{(\pm 2)z}, \qquad s_{(0)} = s_{(0)z}, \tag{157}$$

relating the present-day polarization to the original polarization at redshift z. Here, the change $\delta\Psi_z$ in polarization is given by the integral

$$\delta\Psi_z = E^{d-3}\int_0^z \frac{(1+z)^{d-4}}{H_z}dz \sum_{jm}{}_0Y_{jm}(\hat{\boldsymbol{n}})k^{(d)}_{(V)jm}. \tag{158}$$

The linear-polarization angle ψ at the present epoch is then related through

$$\psi = \psi_z + \delta\Psi_z \tag{159}$$

to the blueshifted angle ψ_z.

In the CPT-even case with a single even value of d, the eigenmodes are linearly polarized and the rotation is more complicated. It is convenient in this case to define the direction-dependent phase

$$e^{-i\xi(\hat{\boldsymbol{n}})} = \frac{\mathfrak{s}_{(+2)}(\hat{\boldsymbol{n}})}{|\mathfrak{s}_{(+2)}(\hat{\boldsymbol{n}})|}, \tag{160}$$

which controls the evolution of the polarization. The phase angle ξ is twice the polarization angle of the eigenmode of propagation. Consequently, linear polarizations with angle $\psi = \xi/2$ or $\psi = \xi/2 + 90°$ remain unaffected as the radiation propagates. Calculation shows that the redshift integral can be expressed using this phase and the angle

$$\Phi_z = E^{d-3}\int_0^z \frac{(1+z)^{d-4}}{H_z}dz \times \left|\sum_{jm}{}_2Y_{jm}(\hat{\boldsymbol{n}})(k^{(d)}_{(E)jm} \pm ik^{(d)}_{(B)jm})\right|. \tag{161}$$

The net rotation is given by

$$\boldsymbol{s} = m_z \cdot \boldsymbol{s}_z, \tag{162}$$

where the Müller matrix m_z takes the form

$$m_z = \begin{bmatrix} \cos^2\Phi_z & -i\sin 2\Phi_z e^{-i\xi} & \sin^2\Phi_z e^{-2i\xi} \\ -\frac{i}{2}\sin 2\Phi_z e^{i\xi} & \cos 2\Phi_z & \frac{i}{2}\sin 2\Phi_z e^{-i\xi} \\ \sin^2\Phi_z e^{2i\xi} & i\sin 2\Phi_z e^{i\xi} & \cos^2\Phi_z \end{bmatrix} \tag{163}$$

in the spin-weighted Stokes basis.

2. Point sources

We next use the above theoretical results to obtain bounds on spherical coefficients from polarimetry of astrophysical point sources. Some of the tightest existing constraints on Lorentz violation have been achieved in birefringence searches involving high-frequency sources such as gamma-ray bursts [21,72,76,85]. However, point sources have the disadvantage that a single line of sight $\hat{\boldsymbol{n}}$ is involved, which provides sensitivity to only a restricted portion of the space of coefficients for Lorentz violation. As with astrophysical dispersion tests, multiple sources are therefore required to perform a comprehensive search, even for a fixed value of d. For example, for the case of $d = 3$ a multiple-source search involving a large number of radio galaxies [19] has placed a limit on a quantity $p_\alpha \equiv -2(k^{(3)}_{AF})_\alpha$ corresponding to the constraint

$$\left|\sum_{jm}{}_0Y_{jm}k^{(3)}_{(V)jm}\right| < 6\times 10^{-43}\ \text{GeV} \tag{164}$$

at the 95% confidence level in terms of spherical coefficients. In the isotropic limit, this gives the limit $k^{(3)}_{(V)00} < 2\times 10^{-42}$ GeV, although sharper bounds have recently emerged from CMB polarimetry as discussed below. Multiple-source searches for the case of $d = 4$ have also been performed [11,20,21,23]. For example, a search using 16 sources [11] places a limit that translates in the present context to the rotationally invariant constraint

$$\sqrt{\sum_m (|k^{(4)}_{(E)2m}|^2 + |k^{(4)}_{(B)2m}|^2)} < 5\times 10^{-32} \tag{165}$$

at the 95% confidence level. For larger values of d, multiple-source birefringence analyses offer excellent prospects for systematic tests of Lorentz violation at extreme sensitivity.

In this subsection, we illustrate the procedure and obtain first constraints on some spherical coefficients with larger d, by analyzing the recent evidence for significant polarized components in the radiation from the gamma-ray bursts GRB 930131 and GRB 960924 [86]. Observations of gamma rays associated with these two sources suggest that they are polarized at levels of $\Pi_{930131} > 35\%$ and $\Pi_{960924} > 50\%$, respectively. Ideally, if we knew the degree of polarization and polarization angles at the source, we could search directly for changes due to birefringence. Without this information, however, we can still place limits on decoherence effects caused by birefringence. The point is that significant birefringence would lead to large differences in observed polarizations at slightly different frequencies, effectively unpolarizing the radiation. Evidence for polarization can therefore be used to constrain the frequency-dependent birefringence caused by violations with dimension $d > 3$.

Figures 2 and 3 show the calculated effective degrees of polarization and the changes in the polarization angles for the above two gamma-ray bursts in scenarios with nonzero spherical coefficients corresponding to *CPT*-odd Lorentz-violating operators of mass dimensions $d = 5$, 7, 9. In constructing these plots, we assume the radiation is initially 100% linearly polarized, which is a maximally conservative assumption in the present context. The displayed results are then obtained by numerically calculating the change in the effective polarization $\Pi_{\rm eff} = \sqrt{\langle s^1\rangle^2 + \langle s^2\rangle^2}$ smeared over observed frequencies, following the basic procedure outlined in Ref. [21]. The shaded regions in Figs. 2 and 3 show the ranges of coefficient space that

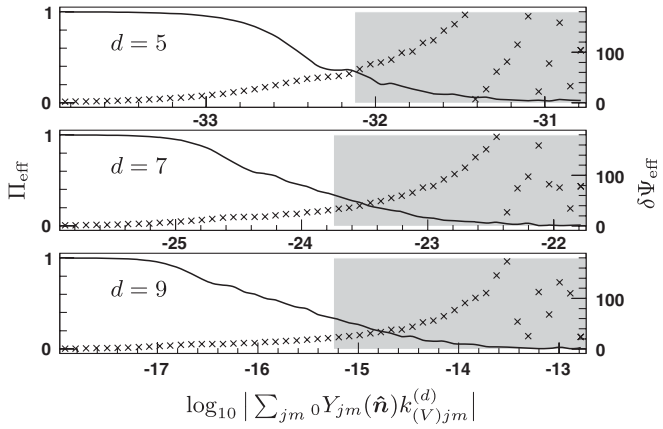

FIG. 2. Spectropolarimetry bounds from GRB 930131 on spherical coefficients corresponding to Lorentz-violating operators of mass dimensions $d = 5$, 7, 9. The source direction is given by the angles $\hat{\boldsymbol{n}} = (98.2°, 182.1°)$. The solid curve represents the effective degree of polarization $\Pi_{\rm eff} = \sqrt{\langle s^1\rangle^2 + \langle s^2\rangle^2}$. The effective polarization angle $\psi_{\rm eff} = \tan^{-1}\langle s^2\rangle/2\langle s^1\rangle$ in degrees is displayed with crosses. The shaded area is the disallowed region with $\Pi_{\rm eff} < 35\%$. All coefficients are in units of GeV^{4-d}.

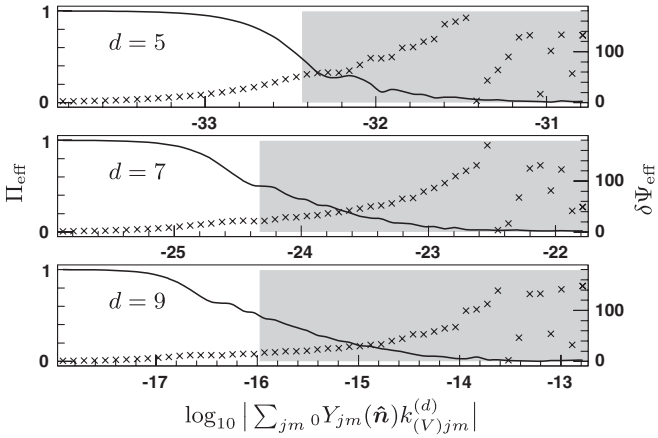

FIG. 3. Spectropolarimetry bounds from GRB 960924 on spherical coefficients corresponding to Lorentz-violating operators of mass dimensions $d = 5$, 7, 9. The source direction is given by the angles $\hat{\boldsymbol{n}} = (87.3°, 37.3°)$. The solid curve represents the effective degree of polarization $\Pi_{\rm eff} = \sqrt{\langle s^1\rangle^2 + \langle s^2\rangle^2}$. The effective polarization angle $\psi_{\rm eff} = \tan^{-1}\langle s^2\rangle/2\langle s^1\rangle$ in degrees is displayed with crosses. The shaded area is the disallowed region with $\Pi_{\rm eff} < 50\%$. All coefficients are in units of GeV^{4-d}.

are excluded by the observation of polarization in the radiation from these sources. Coefficients lying in these regions would cause depolarization beyond what is observed. The resulting constraints for the vacuum coefficients and for the limiting case of the vacuum isotropic model are summarized in Table XIV.

In the *CPT*-even case, the linear polarization of the source could in principle coincide with one of the eigenmodes of propagation. This situation occurs when the phase angle $\xi(\hat{\boldsymbol{n}})$ is twice the initial polarization angle ψ_0, as discussed above. Consequently, the results for any given point source contain unbounded regions of coefficient space, and so definitive constraints on the spherical coefficients cannot be obtained. However, the analysis does achieve high sensitivities to Lorentz violation in certain regions of coefficient space. Figures 4 and 5 show the portions of coefficient space excluded by the observations of GRB 930131 and GRB 960924 for *CPT*-even operators of mass dimensions $d = 4$, 6, 8 [87]. The shaded areas in these figures represent disallowed regions. Their shape and extent demonstrates that part of the coefficient space is excluded at high sensitivity, while emphasizing the need for simultaneous analysis of multiple sources to obtain definitive constraints. The approximate sensitivities to the vacuum coefficients achieved from the two sources are summarized in Table XIV.

The above examples show that high-frequency polarimetry of gamma-ray bursts has the ability to probe Lorentz violation at extreme sensitivity. The use of multiple sources offers the potential to constrain all of the vacuum coefficients $k^{(d)}_{(E)jm}$, $k^{(d)}_{(B)jm}$, and $k^{(d)}_{(V)jm}$ associated

TABLE XIV. Constraints on spherical coefficients from polarization observations of the gamma-ray bursts GRB 930131 and GRB 960924. The first three rows give constraints on the vacuum coefficients for the *CPT*-odd cases with $d = 5, 7, 9$. The arguments of the spherical harmonics are $\hat{\boldsymbol{n}} = (98.2°, 182.1°)$ for GRB 930131 and $\hat{\boldsymbol{n}} = (87.3°, 37.3°)$ for GRB 960924. The next three rows give the constraints on coefficients in the isotropic limit, for which there is exactly one nonzero coefficient for each d. The final three rows give the approximate sensitivities achieved for vacuum coefficients in the *CPT*-even cases with $d = 4, 6, 8$. Unlike the constraints in the first six rows, the results in the final three rows cannot be interpreted as definitive bounds because the amount of birefringence in the *CPT*-even case depends on details of the source polarization. All constraints are at the 95% confidence level.

Model	Coefficients	GRB 930131	GRB 960924
Vacuum	$\lvert\sum_{jm\,0} Y_{jm}(\hat{\boldsymbol{n}}) k^{(5)}_{(V)jm}\rvert$	$<7\times10^{-33}$ GeV^{-1}	$<4\times10^{-33}$ GeV^{-1}
	$\lvert\sum_{jm\,0} Y_{jm}(\hat{\boldsymbol{n}}) k^{(7)}_{(V)jm}\rvert$	$<2\times10^{-24}$ GeV^{-3}	$<5\times10^{-25}$ GeV^{-3}
	$\lvert\sum_{jm\,0} Y_{jm}(\hat{\boldsymbol{n}}) k^{(9)}_{(V)jm}\rvert$	$<6\times10^{-16}$ GeV^{-5}	$<1\times10^{-16}$ GeV^{-5}
Vacuum isotropic	$\lvert k^{(5)}_{(V)00}\rvert$	$<2\times10^{-32}$ GeV^{-1}	$<1\times10^{-32}$ GeV^{-1}
	$\lvert k^{(7)}_{(V)00}\rvert$	$<7\times10^{-24}$ GeV^{-3}	$<2\times10^{-24}$ GeV^{-3}
	$\lvert k^{(9)}_{(V)00}\rvert$	$<2\times10^{-15}$ GeV^{-5}	$<4\times10^{-16}$ GeV^{-5}
Vacuum	$\lvert\sum_{jm\,2} Y_{jm}(\hat{\boldsymbol{n}})(k^{(4)}_{(E)jm} + ik^{(4)}_{(B)jm})\rvert$	$\lesssim 10^{-37}$	$\lesssim 10^{-37}$
	$\lvert\sum_{jm\,2} Y_{jm}(\hat{\boldsymbol{n}})(k^{(6)}_{(E)jm} + ik^{(6)}_{(B)jm})\rvert$	$\lesssim 10^{-29}$ GeV^{-2}	$\lesssim 10^{-29}$ GeV^{-2}
	$\lvert\sum_{jm\,2} Y_{jm}(\hat{\boldsymbol{n}})(k^{(8)}_{(E)jm} + ik^{(8)}_{(B)jm})\rvert$	$\lesssim 10^{-20}$ GeV^{-4}	$\lesssim 10^{-20}$ GeV^{-4}

with leading-order birefringent Lorentz violation at large d. In the *CPT*-odd case, the limits can completely constrain the single vacuum isotropic coefficient at each odd d because the direction of propagation is irrelevant.

The power of this type of analysis is apparent in comparing the sensitivities in Table XIV to those achieved via the astrophysical dispersion tests discussed in Sec. VI A. For $d = 6$, the polarimetry of gamma-ray bursts attains a sensitivity roughly a million times beyond that of the dispersion tests involving Markarian 501, despite the million-fold difference in energy. This confirms the suitability of dispersion tests to constrain instead only the vacuum coefficients $c^{(d)}_{(I)jm}$, which are associated with Lorentz-violating operators that have no leading-order birefringence.

3. CMB tests

In principle, an extended source can provide access to all birefringent Lorentz-violating operators and hence bypass the major limitation of point sources described above. A prime example of an extended source is the CMB. Since the CMB is the oldest observable untainted radiation and hence represents the longest available baseline, an analysis

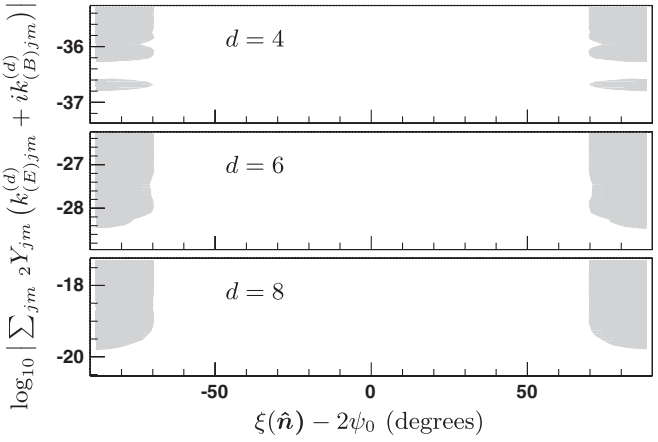

FIG. 4. Spectropolarimetry bounds from GRB 930131 on spherical coefficients corresponding to Lorentz-violating operators of mass dimensions $d = 4, 6, 8$. The source direction is given by the angles $\hat{\boldsymbol{n}} = (98.2°, 182.1°)$. The shaded area is the disallowed region with $\Pi_{\text{eff}} < 35\%$. All coefficients are in units of GeV^{4-d}.

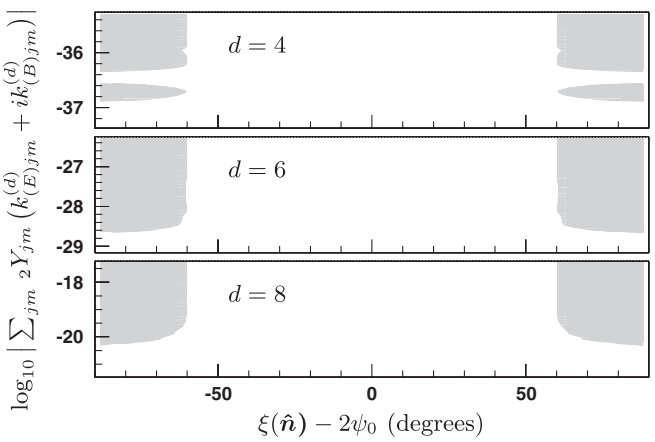

FIG. 5. Spectropolarimetry bounds from GRB 960924 on spherical coefficients corresponding to Lorentz-violating operators of mass dimensions $d = 4, 6, 8$. The source direction is given by the angles $\hat{\boldsymbol{n}} = (87.3°, 37.3°)$. The shaded area is the disallowed region with $\Pi_{\text{eff}} < 50\%$. All coefficients are in units of GeV^{4-d}.

of CMB polarization might be expected to yield high sensitivities to Lorentz violation. However, this expectation may fail for operators at larger d due to the comparatively low CMB frequencies. Nonetheless, the CMB does provide interesting opportunities for lower-dimensional violations, and, in particular, it is the best available source for studies of coefficients with $d = 3$. In this subsection, we discuss and illustrate some of the unusual features that can arise in the CMB in the event of significant birefringence [22,23,88].

The accepted description of the CMB uses a decomposition of the temperature T and the Stokes parameters into spin-weighted spherical harmonics [59], analogous to the discussion in Sec. IV C. Typically, power spectra are introduced to characterize the strength of each mode and the correlations between them, according to

$$C_j^{X_1X_2} = \frac{1}{2j+1}\sum_m \langle (a_{jm}^{(X_1)})^* a_{jm}^{(X_2)}\rangle, \tag{166}$$

where X_1, X_2 range over T, E, B, V and where $a_{jm}^{(X)}$ are the coefficients in the spherical-harmonic expansion of X. While temperature anisotropies have been firmly established, the detection of polarization in the CMB by several experiments [89–92] is of more significance in the present context.

In the conventional Lorentz-invariant picture, temperature and density fluctuations at recombination provide the necessary anisotropies to produce a net polarization [93]. In addition, these processes lead to a correlation between temperature and the E-parity component of the CMB. The E component makes up only a tiny fraction of approximately 10^{-6} of the total radiation. Several measurements of this small degree of polarization have been made. The B-type polarization is expected to be even smaller and uncorrelated with temperature. The standard picture predicts no significant V polarization because Thomson scattering produces only linear polarization.

The presence of Lorentz violation may alter many of the above properties. It can introduce unexpected types of polarization, and it can induce mixing between initially uncorrelated modes during the nearly 14×10^9 years of propagation. The associated violations of rotational symmetry can also cause mixing across multipoles in j and m, including for modes of the same polarization type. Here, we provide a discussion of general features based on a numerical survey of some Lorentz-violating models exhibiting these effects. The calculations parallel those presented in Refs. [22,23].

Some qualitative features can be determined directly using the intuition provided by the Stokes rotations described in Sec. VI B 1. For example, the vacuum coefficients $k_{(V)jm}^{(d)}$ are associated with CPT-violating operators and produce local rotations of the Stokes vector about the s^3 axis. This causes a global mixing of the linearly polarized E and B modes. The result can be unconventionally large B polarization, although no circular V modes can appear. In contrast, the vacuum coefficients $k_{(E)jm}^{(d)}$ and $k_{(B)jm}^{(d)}$ associated with CPT-even operators cause both mixing between E and B modes and also the emergence of V modes, since in this case the Stokes vector rotates out of the s^1-s^2 plane. Consequently, mixing between the three types of polarization are possible in this scenario, although details of the mixing depend strongly on the specifics of the Lorentz-violating operators involved.

Other key features that may be present for some types of violations include dependences on the photon frequency and birefringence varying with the direction of propagation. Only the $d = 3$ vacuum coefficients lead to frequency-independent rotations. Also, only the $j = 0$ coefficients generate direction-independent rotations. Consequently, the isotropic vacuum coefficient $k_{(V)00}^{(3)}$ provides a particularly simple special case. It causes a frequency-independent mixing that is uniform across the sky and that leads to a simple rotation between E and B modes. Using Eq. (158), we estimate this rotation for CMB radiation to be

$$\delta\Psi \simeq k_{(V)00}^{(3)} 10^{43}\ \text{degree/GeV}. \tag{167}$$

Simple frequency-independent rotations of this type have been considered by several groups [22,23,94–99], and the existing measurements are listed as part of Table XV. Figure 6 illustrates the type of mixing that results. We see that initial E power partially rotates into B power. Also, the initial TE correlation induces a TB correlation. Furthermore, since the B polarization is generated from the original E polarization, these two modes become correlated and so a significant EB component emerges.

Other isotropic rotations from CPT-odd operators of larger d, such as the one associated with the isotropic

TABLE XV. Constraints on spherical coefficients with $d = 3$ from CMB studies. The table lists some existing 1-σ results for the scalar magnitude $|\boldsymbol{k}_{AF}^{(3)}|$ defined in Eq. (168) and for the isotropic component $k_{(V)00}^{(3)}$, all obtained via CMB analyses. Constraints on these quantities from other sources are compiled in the data tables of Ref. [6].

Coefficients	Result	Reference
$\lvert\boldsymbol{k}_{AF}^{(3)}\rvert$	$(15 \pm 6) \times 10^{-43}$ GeV	[22]
	$(10^{+4}_{-8}) \times 10^{-43}$ GeV	[23]
$k_{(V)00}^{(3)}$	$(6.0 \pm 4.0) \times 10^{-43}$ GeV	[94]
	$(2.5 \pm 3.0) \times 10^{-43}$ GeV	[95]
	$(12 \pm 7) \times 10^{-43}$ GeV	[22]
	$(1.2 \pm 2.2) \times 10^{-43}$ GeV	[96]
	$(2.6 \pm 1.9) \times 10^{-43}$ GeV	[97]
	$<2.5 \times 10^{-43}$ GeV	[98]
	$(2.3 \pm 5.4) \times 10^{-43}$ GeV	[23]
	$(-1.4 \pm 0.9 \pm 0.5) \times 10^{-43}$ GeV	[99]

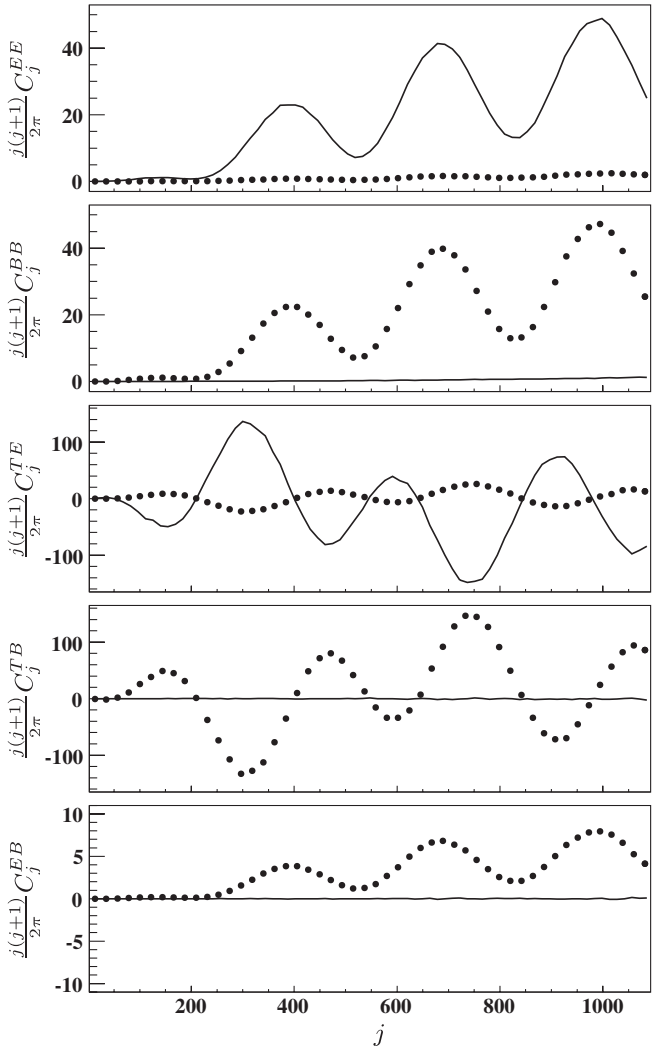

FIG. 6. Correlation spectra for isotropic *CPT*-odd Lorentz violation. Circles show the effects of Lorentz violation due to the spherical coefficient $k^{(3)}_{(V)00} = 12 \times 10^{-42}$ GeV, while lines show the Lorentz-invariant case. Power is transferred from E to B, and an EB correlation is generated. Also, the initial TE correlation induces a TB correlation. As expected for *CPT*-odd Lorentz violation, no significant V polarization or correlation appears. The coefficients C_j have units of $\mu\mathrm{K}^2$.

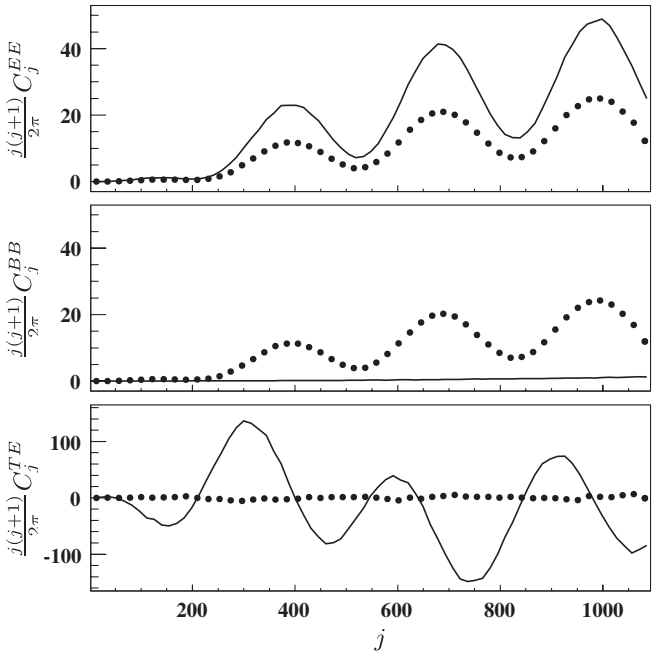

FIG. 7. Correlation spectra for anisotropic *CPT*-odd Lorentz violation. Circles show the effects of Lorentz violation due to a large value of the spherical coefficient $k^{(3)}_{(V)10} = 64 \times 10^{-42}$ GeV, while lines show the Lorentz-invariant case. Power is transferred from E to B, and a loss of TE correlation is evident. As expected for *CPT*-odd Lorentz violation, no significant V polarization or correlation appears. The coefficients C_j have units of $\mu\mathrm{K}^2$.

vacuum coefficient $k^{(5)}_{(V)00}$, lead to similar effects. However, the frequency dependence introduced by coefficients at larger d implies that the amount of rotation depends on the photon frequency. Spectral signatures of this type should be accessible to observations having sensitivity to a wide range of frequencies.

Any *CPT*-odd Lorentz-violating operator with nonzero j produces direction-dependent rotations. An example is shown in Fig. 7, where a comparatively large value of the anisotropic vacuum coefficient $k^{(3)}_{(V)10}$ has been chosen to illustrate the effects. While the local polarization rotations are similar to those from the presence of a nonzero $k^{(3)}_{(V)00}$, the anisotropies in this case cause the correlations to disappear globally. The effects saturate for large rotations, and the net result is roughly equal amounts of E and B. The overall degree of polarization is unaltered, and there is little correlation between any two modes.

Birefringent operators that are *CPT*-even are necessarily both frequency dependent and anisotropic, resulting in similar behavior to the previous case. However, a distinctive feature of *CPT*-even violations is the mixing of linear and circular polarizations. Figure 8 illustrates the generation of V polarization in the presence of a nonzero vacuum coefficient $k^{(4)}_{(E)20}$. In this case, we find that the anisotropic mixing causes a depletion of E polarization, which is rotated into roughly comparable amounts of B and V polarization. As in the case of nonzero $k^{(3)}_{(V)10}$ and indeed in all cases we have studied involving nonzero coefficients with $j \neq 0$, the anisotropic effects tend to deplete correlations when Lorentz violations are large.

Our survey reveals that similar features as those illustrated above also recur for other vacuum coefficients for Lorentz violation that control birefringent operators. We thereby find that generic signals of Lorentz violation in the CMB can incorporate one or more of the following basic features: (a) a depletion in the EE and TE spectra; (b) the

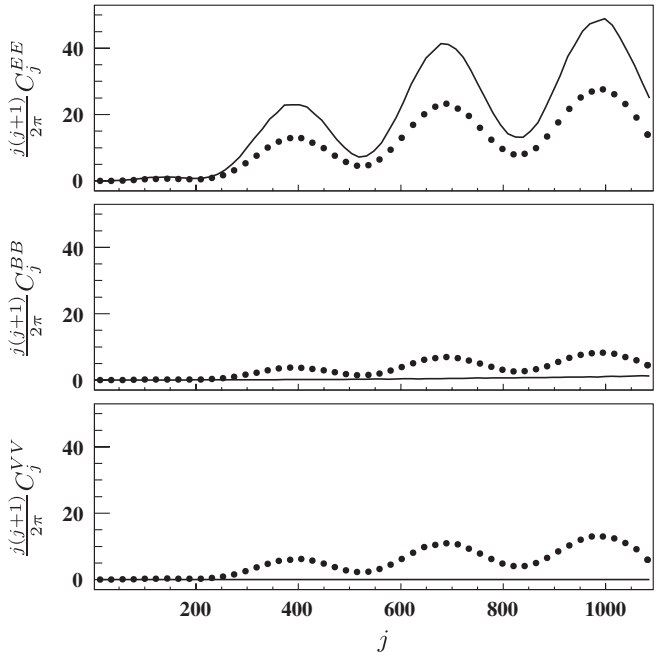

FIG. 8. Correlation spectra for anisotropic *CPT*-even Lorentz violation at photon frequency $\omega = 380$ GHz. Circles show the effects of Lorentz violation due to a large value of the spherical coefficient $k^{(4)}_{(E)20} = 16 \times 10^{-29}$, while lines show the Lorentz-invariant case. Power is transferred from E to B and V, while no significant correlations appear. The coefficients C_j have units of $\mu\mathrm{K}^2$.

introduction of unconventionally large B polarization; (c) the appearance of TB or EB correlations; (d) the development of significant V polarization; and (e) frequency dependences of the power spectra.

None of these basic features is readily apparent in the observed data, which suggests that any Lorentz violation in the CMB must be small. A study of the high-frequency BOOMERANG data [91] places constraints on several of the vacuum coefficients with $d \leq 6$, finding some evidence for nonzero Lorentz violation [22]. A more recent analysis of the $d = 3$ coefficients using the five-year data from the Wilkinson Microwave Anisotropy Probe [90] finds no evidence for isotropic violations involving the coefficient $k^{(3)}_{(V)00}$, but uncovers some support for nonzero anisotropic vacuum coefficients $k^{(3)}_{(V)1m}$ [23]. This study constrains the coefficients $k^{(3)}_{(V)jm}$ at the level of 10^{-43} GeV. For purposes of reporting constraints, the spherical coefficients with $d = 3$ can conveniently be separated into the isotropic component $k^{(3)}_{(V)00}$ and the scalar magnitude

$$|\boldsymbol{k}^{(3)}_{\boldsymbol{AF}}| = \frac{1}{\sqrt{4\pi}}(6|k^{(3)}_{(V)11}|^2 + 3|k^{(3)}_{(V)10}|^2)^{1/2}. \tag{168}$$

Table XV lists existing constraints on these quantities obtained from studies of the CMB. Other limits are given in the data tables of Ref. [6]. Improved sensitivities can be expected from future CMB data to be obtained by various experiments and missions including, for example, the Planck satellite [100], the Q/U Imaging Experiment (QUIET) [101], the CMBPol mission [102], the *E* and *B* Experiment (EBEX) [103], the Experimental Probe of Inflationary Cosmology (EPIC) [104], and the Spider balloon observatory [105].

VII. CAVITY EXPERIMENTS

Laboratory experiments provide alternative methods to search for Lorentz violation in electrodynamics and have the ability to probe many coefficients inaccessible in astrophysical searches. The most common Earth-based tests are contemporary versions of the classic Michelson-Morley [1] and Kennedy-Thorndike [2] experiments and are based on electromagnetic resonant cavities [12–17]. In this section, we discuss possible laboratory studies of the effects of Lorentz-violating operators of arbitrary mass dimension d. We outline a theoretical approach for determining the resonance frequency of a cavity in the presence of Lorentz violation. The approach is illustrated by applying it in the context of the camouflage model, for which the Lorentz violation has no leading-order birefringent or dispersive effects in astrophysical photon propagation. As a specific example of the techniques, we derive an explicit result for the fractional frequency shift of the TM_{010} mode in a cylindrical cavity with circular cross section, including the time dependence induced in the signal by the rotation of the Earth. While we focus specifically on resonant cavities, many of the ideas discussed here are generic and can be applied in the context of other laboratory-based experiments, including space-based missions such as the Atomic Clock Ensemble in Space (ACES) [106] or the Space and Time Anisotropy Tests (STAT) combining the former Space Time Asymmetry Research (STAR) and OPTIS missions [107].

A. General theory

The strategy behind many laboratory tests of Lorentz invariance is a search for minute variations in some observable with changes in the orientation or velocity of the apparatus. For cavity experiments, a suitable observable is typically the fractional frequency shift $\delta\nu/\nu$ induced by the Lorentz violation [11]. At leading order in coefficients for Lorentz violation, the fractional frequency shift takes the generic form $\delta\nu/\nu = \sum_{jm} \mathcal{M}_{jm}\mathcal{K}_{jm}$, where $\mathcal{M}_{jm}$ is an experiment-dependent matrix factor and $\mathcal{K}_{jm}$ represents the relevant spherical coefficients for Lorentz violation discussed in Sec. III.

Normally the experiment-dependent matrix factors are determined in a cavity frame that is fixed with respect to the system in question. In this frame, the matrices are denoted $\mathcal{M}^{\mathrm{cav}}_{jm}$ and are constant. However, since this frame

is noninertial, the cavity-frame coefficients $\mathcal{K}^{\rm cav}_{jm}$ for Lorentz violation vary with changes in the orientation and velocity of the apparatus with respect to the standard Sun-centered frame. In practice, boost effects are suppressed by one or more powers of the typically small velocities $\sim 10^{-4}$ involved, so for simplicity in what follows we neglect boost effects and focus on violations of rotation invariance.

The rotations relating spherical coefficients in the cavity, laboratory, and Sun-centered frames are given in Eqs. (139) and (142). Since the rotation between the cavity frame and the laboratory frame is often constant, it is convenient to define laboratory-frame matrices $\mathcal{M}^{\rm lab}_{jm}$ via

$$\mathcal{M}^{\rm lab}_{jm} = \sum_{m'} \mathcal{M}^{\rm cav}_{jm'} D^{(j)}_{m'm}(-\gamma, -\beta, -\alpha). \tag{169}$$

In terms of these and the spherical coefficients in the Sun-centered frame, the fractional frequency shift takes the form

$$\frac{\delta\nu}{\nu} = \sum_{jmm'} \mathcal{M}^{\rm lab}_{jm} e^{im\phi} e^{im'\omega_\oplus T_\oplus} d^{(j)}_{mm'}(-\chi) \mathcal{K}^{\rm Sun}_{jm'}, \tag{170}$$

which explicitly reveals the sidereal dependence. For experiments involving turntables, where the cavity and laboratory frames rotate relative to each other, the variations resulting from the turntable rotation are incorporated through the phase $\phi = \omega_{\rm tt} T_{\rm tt}$.

Manipulation of the modified Maxwell equations (16) leads to a perturbative estimate for the fractional frequency shift given by [11]

$$\begin{aligned}\frac{\delta\nu}{\nu} &\approx -\frac{1}{4\langle U\rangle}\int d^3x (\boldsymbol{E}^*\cdot\boldsymbol{\delta D} - \boldsymbol{B}^*\cdot\boldsymbol{\delta H}) \\ &= \frac{1}{8\langle U\rangle}\int d^3x F^*_{\mu\nu}(\delta G)^{\mu\nu},\end{aligned} \tag{171}$$

where

$$\langle U\rangle = \frac{1}{4}\int d^3x (\boldsymbol{E}^*\cdot\boldsymbol{D} + \boldsymbol{B}^*\cdot\boldsymbol{H}) \tag{172}$$

is the unperturbed energy inside the resonator. This formulation allows for a general linear and lossless medium inside the cavity in addition to modifications due to Lorentz violation. The fields $\boldsymbol{E}$, $\boldsymbol{B}$, $\boldsymbol{D}$, and $\boldsymbol{H}$ are understood to be solutions of conventional electrodynamics in the absence of Lorentz violation, while

$$\begin{aligned}\boldsymbol{\delta D} &= \hat\kappa_{DE}\cdot\boldsymbol{E} + \hat\kappa_{DB}\cdot\boldsymbol{B} + 2\hat{\boldsymbol{k}}_{\boldsymbol{AF}}\times\boldsymbol{A}, \\ \boldsymbol{\delta H} &= \hat\kappa_{HE}\cdot\boldsymbol{E} + \hat\kappa_{HB}\cdot\boldsymbol{B} - 2(\hat k_{AF})_0\boldsymbol{A} + 2\hat{\boldsymbol{k}}_{\boldsymbol{AF}}A_0\end{aligned} \tag{173}$$

represent leading-order perturbations to the $\boldsymbol{D}$ and $\boldsymbol{H}$ fields due to Lorentz violation. The result (171) assumes that the fields vanish outside the cavity volume V. For simplicity in what follows, we suppose that the resonant modes under consideration are nondegenerate. In the case of degenerate resonances, Eq. (171) yields a weighted average value for the fractional frequency shift.

To express the fractional frequency shift in terms of the spherical coefficients introduced in Sec. III, we next convert to momentum space. However, some care is required to avoid divergences arising from discontinuities at the boundary of the cavity. This technical issue stems from the differential nature of the operators $\hat k_F$ and $\hat k_{AF}$. Although the fields are taken to be continuous throughout the interior volume V of the cavity, they may be discontinuous across the surrounding surface S. As a result, the fields may not be strictly differentiable over all space, and the derivatives in Eq. (173) may be associated with δ-function behavior on the surface S. The usual reciprocal nature of position and momentum spaces then leads to momentum-space representations that fail to vanish sufficiently rapidly at infinite momentum, which introduces divergences in the integral. This issue is absent in the minimal SME with $d = 3$ and $d = 4$ because no derivatives appear in the constitutive relations for that case, but it is endemic for Lorentz-violating operators with $d \geq 5$ and requires a procedure to eliminate the divergences.

One way to address this technical issue is to define new everywhere-differentiable fields $\underline{\boldsymbol{E}}$ and $\underline{\boldsymbol{B}}$ that are equal to $\boldsymbol{E}$ and $\boldsymbol{B}$ inside V but that may be nonzero in the region outside V where the original fields $\boldsymbol{E}$ and $\boldsymbol{B}$ vanish. We then have two sets of fields, both satisfying the Maxwell equations inside V. Derivatives of the extended fields $\underline{\boldsymbol{E}}$ and $\underline{\boldsymbol{B}}$ remain finite everywhere, including on the surface S of the cavity, but $\underline{\boldsymbol{E}}$ and $\underline{\boldsymbol{B}}$ need not satisfy the Maxwell equations outside the cavity. Using both sets of fields, we can construct a finite version of the fractional frequency shift (171) by replacing the fields in Eq. (173) with their extended versions. This procedure removes the divergences at the cavity boundaries.

Performing a Fourier transform, we obtain a convergent momentum-space expression for the fractional frequency shift (171) given by

$$\begin{aligned}\frac{\delta\nu}{\nu} = -\frac{1}{4\langle U\rangle}\int d^3p \Big(&\boldsymbol{E}^*\cdot\hat\kappa_{DE}\cdot\underline{\boldsymbol{E}} - \boldsymbol{B}^*\cdot\hat\kappa_{HB}\cdot\underline{\boldsymbol{B}} \\ &+ \boldsymbol{E}^*\cdot\hat\kappa_{DB}\cdot\underline{\boldsymbol{B}} - \boldsymbol{B}^*\cdot\hat\kappa_{HE}\cdot\underline{\boldsymbol{E}} \\ &+ \frac{2i}{\omega^2}(\omega\hat{\boldsymbol{k}}_{\boldsymbol{AF}} - \boldsymbol{p}(\hat k_{AF})_0)\cdot(\boldsymbol{E}^*\times\underline{\boldsymbol{E}})\Big).\end{aligned} \tag{174}$$

This result is independent of gauge choice, as expected. Since the fields and their extensions agree inside V, the cavity energy $\langle U\rangle$ can be calculated using either of the forms

$$\begin{aligned}\langle U\rangle &= \frac{1}{4}\int d^3p (\boldsymbol{E}^*\cdot\boldsymbol{D} + \boldsymbol{B}^*\cdot\boldsymbol{H}) \\ &= \frac{1}{4}\int d^3p (\boldsymbol{E}^*\cdot\underline{\boldsymbol{D}} + \boldsymbol{B}^*\cdot\underline{\boldsymbol{H}}).\end{aligned} \tag{175}$$

Note that both sets of fields are needed in the integral (174) for this procedure to work. The extended fields control divergences in momentum space, while the unextended fields restrict the integration to the volume V of the cavity in position space.

The general procedure for determining the effects of Lorentz violation on the resonant frequency of a given cavity then involves the following steps. First, obtain the fields $\boldsymbol{E}$, $\boldsymbol{B}$, $\boldsymbol{D}$, $\boldsymbol{H}$ in the cavity in the context of conventional electrodynamics, incorporating in the usual way any permittivity and permeability of the media involved. Next, construct extensions of the fields that are everywhere smooth beyond the cavity volume. Perform the Fourier transform to derive the corresponding momentum-space fields. Then, using the spherical-harmonic expansions of $\hat{k}_{AF}$ and the $\hat{\kappa}$ matrices described in Sec. III, calculate the cavity-frame matrices $\mathcal{M}^{\rm cav}_{jm}$ from Eq. (174). Finally, combine the results using Eq. (170) to extract the desired fractional frequency shift $\delta\nu/\nu$ displaying the explicit sidereal time dependences.

B. Example: camouflage model

A general analysis of cavity experiments incorporating all spherical coefficients for Lorentz violation is challenging due to the large variety of effects. Moreover, although terrestrial tests can provide valuable independent and fully controlled checks on vacuum birefringence and dispersion, the high sensitivities attainable in astrophysical searches for birefringence and dispersion make it reasonable to neglect effects from vacuum coefficients in the context of resonator experiments. Laboratory searches using cavities are therefore well suited to study the vacuum-orthogonal coefficients for Lorentz violation, which play no role in the vacuum propagation of light.

In this subsection, we illustrate the treatment of the spherical coefficients in the derivation of the cavity-frame matrices $\mathcal{M}^{\rm cav}_{jm}$. For simplicity, we focus primarily on Lorentz-violating operators that produce no leading-order birefringence or vacuum dispersion. For $d = 4$, this class of operators includes ones corresponding to the coefficients $c^{(4)}_{(I)jm}$ that have already been widely studied in cavity experiments [12–17]. For general d, it corresponds to the special subset of the coefficients $(c_F^{(d)})^{(0E)}_{njm}$ formed by the camouflage coefficients $(\vec{c}_F^{(d)})^{(0E)}_{njm}$ introduced in Sec. IV D.

We begin by considering a scenario involving the coefficients $(c_F^{(d)})^{(0E)}_{njm}$ controlling nonbirefringent effects. We seek an expression for the fractional frequency shift of the form

$$\frac{\delta\nu}{\nu} = \sum_{dnjm} \mathcal{M}^{(d)}_{(c_F)njm} (c_F^{(d)})^{(0E)}_{njm}. \tag{176}$$

To find the matrices $\mathcal{M}^{(d)}_{(c_F)njm}$, note that the fractional frequency shift in the nonbirefringent case may be written as

$$\begin{aligned}\frac{\delta\nu}{\nu} &= \frac{1}{4\langle U\rangle}\int d^3p F^*_{\mu\nu}\underline{F}^{\mu}{}_{\rho}(\hat{c}_F)^{\nu\rho} \\ &= \frac{1}{4\langle U\rangle}\int d^3p F^*_{\mu\nu}\underline{F}^{\mu}{}_{\rho}\partial^{\nu}\partial^{\rho}\hat{\Phi}_F,\end{aligned} \tag{177}$$

where $\hat{\Phi}_F$ is given by Eq. (60) and the derivatives act in momentum space, $\partial^{\nu} = \partial/\partial p_{\nu}$. Separating explicitly the temporal and spatial components gives

$$\begin{aligned}\frac{\delta\nu}{\nu} = \frac{1}{4\langle U\rangle}\int d^3p\Big[&-\boldsymbol{E}^*\cdot\underline{\boldsymbol{E}}\frac{\partial^2}{\partial\omega^2} \\ &+ (\boldsymbol{B}^*\times\underline{\boldsymbol{E}} - \boldsymbol{E}^*\times\underline{\boldsymbol{B}})^a\nabla_a\frac{\partial}{\partial\omega} \\ &+ \frac{1}{2}((E^*)^{(a}\underline{E}^{b)} + (B^*)^{(a}\underline{B}^{b)} - 2g^{ab}\boldsymbol{B}^*\cdot\underline{\boldsymbol{B}})\nabla_a\nabla_b\Big]\hat{\Phi}_F.\end{aligned} \tag{178}$$

Inserting the spherical-harmonic expansion (60) of $\hat{\Phi}_F$ and using the identities in Appendix A 2, we can determine the contribution to the fractional frequency shift from each coefficient $(c_F^{(d)})^{(0E)}_{njm}$ and hence identify the matrices $\mathcal{M}^{(d)}_{(c_F)njm}$.

To obtain an explicit integral expression for the matrices $\mathcal{M}^{(d)}_{(c_F)njm}$, we can eliminate the magnetic fields using the momentum-space Faraday law $\omega\boldsymbol{B} = \boldsymbol{p}\times\boldsymbol{E}$. This determines the matrices $\mathcal{M}^{(d)}_{(c_F)njm}$ as integrals over the fields $\boldsymbol{E}$ and $\underline{\boldsymbol{E}}$. In terms of the coordinate basis described in Appendix A 2, there are six field combinations contributing to the integrals. They can be specified as

$$\begin{aligned}&\underline{s}^0 = (E_+)^*\underline{E}_+ + (E_-)^*\underline{E}_-, \qquad \underline{s}_{(\pm2)} = 2(E_\pm)^*\underline{E}_\mp, \\ &\underline{\tilde{s}}_{(\pm1)} = E_r^*\underline{E}_\mp + (E_\pm)^*\underline{E}_r, \qquad \underline{\tilde{s}}_{(0)} = (E_r)^*\underline{E}_r,\end{aligned} \tag{179}$$

where

$$E_\pm = \tfrac{1}{\sqrt{2}}(E_\theta \pm iE_\phi). \tag{180}$$

The combinations $\underline{s}^0$ and $\underline{s}_{(\pm2)}$ represent smoothed versions of the usual Stokes parameters s^0 and $s_{(\pm2)}$. The combinations $\underline{\tilde{s}}_{(\pm1)}$ and $\underline{\tilde{s}}_{(0)}$ are helicity-(±1) and helicity-0 combinations, which provide two new transverse Stokes parameters vanishing when $E_r = \underline{E}_r = 0$. In terms of these quantities, the explicit integral expression for the matrices $\mathcal{M}^{(d)}_{(c_F)njm}$ is

$$\mathcal{M}^{(d)}_{(c_F)njm} = \frac{\omega^{d-4-n}}{4\langle U\rangle}\int d^3p\, p^{n-2}\Big[\frac{1}{4}(\omega^2-p^2)\sqrt{\frac{(j+2)!}{(j-2)!}}({}_{+2}Y_{jm}(\hat{\boldsymbol{p}})\underline{s}_{(+2)}(\boldsymbol{p}) + {}_{-2}Y_{jm}(\hat{\boldsymbol{p}})\underline{s}_{(-2)}(\boldsymbol{p}))$$
$$-((n-1)\omega^2+(d-2-n)p^2)\sqrt{\frac{j(j+1)}{2}}({}_{+1}Y_{jm}(\hat{\boldsymbol{p}})\underline{\tilde{s}}_{(+1)}(\boldsymbol{p}) - {}_{-1}Y_{jm}(\hat{\boldsymbol{p}})\underline{\tilde{s}}_{(-1)}(\boldsymbol{p}))$$
$$+\Big(\Big(n-\frac{j(j+1)}{2}\Big)(\omega^2-p^2)-(d-2-n)(d-3-3n)p^2-n(n-1)p^2\Big){}_0Y_{jm}(\hat{\boldsymbol{p}})\underline{s}^0(\boldsymbol{p})$$
$$+(n(n-1)\omega^2-(d-2-n)(d-3-n)p^2){}_0Y_{jm}(\hat{\boldsymbol{p}})\underline{\tilde{s}}_{(0)}(\boldsymbol{p})\Big], \tag{181}$$

where ω is the usual resonant angular frequency.

The result (181) applies both to empty cavities and to ones containing a material medium, provided the medium is lossless. The form of the integral reveals that the sensitivity to Lorentz violation depends both on the shape of the cavity and on the properties of any material medium it contains. This means that different geometries or media can be adopted to access different combinations of coefficients for Lorentz violation. For example, parity-breaking resonators may be used to access parity-odd Lorentz violations that cannot be detected at unsuppressed levels using parity-symmetric systems [108]. The properties of the resonator enter implicitly through the conventional fields $\boldsymbol{E}$, which are determined by solving the conventional Maxwell equations inside the cavity in the presence of the medium, if any. We emphasize that the frequency ω is fixed for a given mode, but any momentum $\boldsymbol{p}$ can contribute to the integral and hence to the matrices $\mathcal{M}^{(d)}_{(c_F)njm}$.

Next, we focus attention specifically on the combinations of the coefficients $(c_F^{(d)})^{(0E)}_{njm}$ that govern nondispersive effects. For $d=4$, the $(c_F^{(4)})^{(0E)}_{njm}$ coefficients correspond directly to the vacuum coefficients $c^{(4)}_{(I)jm}$, as described in Sec. IV A. The matrices $\mathcal{M}^{(4)}_{(I)jm}$ can therefore be expressed in terms of the matrices $\mathcal{M}^{(4)}_{(c_F)njm}$. We find

$$\mathcal{M}^{(4)}_{(I)00} = \tfrac{3}{4}\mathcal{M}^{(4)}_{(c_F)000} + \tfrac{1}{4}\mathcal{M}^{(4)}_{(c_F)000},$$
$$\mathcal{M}^{(4)}_{(I)1m} = -2\mathcal{M}^{(4)}_{(c_F)11m}, \qquad \mathcal{M}^{(4)}_{(I)2m} = \mathcal{M}^{(4)}_{(c_F)22m}. \tag{182}$$

For $d>4$, the relevant matrices are associated with the camouflage coefficients $(\bar{c}_F^{(d)})^{(0E)}_{njm}$ instead. Using the relation (90), we find

$$\mathcal{M}^{(d)}_{(\bar{c}_F)njm} = \mathcal{M}^{(d)}_{(c_F)njm} - \mathcal{M}^{(d)}_{(c_F)(n+2)jm}. \tag{183}$$

With these results and Eq. (181), the sensitivity of any given cavity to camouflage operators for Lorentz violation can be determined.

Typically, the above analysis is performed in the cavity frame, although many of the equations hold for an arbitrary inertial frame. Given the results for the cavity-frame matrices $\mathcal{M}$, the corresponding expressions for the laboratory-frame matrices follow from Eq. (169) and from the orientation of the cavity in the laboratory. Applying Eq. (170), we finally obtain the fractional frequency shift

$$\frac{\delta\nu}{\nu} = \sum_{dnjmm'}\mathcal{M}^{(d)\mathrm{lab}}_{(\bar{c}_F)njm}e^{im\phi}e^{im'\omega_\oplus T_\oplus}d^{(j)}_{mm'}(-\chi)(\bar{c}_F^{(d)})^{(0E)}_{njm'} + \sum_{jmm'}\mathcal{M}^{(4)\mathrm{lab}}_{(I)jm}e^{im\phi}e^{im'\omega_\oplus T_\oplus}d^{(j)}_{mm'}(-\chi)c^{(4)}_{(I)jm'} \tag{184}$$

which exhibits the variation with sidereal time.

C. Example: circular-cylindrical cavity

As an explicit illustration, we calculate in this subsection a number of elements of the matrix $\mathcal{M}$ for the TM_{010} mode of a cylindrical cavity with circular cross section. The cavity is centered at the origin of a cavity frame, with the z' direction aligned with the symmetry axis. For definiteness, let R be the cavity radius and $2R$ be its length, so that its ends lie at $z'=\pm R$. Here, we consider the case of a vacuum cavity for simplicity. The solutions for the TM_{010} mode in the absence of Lorentz violation are given by

$$\boldsymbol{E} = \begin{cases} J_0(\rho' x_{01}/R)\hat{\boldsymbol{\rho}}' & \text{inside } V, \\ 0 & \text{outside } V, \end{cases} \tag{185}$$

where x_{01} is the first zero of the Bessel function J_0, and where $\hat{\boldsymbol{\rho}}'$ represents the radial unit vector.

The electric field $\boldsymbol{E}$ is discontinuous at the ends of the cavity, and its derivatives are discontinuous at the sides $\rho'=R$. We therefore must seek a differentiable extension $\underline{\boldsymbol{E}}$ of the electric field of the type described in Sec. VII A. This is relatively straightforward to find in the present case because we have an analytic solution that could be extended to infinity. However, for the purposes of numerical calculation it is beneficial to construct instead a field $\underline{\boldsymbol{E}}$ that vanishes outside a larger volume V' containing the cavity volume V. With a field of this type, the Fourier transforms can be accurately determined by numerical integration over only a finite region V' of space.

An extension suitable for numerical work can be constructed with the aid of the C^q smoothing function

$g_q(x;a,b)$, defined by $g_q(x;a,b) \equiv 0$ for $x < a < b$ or $b < a < x$, $g_q(x;a,b) \equiv 1$ for $a < b < x$ or $x < b < a$, and

$$g_q(x;a,b) = \frac{(2q+1)!}{(b-a)^{2q+1}} \sum_{n=0}^{q} \frac{(x-a)^{q+1+n}(b-x)^{q-n}}{(q+1+n)!(q+n)!} \tag{186}$$

otherwise. This function continuously interpolates from 0 at $x = a$ to 1 at $x = b$, is constant outside that interval, and is q-times differentiable everywhere. Note that C^∞ functions of this type also exist, but for numerical calculations the above polynomial is easier to handle and suffices for our purposes.

Using this smoothing function, we can define an extended electric field by

$$\underline{\boldsymbol{E}} = g_q(\rho';2R,R)g_q(z';2R,R)g_q(z';-2R,-R) \times J_0(\rho' x_{01}/R)\hat{\boldsymbol{\rho}}'. \tag{187}$$

Taking the integration volume V' as a cube of side length $4R$, we see that the extended field $\underline{\boldsymbol{E}}$ matches $\boldsymbol{E}$ inside cavity volume V, vanishes outside V', and is q-times differentiable. The value of q that is required to ensure the finiteness of the integrals depends on the mass dimension d of the Lorentz-violating operators being considered. For a given dimension d, the matrices $\hat{\kappa}_{DE}$, $\hat{\kappa}_{HB}$, and $\hat{\kappa}_{DB}$ involve $d-4$ derivatives. Use of the Faraday law to eliminate the magnetic field B introduces another derivative. Consequently, the extended field $\underline{\boldsymbol{E}}$ must be at least C^{d-3}, so choosing $q > d-4$ should be sufficient.

The next step involves obtaining the Fourier transforms of the field components $E_{x'}$, $E_{y'}$, $E_{z'}$, $\underline{E}_{x'}$, $\underline{E}_{y'}$, $\underline{E}_{z'}$. We implement these via fast Fourier transform over an $N \times N \times N$ grid in the volume V'. We use the transformed fields to determine the momentum-space Stokes parameters from Eq. (179), and we then perform numerical integration to evaluate the integral (181) and obtain values for $\mathcal{M}^{(d)\mathrm{cav}}_{(c_F)njm}$. Lastly, we use Eqs. (182) and (183) to determine the components of interest for the matrices $\mathcal{M}^{(4)\mathrm{cav}}_{(I)jm}$ and $\mathcal{M}^{(d)\mathrm{cav}}_{(\tilde{c}_F)njm}$. As expected, the results converge to stable q-independent values for large N, provided q is sufficiently large. Table XVI summarizes the results obtained through this procedure for $d = 4, 6, 8$. Note that the symmetry of the mode implies no contribution from parity-breaking coefficients with odd j or from coefficients with $m \neq 0$, a result that is recovered numerically.

Cavity experiments searching for Lorentz violation typically compare two identical cavities with different orientations. In the present example, the cavity-frame matrices $\mathcal{M}$ are then identical for the two cavities. However, their differing orientation implies their laboratory-frame values would differ. This leads to the slight frequency difference that constitutes the signal for Lorentz violation.

TABLE XVI. Nonzero matrix elements $\mathcal{M}^{(4)\mathrm{cav}}_{(I)jm}$ and $\mathcal{M}^{(d)\mathrm{cav}}_{(\tilde{c}_F)njm}$ for the fundamental mode of a circular cylindrical cavity. Values for the cases $d = 4, 6, 8$ are displayed. The units are R^{4-d}, where R is the radius and half the length of the cavity.

j	m	$\mathcal{M}^{(4)\mathrm{cav}}_{(I)jm}$
0	0	−0.28
2	0	0.32

n	j	m	$\mathcal{M}^{(6)\mathrm{cav}}_{(\tilde{c}_F)njm}$
0	0	0	−13
2	0	0	13
2	2	0	−12

n	j	m	$\mathcal{M}^{(8)\mathrm{cav}}_{(\tilde{c}_F)njm}$
0	0	0	−150
2	2	0	26
4	0	0	150
4	2	0	−170
4	4	0	56

VIII. SUMMARY AND DISCUSSION

In this paper, we derive and study gauge-invariant Lorentz- and CPT-violating terms associated with the effective photon propagator in the Lagrange density of the SME, allowing for operators of arbitrary mass dimension d. We begin by showing that Lorentz violation at mass dimension d is characterized by a set of $(d+1)(d-1) \times (d-2)/2$ independent coefficients for the CPT-odd case and another set of $(d+1)d(d-3)$ independent coefficients for the CPT-even case. The compact Lagrange density (8) incorporates these effects for all d. It includes and extends the pure-photon sector of the minimal SME [7,11].

The Lagrange density (8) implies the equations of motion (11) for the photon field. An interpretation of these equations is elaborated in terms of electrodynamics in macroscopic media via the introduction of the operator constitutive tensors (14). We derive the covariant scalar dispersion relation (30), which must be satisfied by nontrivial plane-wave solutions. For the CPT-even violations, we extend the widely used κ matrices [11] of the minimal SME to general $\hat{\kappa}$ operators (32) that are relevant for studies at arbitrary d.

The unconventional properties of the Lorentz-violating eigenmodes can be characterized in terms of birefringence, dispersion, and anisotropy. All CPT-odd operators lead to birefringence. We study the conditions for leading-order birefringence from CPT-even operators via a Weyl decomposition of the constitutive tensor. For this case, we conjecture that nonbirefringent terms are uniquely associated with the non-Weyl part of the constitutive tensor when the decomposition is expressed in terms of a suitable effective

metric. For arbitrary Lorentz violation, we introduce a duality symmetry determined by the effective metric and argue that birefringence is a consequence of the breaking of this symmetry.

In Sec. III, we obtain a complete classification of the coefficients for Lorentz violation at arbitrary d, using an SO(3) decomposition in terms of spin-weighted spherical harmonics. A review of the spin-weighted spherical harmonics and derivations of some useful mathematical results are provided in the appendix, along with a discussion of the relationships to angular momentum, helicity, and parity. The SO(3) decomposition reveals a total of nine independent sets of spherical coefficients for Lorentz violation that control birefringence, dispersion, and anisotropy in the photon propagator. Table XVII lists these spherical coefficients and displays the ranges of their indices and their counting. The labels and indices on a given spherical coefficient identify the key properties of the corresponding Lorentz-violating operator, and their interpretation is summarized in the paragraph containing Eq. (45). More detailed properties of these nine sets are compiled in Tables I, III, IV, and V.

Table XVII reveals the existence of several classes of operators that are absent in the minimal SME, which is restricted to $d = 3$ and $d = 4$. The CPT-odd case at $d = 3$ involves two sets containing four independent spherical coefficients, while the CPT-even case at $d = 4$ involves three sets with 20 coefficients, one of which is an unobservable constant. However, the CPT-odd case at $d = 5$ has 35 coefficients distributed among three sets rather than two. The additional set $(\overline{k}^{(5)}_{AF})^{(1E)}_{njm}$ controls E-parity CPT-odd effects, which are absent in the minimal SME. Similarly, the CPT-even case at $d = 6$ has 126 coefficients distributed among six sets rather than three. The additional sets $(\overline{k}^{(6)}_{F})^{(1E)}_{njm}$, $(\overline{k}^{(6)}_{F})^{(2E)}_{njm}$, $(\overline{k}^{(6)}_{F})^{(2B)}_{njm}$ govern E-parity spin-one operators and also spin-two operators with both E- and B-type parities, all associated with qualitatively new effects.

For applications to observation and experiment, it is valuable to define various limiting cases of the general theory. Section IV presents several of these limits, while Table XVIII summarizes their specific content in terms of spherical coefficients for Lorentz violation. The most widely studied limit to date is the minimal SME, which involves a total of 23 independent nontrivial spherical coefficients. The explicit connections between the spherical coefficients and the usual Cartesian coefficients for the minimal SME is provided via Tables VI, VII, and VIII.

Another useful limit involves the specification of a preferred frame in which all Lorentz violation is isotropic. The corresponding isotropic or fried-chicken models are discussed in Sec. IV B. The isotropic requirement eliminates all but three sets of spherical coefficients and reduces the growth of coefficient numbers to be linear instead of cubic at large d. For CPT-odd isotropic operators with $d = 3, 5, 7\ldots$ there are only $1, 2, 3\ldots$ types of Lorentz violation, all of which are birefringent. Similarly, for CPT-even isotropic operators with $d = 4, 6, 8\ldots$ only $2, 4, 6\ldots$ coefficients arise, of which $0, 1, 2\ldots$ are associated with leading-order birefringence. Note that isotropic CPT-even birefringence is a physical feature only for $d \geq 6$.

A third useful limiting subset of the general theory is obtained by restricting attention to Lorentz-violating operators that are nonbirefringent and also are nondispersive in the vacuum at leading order. Section IV D constructs the corresponding camouflage models. These models involve effects that are challenging to detect in astrophysical stud-

TABLE XVII. Summary of spherical coefficients for Lorentz-violating operators of arbitrary mass dimension. The first column specifies the CPT property and the total number of independent operators at each d. The corresponding spherical coefficient sets are listed in the second column. The remainder of the table provides the allowed ranges for the indices d, n, j and the number of independent components for each coefficient set.

	Coefficient	d	n	j	Number
CPT even, d even	$(c_F^{(d)})^{(0E)}_{njm}$	≥ 4	$0, 1, \ldots, d-2$	$n, n-2, n-4\ldots, \geq 0$	$\frac{(d+1)d(d-1)}{6}$
$(d+1)d(d-3)$	$(k_F^{(d)})^{(0E)}_{njm}$	≥ 4	$0, 1, \ldots, d-4$	2 for $n = 0$, $n+2, n, n-2\ldots, \geq 0$ for $n \neq 0$	$\frac{d^3-d-30}{6}$
	$(\overline{k}_F^{(d)})^{(1E)}_{njm}$	≥ 6	$1, 2, \ldots, d-4$	$n+1, n-1, n-3\ldots, \geq 1$	$\frac{(d-4)(d^2+d+3)}{6}$
	$(\overline{k}_F^{(d)})^{(2E)}_{njm}$	≥ 6	$2, 3, \ldots, d-4$	$n, n-2, n-4\ldots, \geq 2$	$\frac{(d-4)(d^2-2d-9)}{6}$
	$(k_F^{(d)})^{(1B)}_{njm}$	≥ 4	$0, 1, \ldots, d-4$	$n+2, n, n-1\ldots, \geq 1$	$\frac{d^3-4d-18}{6}$
	$(\overline{k}_F^{(d)})^{(2B)}_{njm}$	≥ 6	$1, 2, \ldots, d-4$	$n+1, n-1, n-3\ldots, \geq 2$	$\frac{(d+3)(d-2)(d-4)}{6}$
CPT odd, d odd	$(k_{AF}^{(d)})^{(0B)}_{njm}$	≥ 3	$0, 1, \ldots, d-3$	$n, n-2, n-4\ldots, \geq 0$	$\frac{d(d-1)(d-2)}{6}$
$\frac{(d+1)(d-1)(d-2)}{2}$	$(k_{AF}^{(d)})^{(1B)}_{njm}$	≥ 3	$0, 1, \ldots, d-3$	$n+1, n-1, n-3\ldots, \geq 1$	$\frac{(d-1)(d^2+d-3)}{6}$
	$(\overline{k}_{AF}^{(d)})^{(1E)}_{njm}$	≥ 5	$1, 2, \ldots, d-3$	$n, n-2, n-4\ldots, \geq 1$	$\frac{(d+1)(d-1)(d-3)}{6}$

TABLE XVIII. Summary of limiting cases. The first column specifies the limit, while the corresponding spherical coefficient sets are listed in the second column. The remainder of the table provides the allowed ranges for the indices d, n, j and the number of independent components for each coefficient set.

Limit	Coeff.	d	n	j	Number
vacuum	$c^{(d)}_{(I)jm}$	even, ≥ 4		$0, 1, \ldots, d-2$	$(d-1)^2$
	$k^{(d)}_{(E)jm}$	even, ≥ 4		$2, 3, \ldots, d-2$	$(d-1)^2-4$
	$k^{(d)}_{(B)jm}$	even, ≥ 4		$2, 3, \ldots, d-2$	$(d-1)^2-4$
	$k^{(d)}_{(V)jm}$	odd, ≥ 3		$0, 1, \ldots, d-2$	$(d-1)^2$
vacuum orthogonal	$(\overline{c}^{(d)}_F)^{(0E)}_{njm}$	even, ≥ 4	$0, 1, \ldots, d-4$	$n, n-2, n-4\ldots, \geq 0$	$\frac{(d-1)(d-2)(d-3)}{6}$
	$(\overline{k}^{(d)}_F)^{(0E)}_{njm}$	even, ≥ 6	$1, 2, \ldots, d-4$	$n, n-2, n-4\ldots, \geq 0$	$\frac{(d-1)(d-2)(d-3)}{6}-1$
	$(\overline{k}^{(d)}_F)^{(1E)}_{njm}$	even, ≥ 6	$1, 2, \ldots, d-4$	$n+1, n-1, n-3\ldots, \geq 1$	$\frac{(d-4)(d^2+d+3)}{6}$
	$(\overline{k}^{(d)}_F)^{(2E)}_{njm}$	even, ≥ 6	$2, 3, \ldots, d-4$	$n, n-2, n-4\ldots, \geq 2$	$\frac{(d-4)(d^2-2d-9)}{6}$
	$(\overline{k}^{(d)}_F)^{(1B)}_{njm}$	even, ≥ 6	$1, 2, \ldots, d-4$	$n, n-2, n-4\ldots, \geq 1$	$\frac{d(d-2)(d-4)}{6}$
	$(\overline{k}^{(d)}_F)^{(2B)}_{njm}$	even, ≥ 6	$1, 2, \ldots, d-4$	$n+1, n-1, n-3\ldots, \geq 2$	$\frac{(d+3)(d-2)(d-4)}{6}$
	$(\overline{k}^{(d)}_{AF})^{(0B)}_{njm}$	odd, ≥ 5	$0, 1, \ldots, d-4$	$n, n-2, n-4\ldots, \geq 0$	$\frac{(d-1)(d-2)(d-3)}{6}$
	$(\overline{k}^{(d)}_{AF})^{(1B)}_{njm}$	odd, ≥ 5	$0, 1, \ldots, d-4$	$n+1, n-1, n-3\ldots, \geq 1$	$\frac{(d+1)(d-1)(d-3)}{6}$
	$(\overline{k}^{(d)}_{AF})^{(1E)}_{njm}$	odd, ≥ 5	$1, 2, \ldots, d-3$	$n, n-2, n-4\ldots, \geq 1$	$\frac{(d+1)(d-1)(d-3)}{6}$
camouflage	$(\overline{c}^{(d)}_F)^{(0E)}_{njm}$	even, ≥ 4	$0, 1, \ldots, d-4$	$n, n-2, n-4\ldots, \geq 0$	$\frac{(d-1)(d-2)(d-3)}{6}$
isotropic	$(\mathring{c}^{(d)}_F)_n$	even, ≥ 4	$0, 2, \ldots, d-2$	0	$d/2$
	$(\mathring{k}^{(d)}_F)_n$	even, ≥ 4	$2, 4, \ldots, d-4$	0	$(d-4)/2$
	$(\mathring{k}^{(d)}_{AF})_n$	odd, ≥ 3	$0, 2, \ldots, d-3$	0	$(d-1)/2$
minimal SME	$c^{(4)}_{(I)jm}$	4		0, 1, 2	9
	$k^{(4)}_{(E)jm}$	4		2	5
	$k^{(4)}_{(B)jm}$	4		2	5
	$k^{(3)}_{(V)jm}$	3		0, 1	4

ies of birefringence and dispersion. They are described by the single subset of coefficients $(\overline{c}^{(d)}_F)^{(0E)}_{njm}$ appearing at even d and hence associated with CPT-even Lorentz violation. Table IX summarizes some properties of these coefficients. For $d=4$ only a Lorentz-invariant trace appears, so for most purposes it suffices to take $d>4$. The camouflage coefficients then govern effects outside the minimal SME. For operators of larger mass dimension $d=6, 8, 10\ldots$ there are $10, 35, 84\ldots$ independent effects, with the number of independent coefficients growing rapidly as the cube of d for large d. Also, for $d=4, 6, 8\ldots$ there are $1, 2, 3\ldots$ isotropic camouflage coefficients, which therefore also belong to the general isotropic model.

The extreme sensitivities to Lorentz violation available via studies of birefringence and dispersion of astrophysical sources provides motivation for a further refinement in the classification of spherical coefficients, based on separating those coefficients that affect the propagation of light in the vacuum from all others. We refer to the former as vacuum coefficients and to the complement as vacuum-orthogonal coefficients, and we identify the latter by a negation diacritic $\neg$. This classification is summarized in Table XVIII. The vacuum-orthogonal coefficients appear only for $d \geq 5$, so they represent qualitatively new effects that are absent in the minimal SME. Moreover, the numbers of vacuum and vacuum-orthogonal coefficients grow as d^2 and d^3 for large d, respectively, so the vacuum-orthogonal coefficients represent most of the coefficient space for large d. For example, the vacuum coefficients govern all the physical effects in the minimal SME for which $d=3$ and $d=4$, but for $d=5$ they span only 16 of the 36 possibilities and for $d=6$ only 67 of 126.

The vacuum coefficients are constructed in Sec. IV C. At leading order, they are identified by requiring that the radiation fields are plane waves. This restricts attention to four sets of coefficients $c^{(d)}_{(I)jm}$, $k^{(d)}_{(E)jm}$, $k^{(d)}_{(B)jm}$, $k^{(d)}_{(V)jm}$. The coefficients $c^{(d)}_{(I)jm}$ are associated with CPT-even Lorentz violation that is nonbirefringent at leading order but dispersive for $d>4$. The coefficients $k^{(d)}_{(E)jm}$ and $k^{(d)}_{(B)jm}$ control

CPT-even birefringent effects that are also dispersive for $d > 4$. Only $k^{(d)}_{(V)jm}$ is associated with *CPT*-odd effects, which are also birefringent and dispersive. For any given d, the numbers of each type of vacuum coefficients are roughly the same. For example, at $d = 6$ there are 25 coefficients in $c^{(6)}_{(I)jm}$ and 21 each in $k^{(6)}_{(E)jm}$ and $k^{(6)}_{(B)jm}$.

The vacuum-orthogonal models are introduced in Sec. IV E. There are nine sets of vacuum-orthogonal coefficients, of which four are identical to and five are reduced subsets of the nine sets in the general analysis. One of the latter consists of the camouflage coefficients. Some properties of the remainder are provided in Tables X, XI, and XII. Except for a single constant scale factor in $d = 4$, the vacuum-orthogonal coefficients appear only for $d > 4$. They govern Lorentz-violating operators that produce no leading-order birefringence or dispersion in vacuum propagation, although birefringent or dispersive effects can appear in other physical contexts. For example, all 20 vacuum-orthogonal coefficients for $d = 5$ and 49 of the 59 for $d = 6$ are associated with birefringent and dispersive effects in suitable circumstances. The remaining 10 for $d = 6$ are camouflage coefficients, which govern nonbirefringent effects.

The remainder of the paper is concerned with applications of the theory to observation and experiment. Results of measurements are conventionally reported in the canonical Sun-centered frame, so for some applications it is necessary to perform transformations relating spherical coefficients in the Sun-centered frame to a laboratory or other frame. These transformations are provided explicitly in Sec. V for the case where the boost component is negligible.

Section VI describes some applications in the astrophysical context. We focus on astrophysical studies of vacuum birefringence and dispersion. Birefringence studies offer extreme sensitivity to many vacuum coefficients, while dispersion tests access the remainder at lesser but nonetheless impressive sensitivities. Dispersion constraints are discussed in Sec. VI A. We obtain expressions applicable to both isotropic and anisotropic dispersion, and we use the recent measurements of GRB 080916C made by the Fermi Observatory to obtain new constraints on Lorentz violation involving operators of mass dimension six and eight. A summary of existing constraints from astrophysical dispersion tests is provided in Table XIII.

Birefringence constraints are considered in Sec. VI B. The general theory is outlined, and the net rotation induced by arbitrary spherical coefficients is described quantitatively in terms of Stokes parameters. We use polarimetric data from the gamma-ray bursts GRB 930131 and GRB 960924 to set tight constraints on spherical coefficients associated with Lorentz-violating operators of mass dimensions four through nine. A summary of current limits from GRB polarimetry is provided in Table XIV. We also consider constraints obtained from polarimetric studies of the CMB. The maximal photon-propagation distances and the photon frequencies make the CMB particularly well suited for measurements of spherical coefficients with $d = 3$. A survey is performed to categorize the mixing of polarizations in the CMB induced by Lorentz violation. Table XV compiles some existing limits from the CMB on both isotropic and anisotropic Lorentz violation.

Section VII discusses applications in the laboratory context, focusing on the use of resonant cavities to search for Lorentz violation. These systems offer sensitivities to spherical coefficients that are challenging to access in studies of vacuum birefringence and vacuum dispersion. A general theoretical procedure for deriving the fractional frequency shift in a cavity is presented in Sec. VII A. In the following subsections, the results are applied to nonbirefringent Lorentz violation and, in particular, to the camouflage coefficients, for which some relevant experiment-dependent factors are explicitly obtained. For the specific case of a circular-cylindrical cavity, we provide in Eq. (184) the fractional frequency shift including the explicit time dependence.

The analysis in this work demonstrates that a comprehensive search for Lorentz violation is best performed with multiple types of measurements. The most sensitive tests use astrophysical birefringence, which provides access to some vacuum coefficients. Astrophysical dispersion offers high sensitivity to the remaining vacuum coefficients. However, the bulk of effects involves vacuum-orthogonal coefficients. Direct sensitivity to these requires nonvacuum boundary conditions and hence laboratory studies. Disentangling the various birefringence, dispersion, and anisotropy effects requires a variety of laboratory experiments involving different boundary conditions and different media, and also the exploitation of signals from different rotations and boosts. Even if attention is limited to coefficients with comparatively low values of d, considerable room remains for investigations via both astrophysical observations and laboratory experiments.

ACKNOWLEDGMENTS

This work was supported in part by the United States Department of Energy under Grant No. DE-FG02-91ER40661.

APPENDIX A: SPHERICAL HARMONICS

Angular-momentum eigenstates are irreducible representations of rotations, so tensors in three dimensions can be decomposed into components with definite orbital angular momentum and spin. For spin-zero scalars, the spherical harmonics Y_{jm} provide a basis for this decomposition. For nontrivial tensors, more general tensor spherical harmonics are needed to incorporate the spin. Among the most widely used are the spin-weighted spherical harmonics [57,58], denoted ${}_sY_{jm}$. In this appendix, we briefly

review the definitions and basic features of these spin-weighted spherical harmonics. We also obtain some mathematical properties that are used in Sec. III.

1. Spin-weighted spherical harmonics

A key concept underlying the spin-weighted spherical harmonics is the notion of spin weight. To introduce this idea, consider the problem of characterizing radiation propagating inward toward the Earth from a distant point source in the sky. The electric-field vector $\boldsymbol{E}$ is oriented perpendicular to the line of sight, so it lies in the tangent space of a sphere surrounding the Earth. In spherical polar coordinates, the angular components of $\boldsymbol{E}$ are E_θ and E_ϕ. However, the alternative components $E_\pm \propto E_\theta \mp iE_\phi$ can be considered instead. These have the advantage of transforming elegantly as $E_\pm \to e^{\mp i\delta}E_\pm$ under a rotation of the local coordinates by an angle δ about the line of sight. The irreducible combinations $E_\pm$ are said to be spin-weighted functions of spin weight ± 1. More generally, a function ${}_sf$ is said to have spin weight s if it transforms according to ${}_sf \to e^{-is\delta}{}_sf$ under a local rotation about the line of sight.

The generator of rotations is the angular-momentum operator $\boldsymbol{J}$. Denoting the radial unit vector as $\hat{\boldsymbol{n}}$, the generator of local rotations about the line of sight is the operator $\hat{\boldsymbol{n}} \cdot \boldsymbol{J}$. This is the helicity operator with respect to the line of sight. We see that the spin weight can be understood as the eigenvalue of the helicity operator. For instance, the irreducible combinations $E_\pm$ in the above example are components of definite helicity with respect to the line of sight. In this particular example, the light propagates in the three-momentum direction $\hat{\boldsymbol{p}} = -\hat{\boldsymbol{n}}$, so the helicity operator $\hat{\boldsymbol{n}} \cdot \boldsymbol{J}$ is equivalent up to a sign to the helicity operator with respect to the momentum, $\hat{\boldsymbol{p}} \cdot \boldsymbol{J}$. However, this equivalence fails for nonradial propagation. So in general there are two basic options for defining spin weight, as the eigenvalue up to a sign of either $\hat{\boldsymbol{n}} \cdot \boldsymbol{J}$ or $\hat{\boldsymbol{p}} \cdot \boldsymbol{J}$. The choice of definition can be made based on suitability for the problem at hand.

The helicity operator $\hat{\boldsymbol{p}} \cdot \boldsymbol{J}$ or $\hat{\boldsymbol{n}} \cdot \boldsymbol{J}$ commutes with both the squared total angular momentum $\boldsymbol{J}^2$ and the component J_z, where by convention we choose the projection axis to be the z direction. It is therefore possible to introduce simultaneous eigenfunctions for all three operators. We show in the next subsection that these simultaneous eigenfunctions are the spin-weighted spherical harmonics ${}_sY_{jm}$. However, typical discussions [57–59] of ${}_sY_{jm}$ are based on raising and lowering operators for the spin weight, which connect different harmonics. In this subsection, we define these operators and provide explicit expressions for ${}_sY_{jm}$.

Acting on a function ${}_sf$ of spin weight s, the raising and lowering operators are given by

$$\{{}^{\eth}_{\bar{\eth}}\}{}_sf = -\sin^{\pm s}\theta(\partial_\theta \pm i\csc\theta\partial_\phi)\sin^{\mp s}\theta\,{}_sf. \tag{A1}$$

The raising operator $\eth$ acts on a function of spin weight s to yield a function of spin weight $s+1$. Similarly, the lowering operator $\bar{\eth}$ decreases spin weight by one. The spin-weighted spherical harmonics ${}_sY_{jm}$ of spin weight s can be generated from the usual scalar spherical harmonics $Y_{jm} = {}_0Y_{jm}$ by raising or lowering the spin weight $|s|$ times:

$${}_sY_{jm} = \begin{cases} \sqrt{\frac{(j-s)!}{(j+s)!}}\eth^s\,{}_0Y_{jm}, & 0 < s \le j, \\ (-1)^s\sqrt{\frac{(j+s)!}{(j-s)!}}\bar{\eth}^s\,{}_0Y_{jm}, & -j \le s < 0. \end{cases} \tag{A2}$$

As discussed in the following subsection, the index j corresponds to the eigenvalue of the squared total angular momentum $\boldsymbol{J}^2 = j(j+1)$ and m to the eigenvalue of J_z.

The functions ${}_sY_{jm}$ are nonvanishing for index values $|m| \le j$, as usual. Since the helicity is limited by j, they are also nonvanishing for $j \ge |s|$. They satisfy a relation analogous to that obeyed by the usual scalar spherical harmonics,

$$\begin{aligned} {}_{s_1}Y_{j_1m_1s_2}Y_{j_2m_2} = \sum_{s_3j_3m_3} & \sqrt{\frac{(2j_1+1)(2j_2+1)}{4\pi(2j_3+1)}} \\ & \times \langle j_1j_2(-s_1)(-s_2)|j_3(-s_3)\rangle \\ & \times \langle j_1j_2m_1m_2|j_3m_3\rangle\,{}_{s_3}Y_{j_3m_3}, \end{aligned} \tag{A3}$$

where the symbols $\langle j_1j_2m_1m_2|j_3m_3\rangle$ represent the Clebsch-Gordan coefficients. This implies orthogonality of harmonics of equal spin weight,

$$\int {}_sY^*_{jm}(\hat{\boldsymbol{n}})\,{}_sY_{j'm'}(\hat{\boldsymbol{n}})\sin\theta d\theta d\phi = \delta_{jj'}\delta_{mm'}. \tag{A4}$$

Note, however, that this orthogonality does not extend to ${}_sY_{jm}$ of different spin weight. The harmonics ${}_sY_{jm}$ also satisfy the completeness relations

$$\sum_{jm} {}_sY^*_{jm}(\hat{\boldsymbol{n}})\,{}_sY_{jm}(\hat{\boldsymbol{n}}') = \delta(\hat{\boldsymbol{n}} - \hat{\boldsymbol{n}}'). \tag{A5}$$

Here, we adopt phase conventions ensuring

$${}_sY^*_{jm} = (-1)^{s+m}\,{}_{-s}Y_{j(-m)} \tag{A6}$$

under complex conjugation and

$${}_sY_{jm}(-\hat{\boldsymbol{n}}) = (-1)^j\,{}_{-s}Y_{jm}(\hat{\boldsymbol{n}}) \tag{A7}$$

under parity.

Although Eq. (A2) can be used to generate the spin-weighted spherical harmonics, in practice it is often easier to use the explicit expression

$$
{}_sY_{jm}(\theta,\phi) = \left[\frac{2j+1}{4\pi}\frac{(j+m)!(j-m)!}{(j+s)!(j-s)!}\right]^{1/2} e^{im\phi}\sin^{2j}\frac{\theta}{2} \times \sum_r (-1)^{j+m+s+r}\binom{j-s}{r} \times \binom{j+s}{r+s-m}\cot^{2r+s-m}\frac{\theta}{2}, \tag{A8}
$$

where $\binom{m}{n}$ denotes the binomial coefficients. However, this expression can be numerically troublesome for high values of j. One strategy for numerical applications is to use Eq. (A8) to generate the low-j harmonics but instead to use recursion relations derived from Eq. (A3) to extract the higher-j ones. We find that two recursion relations are useful for this purpose. Taking $s_1 = 0$, $j_1 = 1$, $m_1 = 1$, and $m_2 = \pm j_2$ in Eq. (A3), we obtain the recursion

$$
{}_sY_{j(\pm j)} = \mp\sqrt{\frac{j(2j+1)}{2(j^2-s^2)}}e^{\pm i\phi}\sin\theta\,{}_sY_{(j-1)(\pm j\mp 1)}, \tag{A9}
$$

which relates harmonics with $j = |m|$. Also, taking $s_1 = 0$, $j_1 = 1$, $m_1 = 0$ in Eq. (A3) leads to the recursive formula

$$
{}_sY_{jm} = \sqrt{\frac{j^2((2j)^2-1)}{(j^2-m^2)(j^2-s^2)}}\left[\left(\cos\theta + \frac{ms}{j(j-1)}\right){}_sY_{(j-1)m} - \sqrt{\frac{((j-1)^2-m^2)((j-1)^2-s^2)}{(j-1)^2(2j-1)(2j-3)}}\,{}_sY_{(j-2)m}\right], \tag{A10}
$$

which permits the calculation of higher-j harmonics from lower-j ones with the same m. A practical procedure for determining numerical values of spin-weighted spherical harmonics then involves first using Eq. (A8) to find values for $j = |s|$, followed by using Eq. (A9) to obtain harmonics with $j = |m|$, and finally using Eq. (A10) to fill in all remaining values up to the desired maximum j.

2. Covariant angular momentum

In this subsection, we further explore the relationships between angular momentum, helicity, and the spin-weighted spherical harmonics. For definiteness, we consider helicity with respect to the momentum direction $\hat{\boldsymbol{p}}$, but the following discussion remains valid if $\hat{\boldsymbol{n}}$ is substituted for $\hat{\boldsymbol{p}}$ throughout. Note also that we adopt a metric with positive signature when working with three-dimensional tensors.

We introduce standard angles in spherical polar coordinates, so that the momentum direction can be written as

$$
\hat{\boldsymbol{p}} = \sin\theta\cos\phi\,\hat{\boldsymbol{e}}_x + \sin\theta\sin\phi\,\hat{\boldsymbol{e}}_y + \cos\theta\,\hat{\boldsymbol{e}}_z, \tag{A11}
$$

where $\hat{\boldsymbol{e}}_x$, $\hat{\boldsymbol{e}}_y$, $\hat{\boldsymbol{e}}_z$ form the Cartesian basis vectors. The orthonormal basis vectors in the spherical polar coordinates are taken as

$$
\hat{\boldsymbol{e}}_r = \hat{\boldsymbol{e}}^r = \hat{\boldsymbol{p}}, \qquad \hat{\boldsymbol{e}}_\theta = \hat{\boldsymbol{e}}^\theta, \qquad \hat{\boldsymbol{e}}_\phi = \hat{\boldsymbol{e}}^\phi, \tag{A12}
$$

where $\hat{\boldsymbol{e}}_\theta$ and $\hat{\boldsymbol{e}}_\phi$ are the coordinate unit vectors associated with the spherical coordinates θ and ϕ. We also define complex helicity-basis vectors

$$
\hat{\boldsymbol{e}}_r = \hat{\boldsymbol{e}}^r = \hat{\boldsymbol{p}}, \qquad \hat{\boldsymbol{e}}_\pm = \hat{\boldsymbol{e}}^\mp = \tfrac{1}{\sqrt{2}}(\hat{\boldsymbol{e}}_\theta \pm i\hat{\boldsymbol{e}}_\phi), \tag{A13}
$$

where an explicit choice of phase has been made. Other phase choices would change some of the relations below. With this definition, a rotation of the local coordinates about $\hat{\boldsymbol{p}}$ by an angle δ generates a phase shift in the helicity-basis vectors, $\hat{\boldsymbol{e}}_\pm \to e^{\mp i\delta}\hat{\boldsymbol{e}}_\pm$.

Using the helicity basis, we can readily decompose any tensor into components of definite helicity and spin weight. For example, a vector $\boldsymbol{V}$ has 0-helicity component $V_r = \boldsymbol{V}\cdot\hat{\boldsymbol{e}}_r$ and ±1-helicity components $V^\pm = V_\mp = \boldsymbol{V}\cdot\hat{\boldsymbol{e}}^\pm$, the latter corresponding to spin-weight $= \mp1$. The spin weight and helicity of any tensor component is readily obtained by simple counting, since each $\mp$ contravariant or $\pm$ covariant index adds ±1 to the spin weight.

To construct operators acting to raise or lower the spin weight, it is convenient first to introduce directional derivatives in momentum space with respect to arbitrary basis vectors $\hat{e}_a$, according to

$$
\partial_a = \hat{\boldsymbol{e}}_a\cdot\boldsymbol{\partial}, \qquad \partial_a\boldsymbol{p} = \hat{\boldsymbol{e}}_a. \tag{A14}
$$

The metric is

$$
g_{ab} = \hat{e}_a\cdot\hat{e}_b, \tag{A15}
$$

and we define covariant directional derivatives ∇_a with connection

$$
\Gamma^c{}_{ab} = (\partial_a\hat{\boldsymbol{e}}_b)\cdot\hat{\boldsymbol{e}}^c, \tag{A16}
$$

as usual. For example, acting with ∇_a on the components of a vector $\boldsymbol{V}$ gives

$$
\nabla_a V^b = \partial_a V^b + \Gamma^b{}_{ac}V^c, \qquad \nabla_a V_b = \partial_a V_b - \Gamma^c{}_{ab}V_c. \tag{A17}
$$

In the helicity basis $\{\hat{\boldsymbol{e}}_+, \hat{\boldsymbol{e}}_r, \hat{\boldsymbol{e}}_-\}$, we find the metric takes the explicit form

$$
g_{ab} = g^{ab} = \begin{pmatrix} 0 & 0 & 1 \\ 0 & 1 & 0 \\ 1 & 0 & 0 \end{pmatrix}, \tag{A18}
$$

while the nonzero connection elements are

$$
\begin{aligned} \Gamma^\pm{}_{\pm r} &= -\Gamma^r{}_{\pm\mp} = p^{-1}, \\ \Gamma^\pm{}_{\pm\pm} &= -\Gamma^\pm{}_{\mp\pm} = (\sqrt{2}p\tan\theta)^{-1}, \end{aligned} \tag{A19}
$$

where $p = |\boldsymbol{p}|$. The point is that the derivative ∇_+ operating on an arbitrary tensor acts to create tensor components whose spin weight is increased by one, while ∇_- lowers the spin weight by one.

Our goal is a decomposition in angular momentum, so we seek a covariant description of the angular-momentum

operators. In momentum space, the orbital angular momentum $\boldsymbol{L}$ has components

$$L^a = -i\varepsilon^{abc} p_b \nabla_c \tag{A20}$$

and obeys the algebra

$$[L_a, L_b] = -i\varepsilon_{abc} L^c. \tag{A21}$$

Here, ε^{abc} is the totally antisymmetric tensor, which in the helicity basis satisfies

$$\varepsilon_{+r-} = -\varepsilon^{+r-} = i. \tag{A22}$$

In particular, we have

$$L_r = 0, \qquad L_\pm = \pm p \nabla_\pm, \tag{A23}$$

which implies that orbital angular momentum is perpendicular to $\hat{\boldsymbol{p}}$, as expected.

To complete the description of angular momentum, it is useful to define a covariant spin operator $\boldsymbol{S}$ with components S_a. Acting on a vector V_a, we define

$$S_a V_b = -S^c{}_{ab} V_c, \qquad S_a V^b = S^b{}_{ac} V^c, \tag{A24}$$

where

$$S^c{}_{ab} = i\varepsilon^c{}_{ab}. \tag{A25}$$

This provides a covariant formulation of the general spin relation

$$(\boldsymbol{V}_1 \cdot \boldsymbol{S})\boldsymbol{V}_2 = i\boldsymbol{V}_1 \times \boldsymbol{V}_2 = (V_1)^a \hat{\boldsymbol{e}}^b (S_a(V_2)_b). \tag{A26}$$

The spin operator acting on more general tensors obeys rules like those of the connection. For example, we obtain

$$S_a T^b{}_c = S^b{}_{ad} T^d{}_c - S^d{}_{ac} T^b{}_d. \tag{A27}$$

Since the S_a are covariant operators rather than matrix operators, they obey slightly modified commutation relations

$$[S_a, S_b] = -i\varepsilon_{abc} S^c. \tag{A28}$$

With the above definitions, we can introduce a covariant operator for the total angular momentum as

$$J_a = L_a + S_a. \tag{A29}$$

Like the covariant derivative, this operator has the advantage of maintaining the explicit tensor nature of expressions when operating on tensor components. It obeys the modified commutation relations

$$[J_a, J_b] = -i\varepsilon_{abc} J^c. \tag{A30}$$

An interpretation of these operators is as follows. The radial angular momentum $J_r = S_r$ is the helicity, which is the negative of the spin weight. The operator J^+ raises the helicity and J_+ raises the spin weight, while J^- lowers the helicity and J_- lowers the spin weight. These operators are equivalent to the raising and lowering operators Eq. (A1) via the correspondence

$$J_+ = -\eth/\sqrt{2}, \qquad J_- = \bar{\eth}/\sqrt{2}. \tag{A31}$$

The spin-weighted spherical harmonics ${}_sY_{jm}$ are eigenfunctions of the commuting operators

$$-J_r = s, \qquad J^2 = j(j+1), \qquad J_z = m. \tag{A32}$$

The ladder operators $J_\pm$ can be shown to commute with $\boldsymbol{J}^2$ and J_z. In fact, $J_\pm$ commutes with $\boldsymbol{V} \cdot \boldsymbol{J}$ for any covariantly constant vector $\boldsymbol{V}$, $\nabla_a V_b = 0$. Also, the commutator

$$[J_\pm, -J_r] = i\varepsilon_{\pm r\mp} J^\mp = \mp J_\pm, \tag{A33}$$

implies that J_+ and J_- raise and lower the spin weight, respectively, while leaving j and m unaltered. The ladder nature of the $J_\pm$ can thus be seen either from the differential geometry or from the operator algebra.

Since the spin-weight ladder operators $J_\pm$ are analogous to the conventional ladder operators that raise and lower the eigenvalue of the z component of the angular momentum, many of the usual techniques and results apply. For example, the standard normalization scheme gives

$$J_\pm {}_sY_{jm} = -\sqrt{\frac{1}{2}(j(j+1) - s(s\pm 1))}\, {}_{s\pm 1}Y_{jm}, \tag{A34}$$

where the phase is chosen to match the conventional definitions when expressed in terms of $\eth$ and $\bar{\eth}$. Repeated application gives the useful expressions

$${}_0Y_{jm} = (-1)^s 2^{|s|/2} \sqrt{\frac{(j-|s|)!}{(j+|s|)!}} (J_\pm)^{|s|}{}_{\mp|s|} Y_{jm}, \tag{A35}$$

and

$${}_{\pm|s|}Y_{jm} = (-1)^s 2^{|s|/2} \sqrt{\frac{(j-|s|)!}{(j+|s|)!}} (J_\pm)^{|s|}{}_0 Y_{jm}, \tag{A36}$$

which are equivalent to Eq. (A2).

In practical terms, the above formalism leads to the simple results

$$\nabla_r = \partial/\partial p, \qquad \nabla_\pm = \pm(J_\pm - S_\pm)/p, \tag{A37}$$

which are used extensively in Sec. III. Note, however, that some care is needed when using the results (A37) since they are nontensorial relations, valid only in the helicity basis. For example, the $\pm$ indices on the right-hand side are noncovariant once applied, so further manipulations with covariant operators such as ∇_a, S_a, J_a are inappropriate.

As a simple illustration of the above formalism, consider the covariant momentum-space Laplacian acting on a scalar ψ:

$$\begin{aligned}\nabla_a \nabla^a \psi &= (\nabla_r \nabla^r + \nabla_+ \nabla^+ + \nabla_- \nabla^-)\psi \\ &= \left(\frac{\partial^2}{\partial p^2} + \frac{1}{p}(J_+ - S_+)\nabla^+ - \frac{1}{p}(J_- - S_-)\nabla^-\right)\psi.\end{aligned} \tag{A38}$$

Using the results

$$S_a\nabla^b\psi = S^b{}_{ac}\nabla^c\psi = -i\varepsilon_a{}^{bc}\nabla_c\psi,$$
$$\nabla^\pm\psi = \mp\frac{1}{p}(J^\pm - S^\pm)\psi = \mp\frac{1}{p}J^\pm\psi,$$
$$(J_+J^+ + J_-J^-)\psi = J^2\psi, \tag{A39}$$

we can reexpress $\nabla_a\nabla^a\psi$ as follows:

$$\begin{aligned}\nabla_a\nabla^a\psi &= \left(\frac{\partial^2}{\partial p^2} + \frac{1}{p}(J_+\nabla^+ + \nabla_r) - \frac{1}{p}(J_-\nabla^- - \nabla_r)\right)\psi \\ &= \left(\frac{\partial^2}{\partial p^2} + \frac{2}{p}\frac{\partial}{\partial p} - \frac{1}{p^2}(J_+J^+ + J_-J^-)\right)\psi \\ &= \left(\frac{\partial^2}{\partial p^2} + \frac{2}{p}\frac{\partial}{\partial p} - \frac{1}{p^2}J^2\right)\psi.\end{aligned} \tag{A40}$$

We thereby recover the familiar expression for $\nabla_a\nabla^a\psi$ involving the angular momentum.

It has been noted in the literature that the operators ð and $\bar{\text{ð}}$ are equivalent to covariant derivatives in the two-dimensional tangent space of the sphere [57]. In our present language, this can be made apparent by defining a new covariant derivative as

$$\tilde{\nabla}_a = \nabla_a - i\varepsilon_{arb}S^b/p, \tag{A41}$$

which in the helicity basis gives nonzero connection elements

$$\tilde{\Gamma}^{\pm}{}_{\pm\pm} = -\tilde{\Gamma}^{\pm}{}_{\mp\pm} = (\sqrt{2}p\tan\theta)^{-1}. \tag{A42}$$

The derivative $\tilde{\nabla}_a$ corresponds to the projection of the usual three-dimensional geometry onto the embedded two-sphere. In terms of this derivative, we can express the ladder operators as

$$J_\pm = \pm\tilde{\nabla}_\pm/p. \tag{A43}$$

This relates our three-dimensional picture to the two-dimensional one.

3. Parity

In a typical application of the above formalism, a tensor is decomposed by considering its components in the helicity basis, which are spin-weighted functions, and expanding them using spin-weighted spherical harmonics. In many cases, it is useful to decompose further the results in terms of parity properties [57]. This subsection contains a brief summary of the latter procedure, along with some figures providing insight into the structure of the resulting modes.

Let t represent an arbitrary tensor component with spin weight s. Its expansion then takes the form

$$t(\hat{\boldsymbol{p}}) = \sum_{jm} t_{jm}\,{}_sY_{jm}(\hat{\boldsymbol{p}}). \tag{A44}$$

By exchanging all the + and − indices on t, we obtain another tensor component of spin weight $-s$. Denoting this component as $\bar{t}$, we can expand it as

$$\bar{t}(\hat{\boldsymbol{p}}) = \sum_{jm} \bar{t}_{jm}\,{}_{-s}Y_{jm}(\hat{\boldsymbol{p}}). \tag{A45}$$

The two components t and $\bar{t}$ are parity conjugates, interchanging under parity according to

$$t(\hat{\boldsymbol{p}}) \leftrightarrow (-1)^s\bar{t}(-\hat{\boldsymbol{p}}). \tag{A46}$$

In terms of spherical coefficients, the parity transformation gives

$$t_{jm} \leftrightarrow (-1)^{s+j}\bar{t}_{jm}. \tag{A47}$$

It is then useful to define

$$t_{jm} = E_{jm} + iB_{jm}, \qquad \bar{t}_{jm} = (-1)^s(E_{jm} - iB_{jm}). \tag{A48}$$

The result is a splitting of t and $\bar{t}$ into modes with so-called electric-type parity or E-type parity,

$$E_{jm} \to (-1)^jE_{jm}, \tag{A49}$$

and ones with magnetic-type parity or B-type parity,

$$B_{jm} \to (-1)^{j+1}B_{jm}, \tag{A50}$$

where the nomenclature is borrowed from radiation theory.

As a simple example, consider a scalar function

$$S(\hat{\boldsymbol{p}}) = \sum_{jm} E_{jm}\,{}_0Y_{jm}(\hat{\boldsymbol{p}}). \tag{A51}$$

Under parity, S transforms according to

$$S(\hat{\boldsymbol{p}}) \to S(-\hat{\boldsymbol{p}}), \tag{A52}$$

which in conjunction with Eq. (A7) confirms that scalar functions contain only E-type components. Figure 9 illustrates the angular distribution obtained by considering each mode E_{00}, E_{10}, E_{11}, E_{20}, E_{21}, E_{22} of a real scalar field in turn. For example, the real scalar field $S(E_{11})$ associated with real E_{11} is

$$S(E_{11}) = E_{11}({}_0Y_{11} - {}_0Y_{1(-1)}). \tag{A53}$$

For each of the six images in Fig. 9, the three arrows perpendicular to the spherical surface represent rectangular right-handed coordinate axes with $\hat{\boldsymbol{z}}$ vertical. The solid disks represent positive values of the scalar, while the rings represent negative ones. The radius of each disk or ring is proportional to the magnitude of the scalar at that point. The images reveal the angular and parity symmetries of each scalar mode. Consider, for example, the E_{10} scalar mode. The figure shows that this mode has extremal magnitudes at the poles and equator and is symmetric under rotations about $\hat{\boldsymbol{z}}$, all of which are features of a distribution with $j = 1$ and $m = 0$. Also, the sign of the mode changes on interchanging any two antipodal points, matching its negative parity. Note that the distributions are plotted for

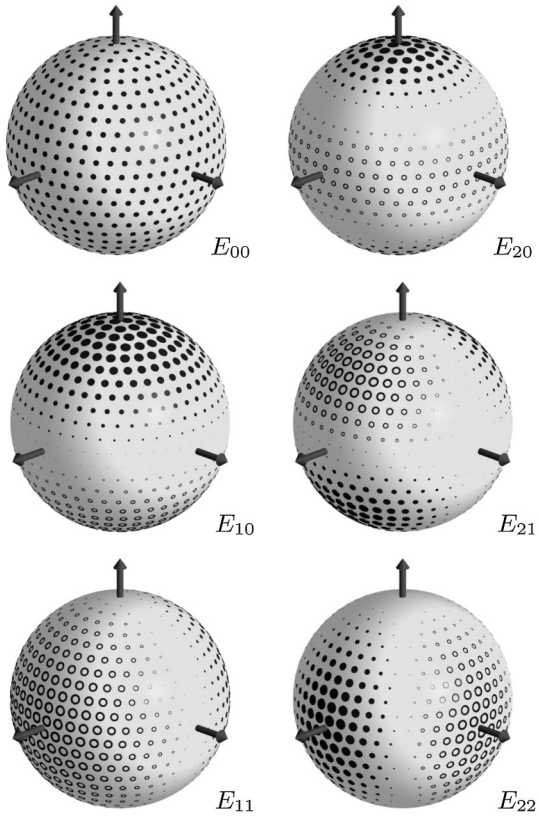

FIG. 9. Angular distributions for electric-type scalar components.

real amplitudes E_{jm}. Inclusion of a phase in an amplitude rotates the corresponding figure about $\hat{z}$.

An example with both E- and B-type content is provided by the components

$$V_{\pm} = \sum_{jm} (\pm E_{jm} + iB_{jm})_{\pm 1} Y_{jm} \tag{A54}$$

of a vector field $\boldsymbol{V}$ in the tangent bundle of the sphere. Figure 10 displays the angular distributions for a real vector field for each separate mode E_{10}, E_{11}, E_{20}, E_{21}, E_{22}, B_{10}, B_{11}, B_{20}, B_{21}, B_{22}. For example, the components of the real vector field $\boldsymbol{V}(E_{11})$ associated with real E_{11} are

$$\begin{aligned} V_+(E_{11}) &= E_{11}({}_1Y_{11} - {}_1Y_{1(-1)}), \\ V_-(E_{11}) &= -E_{11}({}_{-1}Y_{11} - {}_{-1}Y_{1(-1)}). \end{aligned} \tag{A55}$$

In the figure, the vector tangent to a sphere at a given point represents the corresponding mode. The angular and parity symmetries of each vector mode can be seen by inspection. For instance, the E_{10} vector mode has extremal magnitudes at the poles and equator and is symmetric under rotations about $\hat{z}$, as expected for a mode with $j = 1$ and $m = 0$. Also, inspection reveals that applying the parity operation reverses the flow of vectors on the sphere, as is appropriate for a mode with E-type parity and $j = 1$. Note that the E-type modes are curl free while the B-type modes are

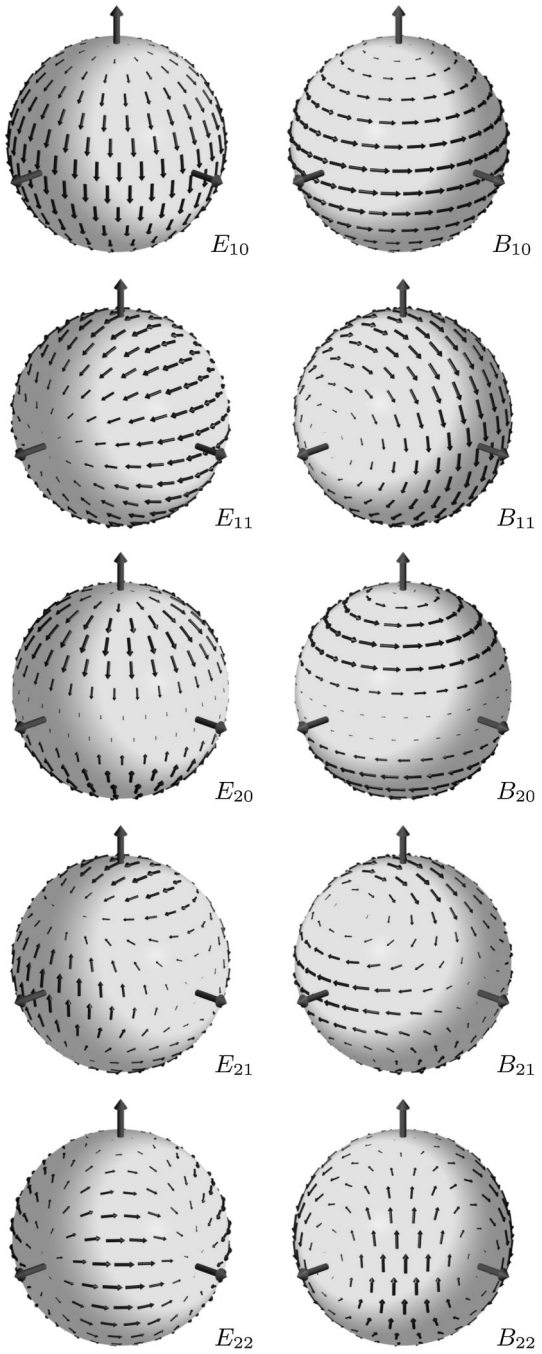

FIG. 10. Angular distributions for electric- and magnetic-type vector components.

divergence free, matching the usual properties in electrodynamics. Note also that for given values of j and m the E- and B-mode field lines are perpendicular everywhere, reflecting the orthogonality of the modes.

For a symmetric traceless two-tensor, we can consider the components

$$T_{\pm\pm} = \sum_{jm} (E_{jm} \pm iB_{jm})_{\pm 2} Y_{jm}. \tag{A56}$$

Figure 11 provides representations of each of the six modes

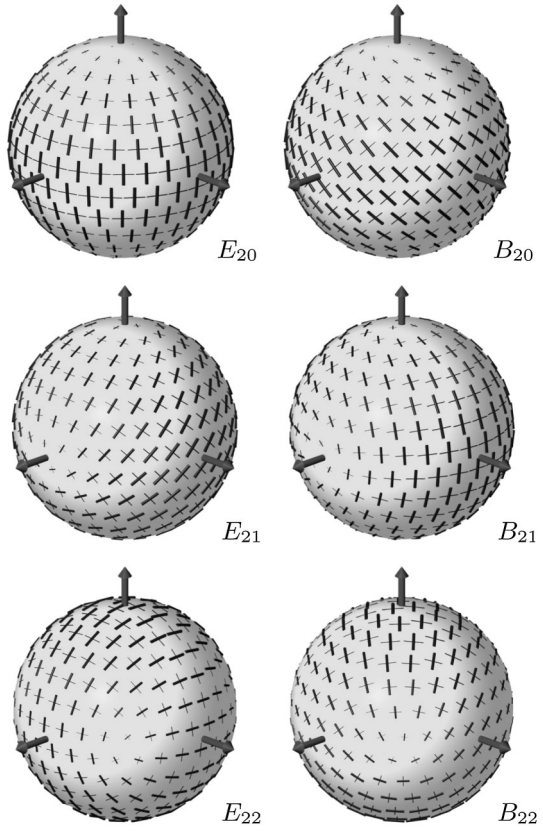

FIG. 11. Angular distributions for electric- and magnetic-type tensor components.

E_{20}, E_{21}, E_{22}, B_{20}, B_{21}, B_{22} for a real tensor. The figure takes advantage of the spectral theorem applied to the decomposition of a real symmetric traceless tensor T that lies in the tangent bundle of the sphere and has nonzero components $T_{\pm\pm}$. In terms of its two orthogonal eigenvectors $\boldsymbol{v}$ and $\boldsymbol{w}$ lying tangent to the sphere, we can write

$$T = \boldsymbol{v} \otimes \boldsymbol{v} - \boldsymbol{w} \otimes \boldsymbol{w}, \tag{A57}$$

where the eigenvalues of T are $|\boldsymbol{v}|^2$ and $-|\boldsymbol{w}|^2 = -|\boldsymbol{v}|^2$. The tensor T can therefore be represented at each point on the sphere by the two vectors $\boldsymbol{v}$ and $\boldsymbol{w}$. We denote the vector $\boldsymbol{v}$ by a thick line and the vector $\boldsymbol{w}$ by a thin one, noting that the vector orientations are unspecified by Eq. (A57) and so the vectors are best represented by unoriented line segments. The angular and parity symmetries of each tensor mode are visible in the figure. For example, the extremal magnitudes of the E_{20} tensor mode occur at the poles and equator, and the mode is symmetric under rotations about $\hat{z}$, as expected for a mode with $j = 2$ and $m = 0$. The symmetry under interchange of two antipodal points is a consequence of the positive parity of this mode. The orthogonality of the E and B modes for given values of j and m implies that each E-B pair of modes is related by interchanging a plus with a cross at each point. As an aside, we remark that this visualization has a parallel in general relativity, where the orthogonality of the plus and cross modes for gravitational radiation also arises from a symmetric real two-tensor tangential to the direction of propagation.

We can also consider various types of pseudotensors. All these acquire an additional sign under parity, which implies that the roles of the E- and B-type coefficients are interchanged in the parity decomposition. For example, pseudoscalars contain only B-type components. Also, the parity decomposition of a pseudovector V' leads to components with spin weight ± 1 of the form

$$V'_{\pm} = \sum_{jm} (\pm B_{jm} + iE_{jm})_{\pm 1} Y_{jm} \tag{A58}$$

instead. Similarly for a pseudotensor T', we have

$$T'_{\pm\pm} = \sum_{jm} (B_{jm} \pm iE_{jm})_{\pm 2} Y_{jm}. \tag{A59}$$

[1] A. A. Michelson and E. W. Morley, Am. J. Sci. **34**, 333 (1887); Philos. Mag. **24**, 449 (1887).
[2] R. J. Kennedy and E. M. Thorndike, Phys. Rev. **42**, 400 (1932).
[3] H. E. Ives and G. R. Stilwell, J. Opt. Soc. Am. **28**, 215 (1938).
[4] G. Joos, Ann. Phys. (Leipzig) **399**, 385 (1930); Naturwissenschaften **19**, 784 (1931); R. S. Shankland *et al.*, Rev. Mod. Phys. **27**, 167 (1955); T. S. Jaseja *et al.*, Phys. Rev. **133**, A1221 (1964).
[5] V. A. Kostelecký and S. Samuel, Phys. Rev. D **39**, 683 (1989); V. A. Kostelecký and R. Potting, Nucl. Phys. **B359**, 545 (1991).
[6] V. A. Kostelecký and N. Russell, arXiv:0801.0287.
[7] D. Colladay and V. A. Kostelecký, Phys. Rev. D **55**, 6760 (1997); **58**, 116002 (1998).
[8] V. A. Kostelecký, Phys. Rev. D **69**, 105009 (2004).
[9] V. A. Kostelecký and R. Potting, Phys. Rev. D **51**, 3923 (1995).
[10] A. Brillet and J. L. Hall, Phys. Rev. Lett. **42**, 549 (1979); D. Hils and J. L. Hall, Phys. Rev. Lett. **64**, 1697 (1990).
[11] V. A. Kostelecký and M. Mewes, Phys. Rev. D **66**, 056005 (2002).
[12] J. Lipa, J. A. Nissen, S. Wang, D. A. Stricker, and D. Avaloff, Phys. Rev. Lett. **90**, 060403 (2003).
[13] H. Müller, S. Herrmann, C. Braxmaier, S. Schiller, and A. Peters, Phys. Rev. Lett. **91**, 020401 (2003).
[14] P. Wolf, M. E. Tobar, S. Bize, A. Clairon, A. N. Luiten, and

G. Santarelli, Gen. Relativ. Gravit. **36**, 2351 (2004); P. Wolf, S. Bize, A. Clairon, G. Santarelli, M. E. Tobar, and A. N. Luiten, Phys. Rev. D **70**, 051902 (2004); M. E. Tobar, P. Wolf, A. Fowler, and J. G. Hartnett, Phys. Rev. D **71**, 025004 (2005); P. L. Stanwix, M. E. Tobar, P. Wolf, M. Susli, C. R. Locke, E. N. Ivanov, J. Winterflood, and F. van Kann, Phys. Rev. Lett. **95**, 040404 (2005); P. L. Stanwix, M. E. Tobar, P. Wolf, C. R. Locke, and E. N. Ivanov, Phys. Rev. D **74**, 081101 (2006).

[15] S. Herrmann, A. Senger, E. Kovalchuk, H. Müller, and A. Peters, Phys. Rev. Lett. **95**, 150401 (2005).

[16] P. Antonini, M. Okhapkin, E. Göklü, and S. Schiller, Phys. Rev. A **71**, 050101 (2005).

[17] H. Müller, P. L. Stanwix, M. E. Tobar, E. Ivanov, P. Wolf, S. Herrmann, A. Senger, E. Kovalchuk, and A. Peters, Phys. Rev. Lett. **99**, 050401 (2007).

[18] H. Müller, C. Braxmaier, S. Herrmann, A. Peters, and C. Lämmerzahl, Phys. Rev. D **67**, 056006 (2003); H. Müller, S. Herrmann, A. Saenz, A. Peters, and C. Lämmerzahl, Phys. Rev. D **68**, 116006 (2003); M. E. Tobar, P. Wolf, A. Fowler, and J. G. Hartnett, Phys. Rev. D **71**, 025004 (2005); H. Müller, Phys. Rev. D **71**, 045004 (2005).

[19] S. M. Carroll, G. B. Field, and R. Jackiw, Phys. Rev. D **41**, 1231 (1990).

[20] V. A. Kostelecký and M. Mewes, Phys. Rev. Lett. **87**, 251304 (2001).

[21] V. A. Kostelecký and M. Mewes, Phys. Rev. Lett. **97**, 140401 (2006).

[22] V. A. Kostelecký and M. Mewes, Phys. Rev. Lett. **99**, 011601 (2007).

[23] V. A. Kostelecký and M. Mewes, Astrophys. J. Lett. **689**, L1 (2008).

[24] B. Altschul, Phys. Rev. D **70**, 056005 (2004); **72**, 085003 (2005); Phys. Rev. Lett. **96**, 201101 (2006); C. D. Carone, M. Sher, and M. Vanderhaeghen, Phys. Rev. D **74**, 077901 (2006); J. P. Cotter and B. T. H. Varcoe, arXiv:physics/0603111; S. Reinhardt *et al.*, Nature Phys. **3**, 861 (2007); M. Hohensee, A. Glenday, C.-H. Li, M. E. Tobar, and P. Wolf, Phys. Rev. D **75**, 049902 (2007); F. R. Klinkhamer and M. Risse, Phys. Rev. D **77**, 117901 (2008); F. R. Klinkhamer and M. Schreck, Phys. Rev. D **78**, 085026 (2008); M. Mewes, Phys. Rev. D **78**, 096008 (2008); M. A. Hohensee, R. Lehnert, D. F. Phillips, and R. L. Walsworth, arXiv:0809.3442; Phys. Rev. Lett. **102**, 170402 (2009).

[25] V. A. Kostelecký, C. D. Lane, and A. G. M. Pickering, Phys. Rev. D **65**, 056006 (2002); B. Altschul and V. A. Kostelecký, Phys. Lett. B **628**, 106 (2005); G. de Berredo-Peixoto and I. L. Shapiro, Phys. Lett. B **642**, 153 (2006); P. Arias, H. Falomir, J. Gamboa, F. Méndez, and F. A. Schaposnik, Phys. Rev. D **76**, 025019 (2007); D. Anselmi, Ann. Phys. (N.Y.) **324**, 874 (2009); Ann. Phys. (N.Y.) **324**, 1058 (2009); D. Colladay and P. McDonald, arXiv:0904.1219 [Phys. Rev. D (to be published)].

[26] D. Colladay and V. A. Kostelecký, Phys. Lett. B **511**, 209 (2001); V. A. Kostelecký and A. G. M. Pickering, Phys. Rev. Lett. **91**, 031801 (2003); C. Adam and F. R. Klinkhamer, Nucl. Phys. **B657**, 214 (2003); C. Kaufhold and F. R. Klinkhamer, Nucl. Phys. **B734**, 1 (2006).

[27] F. W. Stecker and S. L. Glashow, Astropart. Phys. **16**, 97 (2001); R. Lehnert and R. Potting, Phys. Rev. Lett. **93**, 110402 (2004); Phys. Rev. D **70**, 125010 (2004); C. Kaufhold and F. R. Klinkhamer, Phys. Rev. D **76**, 025024 (2007); B. Altschul, Phys. Rev. D **75**, 105003 (2007); Phys. Rev. Lett. **98**, 041603 (2007); Nucl. Phys. **B796**, 262 (2008).

[28] See, for example, Ref. [7] and R. Jackiw and V. A. Kostelecký, Phys. Rev. Lett. **82**, 3572 (1999); M. Pérez-Victoria, J. High Energy Phys. 04 (2001) 032; V. A. Kostelecký, R. Lehnert, and M. J. Perry, Phys. Rev. D **68**, 123511 (2003); B. Altschul, Phys. Rev. D **69**, 125009 (2004); **70**, 101701 (2004); H. Belich, T. Costa-Soares, M. M. Ferreira, and J. A. Helayël-Neto, Eur. Phys. J. C **42**, 127 (2005); A. J. Hariton and R. Lehnert, Phys. Lett. A **367**, 11 (2007); J. R. Nascimento, E. Passos, A. Yu. Petrov, and F. A. Brito, J. High Energy Phys. 06 (2007) 016; J. M. Fonseca, A. H. Gomes, and W. A. Moura-Melo, Phys. Lett. B **671**, 280 (2009); J. Alfaro, A. A. Andrianov, M. Cambiaso, P. Giacconi, and R. Soldati, arXiv:0904.3557.

[29] Q. G. Bailey and V. A. Kostelecký, Phys. Rev. D **70**, 076006 (2004); J. Wu and X. Xue, Eur. Phys. J. C **48**, 257 (2006); A. Kobakhidze and B. H. J. McKellar, Phys. Rev. D **76**, 093004 (2007); S. O. Vellozo, J. A. Helayël-Neto, A. W. Smith, and L. P. G. De Assis, Int. J. Theor. Phys. **47**, 2934 (2008); R. Casana, M. M. Ferreira, and C. E. H. Santos, Phys. Rev. D **78**, 105014 (2008); R. Casana, M. M. Ferreira, A. R. Gomes, and P. R. D. Pinheiro, arXiv:0812.1813.

[30] C. Lämmerzahl, A. Macias, and H. Müller, Phys. Rev. D **71**, 025007 (2005); S. Abel, J. Jaeckel, V. V. Khoze, and A. Ringwald, J. High Energy Phys. 09 (2006) 074; M. Frank and I. Turan, Phys. Rev. D **74**, 033016 (2006); S. Kruglov, Phys. Lett. B **652**, 146 (2007); L. Campanelli and P. Cea, Phys. Lett. B **675**, 155 (2009).

[31] H. Dehmelt *et al.*, Phys. Rev. Lett. **83**, 4694 (1999); R. Mittleman *et al.*, Phys. Rev. Lett. **83**, 2116 (1999); G. Gabrielse *et al.*, Phys. Rev. Lett. **82**, 3198 (1999); R. Bluhm *et al.*, Phys. Rev. Lett. **82**, 2254 (1999); **79**, 1432 (1997); Phys. Rev. D **57**, 3932 (1998); D. Colladay and V. A. Kostelecký, Phys. Lett. B **511**, 209 (2001); B. Altschul, Phys. Rev. D **74**, 083003 (2006).

[32] B. Heckel *et al.*, Phys. Rev. Lett. **97**, 021603 (2006); Phys. Rev. D **78**, 092006 (2008); L.-S. Hou, W.-T. Ni, and Y.-C. M. Li, Phys. Rev. Lett. **90**, 201101 (2003); R. Bluhm and V. A. Kostelecký, Phys. Rev. Lett. **84**, 1381 (2000).

[33] D. Bear *et al.*, Phys. Rev. Lett. **85**, 5038 (2000); D. F. Phillips *et al.*, Phys. Rev. D **63**, 111101 (2001); M. A. Humphrey *et al.*, Phys. Rev. A **68**, 063807 (2003); F. Canè *et al.*, Phys. Rev. Lett. **93**, 230801 (2004); P. Wolf *et al.*, Phys. Rev. Lett. **96**, 060801 (2006); M. Romalis, in *CPT and Lorentz Symmetry IV*, edited by V. A. Kostelecký (World Scientific, Singapore, 2008); V. A. Kostelecký and C. D. Lane, Phys. Rev. D **60**, 116010 (1999); J. Math. Phys. (N.Y.) **40**, 6245 (1999); C. D. Lane, Phys. Rev. D **72**, 016005 (2005); D. Colladay and P. McDonald, Phys. Rev. D **73**, 105006 (2006).

[34] R. Bluhm *et al.*, Phys. Rev. Lett. **88**, 090801 (2002); Phys. Rev. D **68**, 125008 (2003).

[35] O. Bertolami *et al.*, Phys. Lett. B **395**, 178 (1997); G. Lambiase, Phys. Rev. D **72**, 087702 (2005); J. M.

Carmona, J. L. Cortés, A. Das, J. Gamboa, and F. Méndez, Mod. Phys. Lett. A **21**, 883 (2006).
[36] R. Ackerstaff *et al.*, Z. Phys. C **76**, 401 (1997); M. Feindt *et al.*, Report No. DELPHI 97-98 CONF 80 (1997); Y. B. Hsiung *et al.*, Nucl. Phys. B, Proc. Suppl. **86**, 312 (2000); H. Nguyen, arXiv:hep-ex/0112046; J. M. Link *et al.*, Phys. Lett. B **556**, 7 (2003); B. Aubert *et al.*, Phys. Rev. Lett. **100**, 131802 (2008); M. Testa *et al.*, arXiv:0805.1969; V. A. Kostelecký, Phys. Rev. Lett. **80**, 1818 (1998); Phys. Rev. D **61**, 016002 (2000); **64**, 076001 (2001); N. Isgur *et al.*, Phys. Lett. B **515**, 333 (2001); B. Altschul, Phys. Rev. D **75**, 023001 (2007); Phys. Rev. D **79**, 061702 (2009).
[37] V. W. Hughes *et al.*, Phys. Rev. Lett. **87**, 111804 (2001); G. W. Bennett *et al.*, Phys. Rev. Lett. **100**, 091602 (2008); R. Bluhm *et al.*, Phys. Rev. Lett. **84**, 1098 (2000).
[38] L. B. Auerbach *et al.*, Phys. Rev. D **72**, 076004 (2005); M. D. Messier (SK), in *CPT and Lorentz Symmetry III*, edited by V. A. Kostelecký (World Scientific, Singapore, 2005); P. Adamson *et al.*, Phys. Rev. Lett. **101**, 151601 (2008); V. A. Kostelecký and M. Mewes, Phys. Rev. D **69**, 016005 (2004); **70**, 031902 (2004); **70**, 076002 (2004); T. Katori *et al.*, Phys. Rev. D **74**, 105009 (2006); V. Barger, D. Marfatia, and K. Whisnant, Phys. Lett. B **653**, 267 (2007).
[39] D. L. Anderson, M. Sher, and I. Turan, Phys. Rev. D **70**, 016001 (2004); E. O. Iltan, Mod. Phys. Lett. A **19**, 327 (2004).
[40] J. B. R. Battat, J. F. Chandler, and C. W. Stubbs, Phys. Rev. Lett. **99**, 241103 (2007); H. Müller, S. Chiow, S. Herrmann, S. Chu, and K.-Y. Chung, Phys. Rev. Lett. **100**, 031101 (2008); W. M. Jensen, S. M. Lewis, and J. C. Long, in *CPT* and Lorentz Symmetry IV, op. cit.; Q. G. Bailey and V. A. Kostelecký, Phys. Rev. D **74**, 045001 (2006); V. A. Kostelecký, N. Russell, and J. Tasson, Phys. Rev. Lett. **100**, 111102 (2008); V. A. Kostelecký and J. Tasson, Phys. Rev. Lett. **102**, 010402 (2009); Q. G. Bailey, arXiv:0904.0278.
[41] Y. Nambu, Phys. Rev. Lett. **4**, 380 (1960); J. Goldstone, Nuovo Cimento **19**, 154 (1961); J. Goldstone, A. Salam, and S. Weinberg, Phys. Rev. **127**, 965 (1962).
[42] V. A. Kostelecký and R. Potting, Gen. Relativ. Gravit. **37**, 1675 (2005); Phys. Rev. D **79**, 065018 (2009).
[43] V. A. Kostelecký and S. Samuel, Phys. Rev. D **40**, 1886 (1989); Phys. Rev. Lett. **63**, 224 (1989); R. Bluhm and V. A. Kostelecký, Phys. Rev. D **71**, 065008 (2005); O. Bertolami and J. Páramos, Phys. Rev. D **72**, 044001 (2005); R. Bluhm *et al.*, Phys. Rev. D **77**, 065020 (2008); M. D. Seifert, Phys. Rev. D **79**, 124012 (2009).
[44] V. A. Kostelecký and M. Mewes (unpublished).
[45] V. A. Kostelecký and R. Lehnert, Phys. Rev. D **63**, 065008 (2001).
[46] M. Hayakawa, Phys. Lett. B **478**, 394 (2000).
[47] The leading-order action is constructed in S. M. Carroll *et al.*, Phys. Rev. Lett. **87**, 141601 (2001).
[48] M. S. Berger and V. A. Kostelecký, Phys. Rev. D **65**, 091701 (2002); P. A. Bolokhov, S. G. Nibbelink, and M. Pospelov, Phys. Rev. D **72**, 015013 (2005).
[49] H. Boerner, *Representations of Groups* (American Elsevier, New York, 1970).
[50] M. V. Ostrogradski, Mem. Acad. Imp. Sci. St.-Petersbourg **4**, 385 (1850).
[51] See, for example, H. Flanders, *Differential Forms with Applications to the Physical Sciences* (Academic, New York, 1963).
[52] Y. N. Obukhov, T. Fukui, and G. F. Rubilar, Phys. Rev. D **62**, 044050 (2000).
[53] C. Lämmerzahl and F. W. Hehl, Phys. Rev. D **70**, 105022 (2004); Y. Itin, Phys. Rev. D **72**, 087502 (2005).
[54] G. M. Shore, Nucl. Phys. **B717**, 86 (2005).
[55] Y. N. Obukhov and F. W. Hehl, Phys. Lett. B **458**, 466 (1999); F. W. Hehl, Y. N. Obukhov, and G. F. Rubilar, arXiv:gr-qc/9911096.
[56] Y. Itin, Phys. Rev. D **70**, 025012 (2004); F. W. Hehl and Y. N. Obukhov, Gen. Relativ. Gravit. **40**, 1239 (2008).
[57] E. T. Newman and R. Penrose, J. Math. Phys. (N.Y.) **7**, 863 (1966).
[58] J. N. Goldberg, A. J. Macfarlane, E. T. Newman, F. Rohrlich, and E. C. G. Sudarshan, J. Math. Phys. (N.Y.) **8**, 2155 (1967); G. F. T. del Castillo, *3-D Spinors, Spin-Weighted Functions, and their Applications* (Birkhäuser, Boston, 2003).
[59] See, for example, M. Zaldarriaga and U. Seljak, Phys. Rev. D **55**, 1830 (1997).
[60] R. Gambini and J. Pullin, Phys. Rev. D **59**, 124021 (1999); D. Sudarsky, L. Urrutia, and H. Vucetich, Phys. Rev. Lett. **89**, 231301 (2002).
[61] J. Alfaro, H. A. Morales-Técotl, and L. F. Urrutia, Phys. Rev. D **65**, 103509 (2002).
[62] R. C. Myers and M. Pospelov, Phys. Rev. Lett. **90**, 211601 (2003); C. M. Reyes, L. F. Urrutia, and J. D. Vergara, Phys. Rev. D **78**, 125011 (2008).
[63] P. A. Bolokhov and M. Pospelov, Phys. Rev. D **77**, 025022 (2008).
[64] A. G. Cohen and S. L. Glashow, Phys. Rev. Lett. **97**, 021601 (2006).
[65] H. P. Robertson, Rev. Mod. Phys. **21**, 378 (1949).
[66] R. Mansouri and R. U. Sexl, Gen. Relativ. Gravit. **8**, 497 (1977).
[67] For reviews see, for example, J. Kowalski-Glikman, Lect. Notes Phys. **669**, 131 (2005); G. Amelino-Camelia, arXiv:0806.0339.
[68] S. Judes and M. Visser, Phys. Rev. D **68**, 045001 (2003).
[69] J. Lukierski and A. Nowicki, Acta Phys. Pol. B **33**, 2537 (2002); N. Jafari and A. Shariati, AIP Conf. Proc. **841**, 462 (2006).
[70] E. P. Wigner, *Group Theory* (Academic, New York, 1959).
[71] Related results for low d are obtained in R. Lehnert, Phys. Rev. D **68**, 085003 (2003).
[72] T. A. Jacobson, S. Liberati, D. Mattingly, and F. W. Stecker, Phys. Rev. Lett. **93**, 021101 (2004).
[73] M. R. Martínez and T. Piran, J. Cosmol. Astropart. Phys. 04, 006 (2006); J. Ellis, N. E. Mavromatos, D. V. Nanopoulos, A. S. Sakharov, and E. K. G. Sarkisyan, Astropart. Phys. **25**, 402 (2006).
[74] J. Albert *et al.*, Phys. Lett. B **668**, 253 (2008).
[75] G. Amelino-Camelia, J. R. Ellis, N. E. Mavromatos, D. V. Nanopoulos, and S. Sarkar, Nature (London) **393**, 763 (1998).
[76] I. G. Mitrofanov, Nature (London) **426**, 139 (2003).
[77] S. E. Boggs, C. B. Wunderer, K. Hurley, and W. Coburn, Astrophys. J. Lett. **611**, L77 (2004).

[78] A. Abdo *et al.*, Science **323**, 1688 (2009).
[79] F. Aharonian *et al.*, Phys. Rev. Lett. **101**, 170402 (2008).
[80] J. Holder *et al.*, AIP Conf. Proc. **1085**, 657 (2009).
[81] J. Buckley *et al.*, AIP Conf. Proc. **1085**, 902 (2009).
[82] G. Hermann, W. Hofmann, T. Schweizer, and M. Teshima, arXiv:0709.2048.
[83] G. Sinnis, A. Smith, and J. E. McEnery, arXiv:astro-ph/0403096.
[84] See, for example, M. Born and E. Wolf, *Principles of Optics* (Pergamon, New York, 1975), 5th ed..
[85] T. Kahniashvili, G. Gogoberidze, and B. Ratra, Phys. Lett. B **643**, 81 (2006); Y.-Z. Fan, D.-M. Wei, and D. Xu, Mon. Not. R. Astron. Soc. **376**, 1857 (2007).
[86] D. R. Willis *et al.*, Astron. Astrophys. **439**, 245 (2005).
[87] For $d = 4$, these figures differ slightly from those in Ref. [21], where the effective degree of polarization Π_{eff} was taken as $\langle s^1\rangle^2 + \langle s^2\rangle^2$ instead.
[88] A. Lue, L. Wang, and M. Kamionkowski, Phys. Rev. Lett. **83**, 1506 (1999); K. R. S. Balaji, R. H. Brandenberger, and D. A. Easson, J. Cosmol. Astropart. Phys. 12, 008 (2003); J. Gamboa, J. López-Sarrión, and A. P. Polychronakos, Phys. Lett. B **634**, 471 (2006); G.-C. Liu, S. Lee, and K.-W. Ng, Phys. Rev. Lett. **97**, 161303 (2006); R. Casana, M. M. Ferreira, and J. S. Rodrigues, Phys. Rev. D **78**, 125013 (2008); A. P. S. Yadav, R. Biswas, M. Su, and M. Zaldarriaga, arXiv:0902.4466 [Phys. Rev. D (to be published)].
[89] L. Page *et al.*, Astrophys. J. Suppl. Ser. **170**, 335 (2007).
[90] G. Hinshaw *et al.*, Astrophys. J. Suppl. Ser. **180**, 225 (2009); M. Nolta *et al.*, Astrophys. J. Suppl. Ser. **180**, 296 (2009).
[91] T. E. Montroy *et al.*, Astrophys. J. **647**, 813 (2006); F. Piacentini *et al.*, Astrophys. J. **647**, 833 (2006).
[92] A. C. S. Readnead *et al.*, Science **306**, 836 (2004); E. M. Leitch *et al.*, Astrophys. J. **624**, 10 (2005); D. Barkats *et al.*, Astrophys. J. Lett. **619**, L127 (2005).
[93] For a review see, for example, W. Hu and M. White, New Astron. Rev. **2**, 323 (1997).
[94] B. Feng, M. Li, J.-Q. Xia, X. Chen, and X. Zhang, Phys. Rev. Lett. **96**, 221302 (2006).
[95] P. Cabella, P. Natoli, and J. Silk, Phys. Rev. D **76**, 123014 (2007).
[96] E. Komatsu *et al.*, Astrophys. J. Suppl. Ser. **180**, 330 (2009).
[97] J.-Q. Xia, H. Li, X. Wang, and X. Zhang, Astron. Astrophys. **483**, 715 (2008).
[98] T. Kahniashvili, R. Durrer, and Y. Maravin, Phys. Rev. D **78**, 123006 (2008).
[99] E. Y. S. Wu *et al.*, Phys. Rev. Lett. **102**, 161302 (2009).
[100] The Scientific Program of Planck, arXiv:astro-ph/0604069.
[101] D. Samtleben, Nuovo Cimento Soc. Ital. Fis. **122B**, 1353 (2007).
[102] D. Baumann *et al.*, arXiv:0811.3919.
[103] P. Oxley *et al.*, Proc. SPIE Int. Soc. Opt. Eng. **5543**, 320 (2004).
[104] J. Bock *et al.*, arXiv:0805.4207.
[105] B. P. Crill *et al.*, arXiv:0807.1548.
[106] P. Laurent *et al.*, Eur. Phys. J. D **3**, 201 (1998).
[107] R. Byer, S. Buchman, J. Lipa, K.-X. Sun, and J. Hall, Space Time Asymmetry Research (STAR); C. Lämmerzahl, H. Dittus, A. Peters, and S. Schiller, Classical Quantum Gravity **18**, 2499 (2001).
[108] M. Mewes and A. Petroff, Phys. Rev. D **75**, 056002 (2007).